6-30-2016

Development Of Highly Active And Stable Compressive Pt Cathode Catalysts For Polymer Electrolyte Membrane Fuel Cells

Taekeun Kim
University of South Carolina

DEVELOPMENT OF HIGHLY ACTIVE AND STABLE COMPRESSIVE PT CATHODE CATALYSTS FOR POLYMER ELECTROLYTE MEMBRANE FUEL CELLS

by

Taekeun Kim

Bachelor of Science
Seoul National University, 2005

Submitted in Partial Fulfillment of the Requirements

For the Degree of Doctor of Philosophy in

Chemical Engineering

College of Engineering and Computing

University of South Carolina

2016

Accepted by:

Branko N. Popov, Major Professor

Ralph E. White, Committee Member

John W. Weidner, Committee Member

Qian Wang, Committee Member

Lacy Ford, Senior Vice Provost and Dean of Graduate Studies

DEDICATION

I dedicate my dissertation work to God, and my father, parents-in-law, my lovely wife, Sun Young Park and my precious two sons, Jayden and Jacob. I also dedicate this work to my late mother, Chun-Seok Jeon.

ACKNOWLEDGEMENTS

I sincerely thank my advisor, Dr. Popov, for his continuous support and enriching guidance he provided during my study period. I have to mention that he is the most passionate person in the lab including all young students. His ceaseless enthusiasm encouraged me a lot when I had a hard time. His passion for research greatly spurred me whenever I felt down. Even when I failed several times getting good results, he always encouraged me and guided me with valuable suggestions from his enthusiasm and great store of knowledge in electrochemistry. I also appreciate the opportunities he provided me to present my research in several international conferences. I could expand my experience by discussing my work with researchers from all over the world, and get inspired by other peoples' innovative researche. I extend gratitude to Dr. White, Dr. Weidner and Dr. Wang for serving on my committee and providing invaluable advice. I also would like to thank professors who have instructed me in my course works, especially Dr. White for chemical process analysis and Dr. Gadala-Maria for fluid flow analysis who let me get a better understanding of chemical systems.

I am also thankful to the lab members, Prabhu, Tian and Jung for their personal and professional assistance. Prabhu has always been friendly and helped me with many hours of proofreading my papers and the dissertation. Tian has always been friendly and I could get refreshed after sharing our similar hardships. I also wish to acknowledge the help of staff members of the Chemical Engineering Department, Marcia, Vernon, Loretta, Carol, and Sandy.

Special thanks to Hyunseok, Hyomin, Shawn, Seokwon, Youngseok, Brian, Seungmo, Soonkun, Jungho, Sungtak, Youjung, Myunghee, Dooyoung, Chanil, Dr. Woo-Kum Lee and Dr. Joongpyo Shim for making me feel relaxed, secure and joyful with lots of help and agreeable conversations during my Ph.D. years. I also would like to thank my classmates who struggled together with me for the qualifying exam and course works.

I appreciate the continuous prayer and supports of Pastor Dong Yung Kim and members of Columbia Korean Community Presbyterian Church. I'm also thankful to Pastor Daehee Lee, Pastor Jindoo Kim, and Pastor Youngman Won for their prayer and wishes from Korea. I also would like to express my gratitude to Seungshik Shin, Dr. Sungchul Lee, and Dr. Junsik Kim who guided me as a mentor when I worked at Samsung and encouraged me to proceed to a doctoral program. Thanks to my old friends with whom I have spent my life from childhood to college years.

I am deeply indebted to my grandmother Chae-Bok Yu; my father Soo-Young Kim; sister Ji-Young; brother Yu-Geun, his wife Eun-Mee and his adorable children Ye-Seo and Ye-Dam; for their devoted support. My parents-in-law Jonghyuk Park, Chunja Kim and sister-in-law Joo-Young have always trusted me and provided me never-ending assistance and encouragement. I really thank my late mother Chun-Seok Jeon for her endless love and pray.

Finally, I give special thanks to my beloved wife, Sun Young Park, and my wonderful sons, Jayden and Jacob, for being there for me throughout the entire doctorate program. They have provided me a source of strength to finish this work and made me feel like the best husband and dad. Without my wife's devotion and love, this work would not be possible. Two sons, you have been my best cheerleaders.

ABSTRACT

With the limited fossil fuel reserve and increased power demand, polymer electrolyte membrane fuel cells (PEMFC) have been considered to be a promising alternative to the current energy consumption mode due to its high energy conversion, high efficiency, and zero emissions. However, high cost, poor stability, and sluggish kinetic for oxygen reduction reaction (ORR) of Pt/C cathode catalysts are obstacles for the commercialization of PEMFC for automotive application. The observed poor stability is attributed to a corrosion of carbon supports due to low pH, high temperature, and high anodic potentials (1.0-1.5 V) at the cathode interface during start-up/shutdown conditions. Electrochemical oxidation of carbon results in carbon loss leading to Pt detachment/sintering and subsequent loss of electrochemical surface area (ECSA). Another contributing factor is Pt and/or alloying element dissolution and particle sintering in operating conditions (0.6-1.0 V).

In this study, a support material, a Pt catalyst and a compressive Pt lattice catalyst were optimized to develop an active and stable cathode catalyst for PEMFC. A carbon composite catalyst (CCC) was developed from high surface area carbon black (HSACB), which has unique ORR activity and stability compared to those of HSACB. By using CCC support for Pt/C catalysts, the support stability was improved significantly. Also, transition metals embedded in CCC structure were used to synthesize the compressive Pt catalyst by using USC's novel method. The catalyst indicated improved activity when compared with pristine Pt catalyst.

To further enhance activity and stability, a novel activated carbon composite support (ACCS) was developed by optimizing surface area, pore-size distribution, as well as the degree of graphitization and the hydrophobicity. Pt deposition on the ACCS was optimized using a modified polyol process developed in our laboratory in order to control Pt particle size and Pt particle distribution. Fuel cell performance and stability of Pt/ACCS were evaluated using accelerated stress test (AST) protocols recommended by the US Fuel Cell Tech Team for both the catalyst and the support. The Pt/ACCS catalyst showed improved activity and excellent support stability at 1.0-1.5 V over those of commercial catalysts due to the controlled Pt particles and optimized properties of ACCS. Also, a compressive Pt catalyst (Pt*/ACCS) was developed to further increase activity and stability at 0.6-1.0 V. Pt*/ACCS was prepared using the in-house developed procedure in which Co diffuses into the Pt/ACCS catalyst followed by controlled heat-treatment. The pyrolysis temperature and Pt/Co ratio were optimized to initiate formation of compressive Pt catalyst. A protective coating method was used to inhibit particle growth during heat treatment which maintains the catalyst particle size in the range between 3 and 5 nm. Pt*/ACCS showed enhanced catalyst stability at 0.6-1.0 V over that of Pt/ACCS while keeping good performance and good support stability. The good stability of Pt*/ACCS is attributed to a potential shift of Pt oxide formation to a more positive direction which results in less Pt dissolution due to less reduction of Pt oxide when the catalyst is cycled in cathode direction from 1.0 to 0.6 V.

TABLE OF CONTENTS

LIST OF TABLES

LIST OF FIGURES

CHAPTER 1

INTRODUCTION

1.1 Background

Since the first concept of fuel cells was discovered in 1839 by William Grove, enormous research on catalysts, stacks, and systems has been carried out in variety of fuel cell types including solid oxide fuel cells (SOFC), molten carbonate fuel cells (MCFC), alkaline fuel cells (AFC), direct methanol fuel cells (DMFC), phosphoric acid fuel cells (PAFC), and polymer electrolyte membrane fuel cells (PEMFC) [1, 2]. A fuel cell is an electrochemical device that continuously converts chemical energy into electrical energy (and some heat) for as long as fuel and oxidant are supplied. It is a power generating device which has higher efficiency and low emission when compared to batteries and combustion engines [2].

Among various types of fuel cells, PEMFCs have attracted attention for automotive applications due to their high efficiency, high current density output, low-temperature operation, and low emissions [3-7]. Robust cation exchange membranes were originally developed by DuPont and have proved instrumental in combining all the key parts of a fuel cell, anode electrode, cathode electrode, the electrolyte, and the gas diffusion layer (GDL), in a very compact unit which is membrane electrode assembly (MEA). The membrane relies on the presence of liquid water to be able to conduct protons effectively; therefore, to achieve good performance, effective electrocatalyst

technology is required. The catalysts form thin gas-porous electrode layers on either side of the membrane. Ionic contact with the membrane is enhanced by mixing the catalysts with a liquid form of the membrane ionomer while constructing electrodes. The MEA is located between a pair of bi-polar plates (which also have a role of the current collector) with machined flow field for distributing fuel and oxidant to anode and cathode, respectively. Figure 1.1 represents the unit cell cross-section of a fuel cell stack [8].

As shown in Figure 1.1, the hydrogen oxidation reaction (HOR) takes place on the anode catalysts with the following reaction [2].

$$H_2 \rightarrow 2H^+ + 2e^- \ (E^o = 0.00\ V\ vs.RHE) \quad (1)$$

Various metal catalysts show high activity for HOR, but in acidic electrolytes, noble metals show the greatest stability towards corrosion or passivation. The exchange current density, i^o, of the reaction on Pt single crystals is ~ 10^{-3} A cm^{-2} [9]. This high i^o implies that on increasing load, the anode stays at a potential close to the theoretical reversible potential.

The oxygen reduction reaction (ORR) is the primary electrochemical reaction occurring at the cathode of the fuel cells. The ORR in aqueous media is governed by a number of possible reactions. The thermodynamic potentials for the reactions are shown below [10].

$$O_2 + 4H^+ + 4e^- \rightarrow 2H_2O \ (E^o = 1.23\ V\ vs.RHE) \quad (2)$$

$$O_2 + 2H^+ + 2e^- \rightarrow H_2O_2 \ (E^o = 0.67\ V\ vs.RHE) \quad (3)$$

The generalized scheme for the ORR is shown in Figure 1.2 [11]. Based on this scheme, oxygen can be reduced either directly to water with the rate constant k_1 without intermediate formation of $H_2O_{2,ad}$ (direct four-electron reduction) to $H_2O_{2,ad}$ with the rate constant k_2 (series two-electron reduction). The adsorbed peroxide can be electrochemically reduced to water with the rate constant k_3; catalytically decomposed on the electrode surface (k_4) or desorbed into the bulk of the solution (k_5). Ideally, the direct four-electron oxygen reduction path (Eq. 2) is more desirable than two-electron reduction path (Eq. 3) for high efficiency. Since the four-electron oxygen reduction is highly irreversible in aqueous electrolyte, it results in substantial energy losses in PEMFCs. In most instances, the exchange current densities practical for kinetic studies are much larger than the one for ORR; therefore, the information obtained from IV data is confined only to the rate-determining step, which is ORR [12]. Also, it is clear from the above discussion that the oxygen reduction takes place at a high positive potential in acid medium. At such a high potential, most of the metals will dissolve and only noble metals are stable.

To determine the activities of various metals toward ORR, Norskov and co-workers calculated the Gibbs free energy of the ORR intermediates as a function of cathode potential based on a simple dissociative mechanism, i.e., assuming the adsorbed oxygen atoms and the hydroxyl groups being the only intermediates by using density functional theory (DFT) models [13]. As shown in Figure 1.3, the model predicts a volcano-shaped relationship between the rate of the ORR and the oxygen adsorption energy, with platinum (Pt) and palladium (Pd) being the best metals for electrocatalysis for the ORR.

Therefore, Pt and Pt-based alloy catalysts are most commonly used as cathode catalysts for PEMFCs due to their high activity and stability [7, 14, 15]. However, the high cost of Pt metal is an obstacle for the commercialization of PEMFCs for automotive applications [16]. To overcome the cost issues of Pt-based catalysts, many recent studies have focused on decreasing the Pt loadings and increasing the Pt utilization in fuel cell electrodes while maintaining satisfactory activity and stability. These efforts include the design of novel catalysts, the use of new catalyst support materials, development of new methods for catalyst synthesis, optimizing Pt catalyst structures, developing Pt-alloy catalysts, and the optimization of electrode structure and fabrication methods [17-23].

In spite of relatively high stability of Pt metal in acidic medium, the electrochemical durability of Pt-based catalysts under fuel cell operating conditions are not still satisfactory in terms of commercialization of PEMFCs for automotive applications [16]. The durability of Pt-based catalysts can be compromised by Pt sintering and dissolution, especially under the load cycling found in fuel cell vehicles, which accelerates these processes [24-29]. These effects significantly decrease the electrochemically active surface area and Pt utilization in fuel cell cathodes. In addition, the dissolution of non-noble metals in the catalyst alloy not only causes a decrease in the catalyst's activity, but it also poisons the MEAs via ion exchange between the metal cations and the protonic sites on both the Nafion® membrane and the ionomer inside the catalyst layer [26].

Another concern complicating the use of carbon-supported Pt-based catalysts is the corrosion of the high surface area carbon support [21, 23, 28, 30, 31]. During the startup/shutdown cycle, the cathode interface potential of a fuel cell may increase to 1.2–

1.5 V, or even higher. At these high potentials, the corrosion rate of carbon increases drastically resulting in severe degradation of the carbon support [32-35]. Oxidation of the carbon surface increases its hydrophilicity and thus affects water removal, resulting in an increased mass transfer resistance. In addition, the oxidation of carbon increases the electrical resistance of the catalysts, leads to the aggregation of catalyst particles, and even damages the structure of the catalyst layer. In particular, Pt increases the corrosion rate of carbon supports [28, 30, 31]. In spite of world-wide research about durability issues, it is still challenging to obtain a Pt-based fuel cell cathode catalyst with both high activity and durability necessary for automotive application.

1.2 Literature review

1.2.1 Carbon supports for Pt-based cathode catalysts

Carbon black (CB) is a typical catalyst support material for fuel cell applications because of its high electrical conductivity, large surface area, and well-defined pore structure. Pt and Pt-based alloy catalysts supported on high surface area carbons have been used for ORR in PEMFCs [4, 7, 14, 36]. Recent research on PEMFC development mainly focuses on the reliability of the system and durability of the catalysts and catalyst supports. The performance degradation of PEMFCs is affected by several factors including Pt and/or alloying element dissolution [37, 38], Pt particle sintering [37-39], carbon support corrosion [31, 40-43], and membrane thinning [37, 38].

It has been reported that automotive fuel cell systems can experience excursions to very high potential regions due to repetitive shutdown/startup of the fuel cell system or due to local fuel cell starvation [44]. Reiser et al. [45] have shown that the cathode interfacial potential difference can reach ~1.5 V due to the "H_2/air front" mechanism in

the anode compartment during startup/shutdown and carbon corrosion is an inevitable parasitic reaction at these high potentials. This high potential with other favorable conditions such as the presence of Pt, low pH, high oxygen and water contents, and high temperature accelerate the carbon corrosion according to the following reaction [46]:

$$C + 2H_2O \rightarrow CO_2 + 4H^+ + 4e^- \ (E^o = 0.207\ V\ vs.RHE\ at\ 25\ ℃) \qquad (4)$$

In general, carbon corrosion occurs through the formation of oxygen-containing functional groups like carboxyl, carbonyl, hydroxyl, phenol, etc. on the surface at high potentials and temperature (>1.0 V vs. reversible hydrogen electrode (RHE) at room temperature or >0.8 V vs. RHE at 65 °C) [31, 42]. Figure 1.4 shows a schematic of the effects of carbon corrosion on a PEMFC cathode [41]. Carbon corrosion weakens the catalyst interaction with the support resulting in the formation of electrically isolated Pt particles that are detached from the carbon support. Electrochemical oxidation of the carbon support results in carbon support loss which leads to Pt agglomeration and sintering and subsequent loss of electrochemical surface area (ECSA) [39, 40, 43]. Carbon support oxidation can increase the hydrophilicity of the surface which results in a decrease in gas permeability [47] as the pores are filled with water that hinders gas transport [48]. Carbon support loss also causes a decrease in catalyst layer thickness which increases the cell resistance [49] due to poor electrical contact with the GDL [50, 51]. Thus, carbon corrosion is a detrimental factor which affects the cathode catalyst degradation and overall PEMFC performance loss.

In order to overcome the problems associated with carbon supports, alternative materials such as metal oxides [41, 52-55], conducting polymers [56], non-conducting polymers [8, 57], metal nitrides and metal carbides [58, 59], ZrO_2/C [60, 61], CeO_2/C [62] have been explored as catalyst supports for PEMFC application with limited success in terms of achieving desired power density requirements necessary for automotive applications. Hence, high surface area carbons and graphitic carbons are being used as the catalyst support for PEMFC applications.

Carbon corrosion in PEMFC cathode catalysts has been extensively studied in both three-electrode set-up using a rotating ring disk electrode (RRDE) [63-71] and under fuel cell operating conditions [32-35, 44, 72-81]. Mechanistic studies to understand carbon corrosion under PEMFC operating conditions have also been reported [82, 83]. The effect of corrosion of BP-2000 and XC-72 carbon supports on the durability of Pt/C catalyst was studied by Wang et al. [70] by applying a constant potential of 1.2 V under simulated PEMFC conditions. A larger increase in Pt particle size and a higher Pt loss was observed in the Pt/BP-2000 catalyst than in Pt/XC-72 under potential cycling condition between 0.6 and 1.2 V. ECSA loss of 40.9% for the Pt/BP-2000 and 20.6% for the Pt/XC-72 catalysts have been reported. Studies of the corrosion mechanism of Pt/XC-72 and Pt/BP-2000 catalysts using RRDE and observations using a transmission electron microscope indicated that major corrosion occurred inside the catalyst with some minor corrosion on the surface in the case of Pt/XC-72, whereas corrosion predominantly occurred at the surface for Pt/BP-2000 [71].

The microstructure effects on the electrochemical corrosion of furnace blacks, proprietary carbons of the Sibunit family, carbon nanofilaments, and carbon-supported Pt

catalysts have been studied in a three-electrode cell in 2 M H_2SO_4 at 80 °C [64]. Corrosion currents were found to decay with time roughly following the $t^{-0.5}$ dependence. Corrosion current densities (normalized to the surface area) depended strongly on the microstructure of the carbon material. The proprietary Sibunit carbon and carbon nanofiber possess higher corrosion stability than conventional furnace blacks. The electrochemical stability of carbon nanofiber [63], mesoporous carbon [65], nitrogen-doped reduced graphene oxide [67], and graphene oxide (GO) [66, 68] supports in RRDE has also been reported. The experiments on carbon nanofibers showed that the relative increase in surface oxides during the electrochemical oxidation treatment is significantly smaller than on CB [63]. Potential cycling between 0.8 and 1.4 V in an RRDE indicated better stability for catalysts on Vulcan carbon due to the presence of larger average graphitic crystallites than for catalysts supported on high-surface-area ordered mesoporous carbon [65]. The GO has been used as a support for the cathode catalyst in PEMFCs because its oxygen-containing groups act as binding sites for Pt nanoparticles [66-68]. Unlike conventional Pt catalysts, a Pt catalyst supported on nitrogen-doped reduced GO showed no performance degradation after 1000 cycles between 0.6 and 1.2 V in an accelerated durability test (ADT) [67]. He et al. [66] suggested a bifunctional effect of both graphitization and oxygen functional groups on the catalytic activity and stabilization of Pt nanoparticles deposited on reduced graphene oxide (Pt/RGO) catalysts. The support durability test results using three-electrode cell studies offer only limited information about the stability of various carbon supports and do not provide any insight into the durability of these supports in PEMFCs under actual startup/shutdown conditions.

The support durability of various carbon-supported Pt catalysts subjected to different accelerated corrosion tests in PEMFCs has been reported in the literature [32-35, 44, 72-82]. Wang et al. [81] carried out support corrosion characterization studies on multiwall carbon nanotube (MWCNT) and commercial Vulcan XC-72 supports using potentiostatic treatment (0.9 V) for 168 h. They concluded that the multiwall carbon nanotube support is electrochemically more stable than the Vulcan XC-72 support since the former showed 30% lower corrosion current and a 37% loss in ECSA (80% loss in ECSA for Vulcan XC-72) after applying a constant potential of 0.9 V for 168 h. However, the experimental conditions used in this study do not effectively induce carbon corrosion since the extent of carbon corrosion is significant only at potentials >1.0 V. Bi and Fuller [72] studied the effect of temperature on carbon corrosion in Pt/C under accelerated conditions by applying a square-wave potential cycling between 0.87 and 1.2 V vs. RHE. More rapid degradation was observed due to loss of ECSA and Pt deposition on the membrane at 80 °C than at 60 or 40 °C.

Oh et al. [34, 35] and Lim et al. [32, 33] studied carbon corrosion in a variety of carbons such as CB, carbon nanofiber (CNF) and carbon nanocage (CNC) in Pt/CB, Pt/CNF and Pt/CNC catalysts by applying a constant potential of 1.4 V for 30 min. Using on-line mass spectrometry, they measured the amount of CO_2 produced when these catalysts were subjected to a high potential. A comparison study involving Pt/CB, Pt/CNF and Pt/CNC by Oh et al. [35] indicated that the degree of graphitization did not directly correlate to the higher corrosion resistance. The authors concluded that hydrophobicity was a critical factor in enhancing the supports' resistance to corrosion and that carbon nanocage was more resistant to corrosion than carbon nanofiber. Lim et al.

[33] also found significant corrosion resistance for the carbon nanocage support with 2.3% performance degradation at 0.6 V under H_2/O_2 fuel cell polarization after applying 1.4 V to the cathode for 30 min. In a separate study, Lim et al. [32] showed that the presence of water is indispensable for and the presence of gas-phase O_2 has little effect on the electrochemical carbon corrosion.

The durability of graphitic carbon (GrC) [76, 80] and graphitized MWCNT [77] supports was studied through accelerated stress tests (AST) using potentiostatic (potential holding at 1.2 V) [77, 80] and potential cycling (between 0.6 and 1.2 V) [76] experiments. Application of the constant potential to the Pt/GrC and Pt/non-GrC cathodes showed fuel cell performance degradation of only 10% after 70 h for the Pt/GrC and a much higher loss (77%) for the Pt/non-GrC in a H_2/O_2 fuel cell. The AST study for Pt_3Co and Pt catalysts supported on graphitic and non-graphitic carbon supports subjected to potential cycling between 0.6 and 1.2 V indicated an order of durability: Pt_3Co/GrC > Pt/GrC > Pt_3Co/non-GrC > Pt/non-GrC [76]. The comparison study involving Pt/C, pristine, and graphitized Pt/MWCNT catalysts showed Pt particle growth in the Pt/C catalyst after subjecting the AST at 1.2 V [77]. The study concluded that Pt particles have a high tendency to aggregate upon carbon corrosion during AST because of their high surface-energy. Furthermore, in Pt/C, the amorphous nature of carbon with a higher number of defect sites facilitates carbon corrosion resulting in larger particles relative to Pt deposited on pristine and graphitized MWCNTs.

A simple low-temperature self-catalyzed reduction treatment has been shown to improve the support durability at 1.4 V of the carbon nanotube (CNT) supports. Studies consisting of an accelerated test for 6 h followed by electrochemical characterization

studies including ECSA measurement and H_2/O_2 polarization curve indicated an activity loss of 62.5% for the commercial Pt/C and of only 6.2% for the CNT subjected to self-catalyzed reduction treatment. An increase in polarization resistance of 3% for the Pt/CNT as opposed to a 700% increase for the Pt/C has been reported [75].

Dhanushkodi et al. [73] used a variety of voltage waveforms such as two square-wave potential cycling tests (from 1.0 V to 1.4 V and from 1.0 V to 1.5 V) with different dwell times and constant cell voltage of 1.4 V to elucidate the extent of carbon corrosion, mixed-mode degradation, and Pt dissolution.

The durability of Pt/C and of Pt deposited on mesoporous carbon functionalized with poly(3,4-ethylenedioxythiophene) (MC-PEDOT) has been reported by Tintula et al. [79]. They found the degradation rate for Pt/C in an H_2/O_2 fuel cell is three-times higher than that for Pt/MC-PEDOT. The authors concluded that the enhanced durability of Pt/MC-PEDOT is due to the specific interaction of Pt with the MC-PEDOT support and the resistance toward electrochemical oxidation of the mesoporous carbon support.

Other studies of importance with respect to the carbon support corrosion were reported by Makharia et al. [44], Jung et al. [74], and Spernjak et al. [78]. Makharia et al, after studying the support stability by calculating the mass-specific CO_2 currents by online gas analysis as a function of potential (1.1–1.3 V vs. RHE), temperature (50–95 °C), and time (1000 min.), suggested that future R&D efforts should focus on the development of more stable catalyst supports with improved corrosion resistance at high cathodic potentials. Carbon corrosion in 50% Pt/C and 30% Pt-alloy/corrosion-resistant carbon catalysts were evaluated by recording H_2/air polarization curves using a stoichiometry of 3/3 at 80 °C with 50% relative humidity (RH) and 150 kPa_{abs} back

pressure. Their study showed that after 20 h of potentiostatic holding at 1.2 V, the H_2/air performance of a Pt/C catalyst decreases 30 mV at 1500 mA cm^{-2} and much more after 30 h, while the 30% Pt-alloy/corrosion-resistant support showed no decrease in performance even after 100 h of exposure at 1.2 V. A correlation between voltage loss and carbon-support weight loss indicated that both conventional and corrosion-resistant support electrode structures show high performance losses at about 5-10% carbon-support weight loss.

1.2.2 Pt deposition on carbon supports

As the Pt is known to be a good catalyst for ORR, the production of such catalytic surfaces with a range of particle sizes and surface are of prime importance. The reduction of Pt metal salts to the metallic state on support materials has become a focus in material science dealing with nanoparticles [84]. There are mainly two methods for Pt deposition; electrochemical deposition and electroless (chemical) deposition. Historically, electrochemical deposition is a versatile technique by which a desired metallic coating can be obtained on to the surface of another metal by a simple electrolysis of an aqueous solution containing the desired metal ion or its complex with a driving force of external electric power. For fuel cell application, there were several approaches of electrochemical deposition technique for the synthesis of nano-sized electro-catalysts [85-87]. On the other hand, electroless deposition is a method of obtaining desired nano-sized catalyst particles by chemically reducing the metal ion or its complex on to either conducting or non-conducting substrates in a controlled fashion [84]. Table 1 compares the nature of reactions occurring in these two processes. The two processes distinctly differ in their reduction approaches. In the electrochemical method, reduction takes place by supplying

current externally and the sites for the anodic and cathodic reactions are separate. For the electroless deposition method, electrons required for the reduction are supplied by a reducing agent and the anodic/cathodic reactions are on the inseparable work piece. Moreover these reactions proceed only on the catalytically active surface and they are applicable for all platinum group metals (PGM) since all PGMs are catalytically active [84]. Since electroless deposition method is more efficient to control particle size, shape, and support materials, it has been widely used for the synthesis of Pt/C catalysts for fuel cell application [10, 88, 89].

Several methods in electroless deposition have been used to prepare Pt-based catalyst; however, the following two synthesis methods are widely used – impregnation method, and colloidal method. Impregnation method is a simple and the most widely used straightforward chemical preparation technique. In this method, Pt precursors are mixed with a carbon powders in aqueous or organic solution (toluene, ethanol, octyl ether, benzyl ether, acetone) to form a homogeneous mixture followed by heat treatment under a reducing gas (e.g., 5% hydrogen balanced with nitrogen) [90-96]. Alternatively, the mixture is reduced by a chemical reduction in the presence of a suitable reducing agent, such as $NaBH_4$ [97], formic acid [98, 99], formaldehyde [100], borane tert-butylamine [101], etc. Metal chloride and metal acetate salts are commonly used as precursors in the impregnation method due to their easy availability. The heat treatment normally produces a non-uniform composition, resulting in a decrease in the activity. So, the chemical reduction method is preferentially used for the reduction of Pt ion in the liquid phase. Even with chemical reduction method, however, many studies have shown

the difficulty of high metal loadings (which are essential for fuel cell applications) without a significant increase in the Pt particle size [102, 103].

The colloidal method is another extensively used preparation route for the Pt-based catalysts. This method consists of three steps: preparation of the Pt-metal colloids, deposition of the colloids onto the carbon supports, and chemical reduction of the suspension. The colloidal method can be further optimized by using new precursors, reducing agents, stabilizers, solvents, and synthetic procedures [104-106]. In spite of the complexity of the synthesis route, the colloidal method can be an effective method for Pt deposition on carbon supports by producing well-homogenized ultrafine Pt particles with narrow particle size distribution [107]. In the colloidal method, diverse stabilizing agents have been used to control metal particle size. Organic stabilizers such as polyvinylpyrrolidone (PVP) and the dodecyldimethyl(3-sulfopropyl)ammonium hydroxide are widely used in the preparation of metal colloids [108-110]. The stabilizing agents can help to control metal particle size, but some of them remain on the metal surface after synthesis and inhibit the catalytic activity. A typical method to remove the stabilizing agent, heat treatment, results in sintering of metal nano particles which leads to a decrease in the catalytic activity.

In this aspect, polyol process which is one of colloidal reduction methods is preferred since it does not require any type of polymer stabilizer. Bock et al. studied PtRu deposition on high surface area carbon by polyol method [111]. They have shown that the size of PtRu catalyst particles can be varied in the range of 0.7-4 nm by controlling the solution pH. Also, they suggested the mechanism of polyol method in which the formation of the particles involves the reduction of Pt and Ru precursor salts by receiving

electrons from the oxidation of the solvent, ethylene glycol. The glycolic anion which was produced from the oxidation of ethylene glycol acts as a stabilizer for the PtRu colloids, and hence the resulting PtRu particle size is controlled. In another research, the same authors reported that organic materials from a synthesis of polyol method can be removed at relatively low temperature (160 °C) which avoids Pt particle sintering problem [112]. Oh et al. investigated the parameters involved in Pt/C catalyst synthesis using polyol method [113]. The authors also found that initial pH of the reaction mixture is a key factor in controlling the particle size of Pt. Furthermore, they observed a severe reduction in the metal loading with increasing solution pH due to the electrostatic stabilization between Pt particles and carbon supports as confirmed by the zeta potential study. The zeta potential of the carbon support decreased from positive to negative values with increasing solution pH while that of the Pt particles remained constant at a negative charge after pH 6 which results in poor adsorption of Pt particles on the carbon supports. They further optimized the polyol method to improve the product yield and found out final adjustment of pH is an important factor for high yield of the process [114]. It is shown that the surface charge on the carbon supports becomes more electropositive when the final solution pH is changed from alkaline to acidic by monitoring the zeta potential. The yield from the pH adjustment step is 14% higher (96% product yield) than that in the absence of the step (82% product yield). Other studies show that polyol process can be optimized further with the microwave-assisted process [115-124], stabilizing agent [108, 119, 123, 125], and post heat-treatment [126].

1.2.3 Stability of Pt-based catalysts

It is well-known that Pt nanoparticle catalyst on carbon support is one of the best catalysts for PEMFC application. At the same time, nanoparticles inherently show a strong tendency to agglomerate due to their high specific surface energy [39, 127, 128]. For nanoparticles, the smaller the size, the higher the specific surface area, and the easier to agglomerate/sinter [127]. When Pt nanoparticles agglomerate to bigger ones, the ECSA of Pt catalysts decreases and the performance of PEMFC degrades consequently. Additionally, it can be accelerated under the extremely harsh condition of PEMFC. For the cathode, the catalysts are under strongly oxidizing conditions: high oxygen concentration, high potential (>0.6 V vs. SHE, and sometimes >1.2 V for short periods of time [129]). An increase of cathode potential results in the formation of surface oxides of Pt which not only decreases the Pt activity towards ORR but also accelerates the degradation of Pt catalysts. Also, PEMFCs are operated under the condition of low pH (<1), high temperature (80 °C or above), and with significant levels of water in both vapor and liquid phase which increase Pt degradation rate [21].

It is reported that the performance degradation of PEMFC is largely due to the ECSA loss of the cathode catalysts and the decrease in ECSA mainly results from the increase of Pt or Pt-M alloy nanoparticle size, the dissolution of Pt and/or other alloyed metals, and the detachment of Pt and/or Pt-M alloy nanoparticles from the carbon support [130, 131]. As to the increase in Pt nanoparticle size, there are several fundamentally different pathways [27, 49, 132, 133]: (i) Pt dissolution and re-deposition, which is also called “Ostwald ripening” [134, 135], (ii) the coalescence of Pt nanoparticles via Pt nanocrystallite migration on the carbon support [136, 137], (iii) the transport of Pt atoms

on the carbon support, so-called “2D Ostwald ripening” as compared with the case of (i), which is also called “3D Ostwald ripening.” But so far, there is still no agreement on the respective contribution of the above pathways to the total decrease in the ECSA [127].

It has been observed that operating conditions have a great influence on the degradation of Pt-based catalysts, which include the electrode potential, constant potential or potential cycling, the temperature, the humidity, etc. [138, 139]. Wang et al. reported that Pt dissolving rate in acidic solution increases with increasing potentials from 0.65 to 1.1 V vs. SHE under potentiostatic conditions, and above 1.1 V, the dissolution rate decreases which is attributed to the formation of a protective Pt-oxide film [140]. Also, they observed that cycling the potential between the oxide formation and reduction regions leads to higher dissolution rates than potential holding in the oxide formation region, with the latter being three to four orders of magnitude lower than the former. This is because, once the oxide are reduced by the negative potential sweep, Pt^{Z+} ions are formed and dissolved in the electrolyte and accelerated corrosion takes place [141-143]. The humidity is another important parameter that affects the degradation of Pt-based catalysts. For example, Pt surface area loss is largely mitigated by operating the cell at 25% RH as compared to 100% RH [144]. In another study, the degree of Pt oxidation on PEMFC cathode increased significantly with an increase in RH from 20 to 72% [145]. It has also been shown that the growth of Pt particles is accelerated in the presence of a liquid environment, which is attributed to the lowered activation energy of particle growth [146, 147]. The degradation of catalysts is also a function of temperature. Catalyst coarsening rates exhibited a linear increase with temperature [138]. In the experiment of Pt dissolution at a certain potential, it is estimated that the Pt^{2+} equilibrium

concentration on acidic solution at 0.9 V increases by two orders of magnitude from 25 to 80 °C and an additional order of magnitude from 80 to 120 °C.

To investigate the kinetics of Pt dissolution relevant to PEMFCs, a mathematical model has been developed by Darling and Meyers [139]. They showed that Pt dissolution is negligible at low and high potentials but is large at intermediate potentials. In their kinetic model, they explained the effect of potential in the following way, by considering three possible reactions:

$$Pt \rightarrow Pt^{2+} + 2e^{-} \ (Pt\ dissolution) \tag{5}$$

$$Pt + H_2O \rightarrow PtO + 2H^{+} + 2e^{-} \ (Pt\ oxide\ film\ formation) \tag{6}$$

$$PtO + 2H^{+} \rightarrow Pt^{2+} + H_2O \ (chemical\ dissolution\ of\ Pt\ oxide) \tag{7}$$

The model and experimental data indicated that at lower potentials (i.e. under the conditions of normal H_2/air fuel cell operation), the solubility of Pt in acid is quite low. At higher potential and on exposure to air to form PtO, the oxide layer effectively protects the Pt particles from dissolution. At intermediate potentials, however, the uncovered surface is prone to high rates of Pt dissolution.

The investigation of the stability of Pt-based catalyst in real time fame is time-consuming and inefficient since the life requirement for PEMFC is >5000 h for transportation and >40000 h for stationary applications [42]. Therefore, the so-called accelerated degradation test (ADT) is developed including thermal degradation under hot air conditions [129, 148], OCV operation [149], and electrochemically forced aging under simulated cell operating conditions [25, 26, 39, 43]. Between these methods,

electrochemically forced aging method is widely used due to the similarity of the real PEMFC operating conditions. Usually, a constant potential in the range of cathode potential in a working PEMFC or a potential cycling in the potential region between the oxidation and reduction of Pt is applied to the cathode. Among all the above methods, Gasteiger and co-workers proposed the catalyst voltage cycling test method as a reliable and efficient screening tool for fuel cell catalyst development [44, 144]. At the same manner, Fuel Cell Technical Team (FCTT) and Department of Energy (DOE) suggested triangle potential sweep cycles from 0.6 to 1.0 V for catalyst stability test [150].

1.3 Objectives and outline

The objective of this work is to develop a cathode catalyst with high fuel cell performance under H_2/air (power density), optimized mass activity, good support stability and good catalyst stability for transportation applications. To achieve this objective, support material, Pt catalyst, and compressive Pt catalyst were studied and optimized. The specific objectives are (i) Development of activated carbon composite support (ACCS) having desired stability, hydrophilic/hydrophobic property, BET surface area, pore-size distribution. (ii) Modification of the surface of ACCS to facilitate uniform Pt deposition. (iii) Studying Pt/ACCS catalysts in PEM fuel cells with 25 cm^2 MEAs and evaluating the support stability for Pt/ACCCS catalyst under potential cycling conditions (1.0-1.5 V, 5000 cycles) by measuring the cell potential loss and to compare the results with the stability of commercial Pt/C catalyst deposited on high surface area carbon. (iii) Development of compressive Pt catalyst on ACCS support to further improve catalyst stability under 0.6-1.0 V cycling by optimizing synthesis parameter including Pt/Co ratio, annealing temperature, protective layer coating, etc.

To the best of our knowledge, very limited reports are available on the support stability and catalyst stability performance of cathode catalyst under fuel cell condition by testing MEAs. These studies are important for the development of cathode catalysts for automotive applications since it could mimic the fuel cell stack situation effectively. Therefore, the overall objectives of the present study are (i) to develop active and stable cathode catalyst for PEMFC, (ii) to study their support stability using a 1.0-1.5 V potential cycling experiment, and (iii) to study their catalyst stability using a 0.6-1.0 V potential cycling experiment by comparing the ORR activity under fuel cell operating conditions with 25 cm^2 MEA.

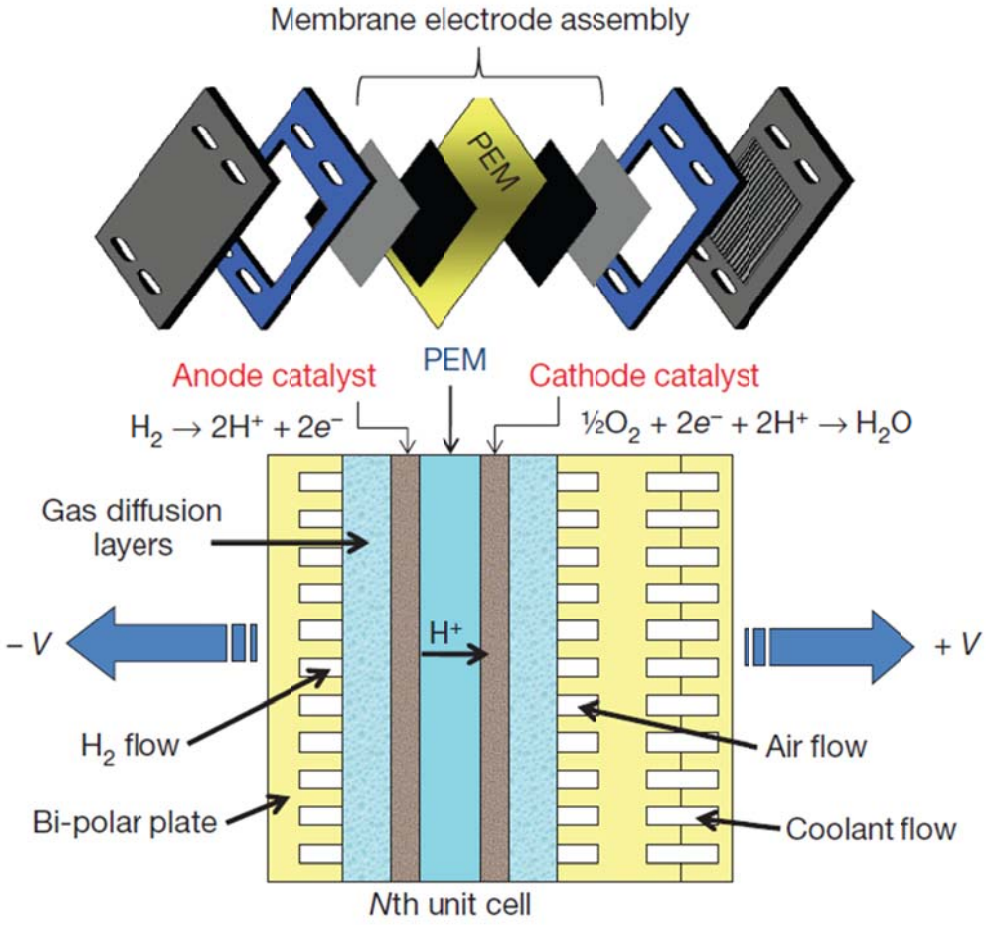

Figure 1.1 PEMFC components. Unit cell cross section of the Nth unit cell in a fuel cell stack, showing the components of an expanded MEA [8].

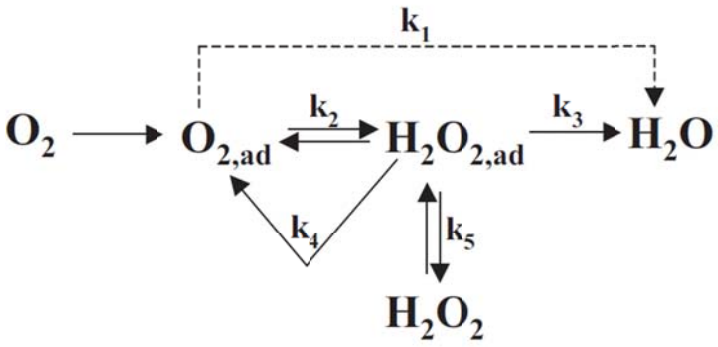

Figure 1.2 Schematic presentation of ORR pathway [11].

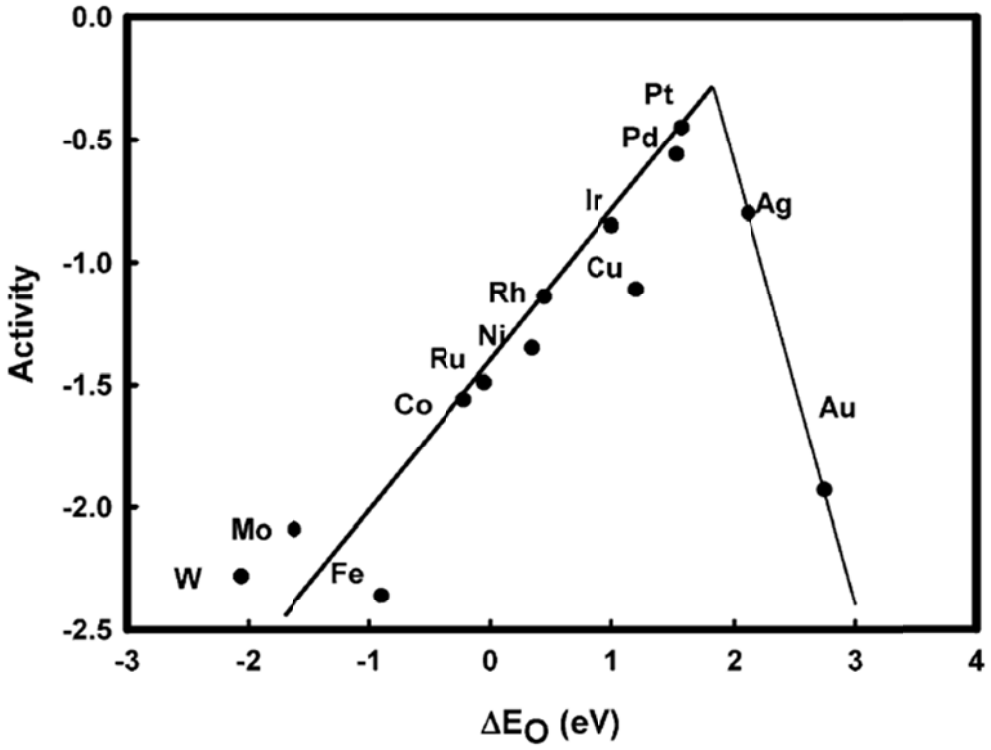

Figure 1.3 Calculated trends in oxygen reduction activity plotted as a function of the O binding energy [13].

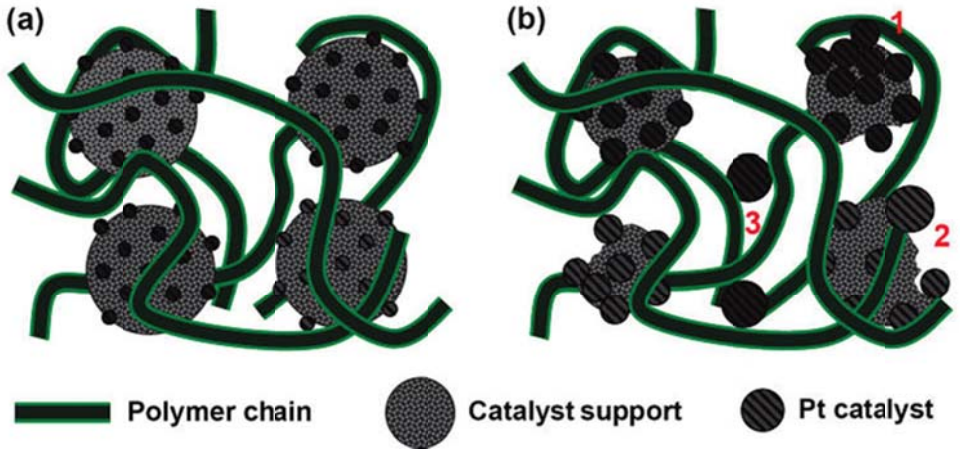

Figure 1.4 Schematic representation of the effect of carbon corrosion on (1) agglomeration, (2) coalescence, and (3) loss of Pt particles during operation of PEMFCs: (a) normal (corrosion-resistant) electrode and (b) corroded electrode [41].

Table 1.1 Nature of reactions and their sites occurring in electrochemical and electroless depositions [84].

Property	Electrochemical deposition	Electroless (chemical) deposition
Driving force	External power supply	Reducing agent [RA] and auto-catalytic property of the deposited metal
Cathode reaction	$M^{n+} + ne^{-} \rightarrow M$	$M^{n+} + RA \rightarrow M$
Anodic reaction	$M - ne^{-} \rightarrow M^{n+}$	$RA - ne^{-} \rightarrow [RA]_{Oxidized\ form}$
Overall reaction	$M_{anode} \rightarrow M_{cathode}$	$M^{n+} + RA \rightarrow M + [RA]_{Oxidized\ form}$
Anodic site	Anode itself	Work piece
Cathodic site	Work piece	Work piece

CHAPTER 2

STUDY OF THE CARBON COMPOSITE CATALYST (CCC) AS A SUPPORT MATERIAL FOR CATHODE CATALYSTS SYNTHESIZED FROM A HIGH SURFACE AREA CARBON BLACK (HSACB)

2.1 Introduction

To achieve high power in PEMFCs, the catalyst layer should be relatively thin to minimize losses from the rate of proton diffusion and the rate of mass transfer of reactants (H_2 and O_2/air) and product (H_2O) within the electrode. To minimize the thickness of the catalyst layer, the Pt loading on carbon must be significantly high (~30 wt. % or higher) compared with the one for normal commercial supported Pt catalysts which are typically less than 5 wt. % [151]. For the synthesis of high Pt loading Pt/C catalysts, high surface area carbon black (HSACB) is the most widely used support material due to large surface area for Pt deposition, well-defined pore structure, and high electrical conductivity [4, 7]. While the Pt catalyst dispersed on HSACB has been shown high power density in many studies, the stability of this catalyst is not satisfactory for automotive PEMFC application, especially for cathode catalysts [40-42]. To improve the stability of support, a modification of HSACB must be considered.

The carbon composite catalyst (CCC) obtained from HSACB could be one of the promising support materials for Pt/C cathode catalyst for PEMFCs. The researchers at the University of South Carolina, has developed CCC as a non-precious cathode catalyst for

PEMFCs [7, 152-159]. It is obtained by the surface modification of HSACB through pyrolysis in the presence of a Co-chelate complex. There are two advantages of CCCs as a cathode catalyst support material: (i) high ORR activity which is similar to that of Pt and (ii) increase of graphitization of carbon through metal-catalyzed pyrolysis. When CCC is used as a support material for Pt cathode catalyst, the ORR activity of CCC can also contribute to the overall ORR activity of Pt/C catalyst. Furthermore, more graphitized carbon structure of CCC can enhance the carbon support stability compared with the pristine HSACB.

The objective of the work in this chapter is to investigate the feasibility of CCC obtained from a commercial HSACB as a support material for cathode catalyst and study the electrochemical characteristics and stability in PEMFCs.

2.2 Experimental

2.2.1 Synthesis of CCC from HSACB

A methodology for CCC has been developed at University of South Carolina and reported in our previous studies [7, 152-159]. The CCC was synthesized from HSACB - Ketjenblack EC-300J. In brief, the as-received HSACB was refluxed in a concentrated HNO_3 solution at 80 °C to introduce oxygen functional groups onto the carbon surface. Then, the oxidized carbons were subjected to a metal-catalyzed pyrolysis process in the presence of transition metals, such as Co, and nitrogen-containing organic compounds, ethylenediamine (EDA), to introduce pyridinic-nitrogen ORR active sites by pyrolysis at different temperatures (800–1500 °C) under N_2 atmosphere. Then, the resulting products were leached in 0.5 M H_2SO_4 to remove excess metals on the surface. Finally, the products were heat treated again using the same temperatures used before.

2.2.2 Material characterization studies

The physical properties of CCCs were studied using a variety of physical characterization techniques such as X-ray diffraction (XRD), Raman spectroscopy, Brunauer-Emmett-Teller (BET) surface area analysis, inductively coupled plasma-atomic emission spectroscopy (ICP-AES) analysis, and high resolution transmission electron microscopy (HRTEM). XRD patterns were recorded using Rigaku 405S5 to identify the crystalline structure of the synthesized CCCs. Raman spectroscopy (HORIBA "LABRAM 1B" with He-Ne 20mW laser, wave length 632.817 nm) was used to evaluate the degree of graphitization of the carbon supports. BET (Quantachrome) was used to determine the surface area and pore-size distribution of the CCCs. ICP-AES (Perkin Elmer) analysis was used to determine the composition CCCs. HRTEM (Hitachi H9500) was used to determine the surface structure of CCCs.

2.2.3 Electrochemical characterization studies

Electrochemical RRDE characterization studies were performed in 0.1 M $HClO_4$ using a Pine bipotentiostat (Model AFCBP1), a Pt-mesh counter electrode, and an Ag/AgCl reference electrode (0.254 V vs. RHE). RRDE with a Pt-ring and a glassy carbon disk (0.248 cm^2) was used as the working electrode. The catalyst ink was prepared by blending the catalyst powder (CCCs) with a 5% solution of Nafion® and isopropanol in an ultrasonic bath. Appropriate quantities of the catalyst inks were deposited on the glassy carbon disk using a micropipette to achieve loadings of 100 μg cm^{-2} of CCCs.

2.3 Results and discussion

2.3.1 Roles of ethylenediamine and cobalt on CCC synthesis

To study roles of Co and nitrogen-containing organic compounds on CCC synthesis, three samples with different combinations of the reactants are prepared and evaluated. EDA was used as a nitrogen-containing organic compound in this study. Sample 1 is prepared using HSACB and Co source without EDA. 0.48 g of $Co(NO_3)_2$ $6H_2O$ was dissolved in 200 ml of IPA and 0.4 g of oxidized HSACB was added to the suspension. The suspension was refluxed at 80 °C for 3 h while continuous stirring. The solvent was removed by rotary evaporator (Buchi, Rotavapor R-210 and B-491) write the other details) followed by drying at 80 °C in a vacuum oven. The collected powder was heat-treated at 800 °C for 1 h with 5 °C/min ramping time under N_2 atmosphere. Finally, the product was acid leached in 0.5 M H_2SO_4 at 80 °C for 2 h. Sample 2 is prepared using only EDA and Co source without HSACB support in the same manner as sample 1 preparation. Sample 3 is prepared using all three reactants namely, HSACB, Co source, and EDA which is a typical CCC synthesis procedure [7, 152-159]. Figure 2.1 shows XRD patterns of HSACB and the three samples prepared using the method described above. Sample 1 shows almost identical XRD pattern with the one of pristine HSACB which indicates that no Co inclusion in the sample and negligible structural change. On the other hand, sample 2 shows similar XRD pattern with the one of CCC-800 °C which indicates Co presence in the sample. Similar observation is also confirmed by HRTEM shown in Figure 2.2. The HRTEM image for sample 1 (Figure 2.2 (b)) shows no Co particles in the carbon similar with pristine HSACB (Figure 2.2 (a)). However, the HRTEM image for sample 2 (Figure 2.2 (c)) shows Co particles in the sample same as

CCC-800 °C sample (Figure 2.2 (d)). This result is attributed to the formation of Co-chelate complex by Co and nitrogen nitrogen-containing organic compounds [160]. When Co and EDA formed Co-chelate complex, thin layers of carbon evolved from EDA encapsulated the Co particles during pyrolysis. In the case of sample 1, no Co-chelate complex was formed due to the absence of EDA resulting in bare Co particles that cannot be protected by carbon layers from EDA and dissolved completely during the acid leaching step.

2.3.2 Electrochemical characterization of CCC

Comparison of ORR kinetics of HSACB and CCC-800 °C are shown in Figure 2.3. The HSACB shows no activity in terms of onset potential for ORR and diffusion current when compared to CCC-800 °C which shows onset potentials of ~0.86 V vs. RHE and well-defined kinetic and mass-transfer regions in 0.1 M $HClO_4$ electrolyte at room temperature. Koutecky–Levich analysis resulted in slopes close to that for the theoretical four-electron transfer reaction with a calculated number of transferred electrons of about 3.6 for CCC-800 °C. The RRDE studies also indicated that the H_2O_2 production on CCCS-800 °C is 2.5% (Figure 2.4). The formation of H_2O_2 is detrimental to the Nafion® membrane and the ionomer in PEM fuel cells [161]. Studies carried out by Sethuraman et al. [162] and Stamenkovic et al. [163] correlate the % H_2O_2 production to the number of electrons transferred during ORR in acid electrolytes. Stamenkovic et al. [163] reported that the kinetics/reaction pathways of the oxygen reduction reaction on Pt-poly and Pt (110) are almost identical, i.e., the 4 e^- reduction (with ca. 5-10% of H_2O_2 production at 0.1 V) is operative on Pt-poly in acid solutions. Since the H_2O_2 production is less than 5% on CCC-800 °C, the ORR kinetics follows the 4 e^- reduction pathways

and is similar to that on Pt catalysts. Similar results have been reported in our previous studies for various non-precious metal catalysts [7, 152-159]. Our previous studies on various non-precious metal catalysts showed that high-temperature pyrolysis produces pyridinic and graphitic-type nitrogen on the surface of CCC and the pyridinic-nitrogen group act as catalytic sites for ORR. Maldonado et al. [164] have reported that a strong Lewis basicity of such nitrogen-modified sites facilitates the reductive adsorption of oxygen without the irreversible formation of oxygen functionalities, due to an increase in the electron-donor property of carbon. The surface analysis using X-ray photoelectron spectroscopy (XPS) did not show the presence of Co and indicated the presence of only carbon, nitrogen, and oxygen on the CCC surface. It is important to note that Co is present only in the bulk as indicated by the ICP-AES analysis. The Co content determined using ICP-AES indicates that approximately a half the amount of Co in the CCC-800 °C is removed within the first 0.5 h and stays the same (~10 wt. % Co) even after 8 h leaching in 0.5 M H_2SO_4 (Figure 2.5). The result shows that ~10 wt. % Co is on the surface of carbon which is easy to be removed by the acid leaching and another ~10 wt. % of Co is encapsulated by the graphitic carbon layers protecting it during acid leaching. This is also confirmed by the HRTEM image of CCC-800 °C which shows a significant amount of Co particles after acid leaching step (Figure 2.2 (d)). Thus, the ORR catalytic activity of CCC is due to the presence of pyridinic-nitrogen groups and an addition of Co for metal-catalyzed pyrolysis helps (i) the inclusion of nitrogen into the CCC and (ii) the formation of graphitic carbon structure during pyrolysis [7, 152-159].

2.3.3 Effect of pyrolysis temperature on CCC synthesis

The XRD patterns of CCC synthesized at heat treatment temperatures between 800 and 1500 °C are shown in Figure 2.6. It is observed that the degree of graphitization increases with an increase in the pyrolysis temperature by analyzing the C (002) peaks of the XRD patterns of different CCCs. It has been reported that higher value of the crystallite thickness (L_c) calculated by Scherrer's formula and lower value of the interlayer spacing (d_{002}) obtained from Bragg's law imply higher degree of graphitization [34, 165]. Also, lower value of the ratio between the D and G peaks (I_D/I_G) obtained from Raman spectroscopy indicates a higher degree of graphitization [67, 166]. The Raman spectroscopy results for CCCs with different heat treatment temperature are shown in Figure 2.7. The L_c value increased and both d_{002} and the I_D/I_G ratio decreased as a function of pyrolysis temperature indicating the increased degree of graphitization of CCCs. As shown in Table 2.1, BET analysis of various carbon supports indicated surface area values of 800, 411, 380, 255, 241, 189, and 158 $m^2\ g^{-1}$ for HSACB, CCC-800 °C, CCC-900 °C, CCC-1000 °C CCC-1100 °C, CCC-1300 °C, and CCC-1500 °C, respectively. The BET surface area decreased for different CCCs as the heat treatment temperature increased due to the removal of micropores and formation of graphitized carbons. The HRTEM images which are shown in Figure 2.8 for various CCCs also confirm the increase of a degree of graphitization with the increase in heat-treatment temperatures. While the starting material, HSACB, is amorphous in nature, the CCCs show graphitic carbon tubes and carbon fiber structure formation during metal-catalyzed pyrolysis. It is observed that carbon nanostructures are formed even in the case of CCC-800 °C (Figure 2.8 (c)). As heat treatment temperature increased, more carbon

nanostructures are observed and CCC-1500 °C (Figure 2.8 (h)) shows the bulk of complete carbon nanostructures. In addition, Co particles are observed in the case of CCC-800 °C (Figure 2.8 (c)) and CCC-900 °C (Figure 2.8 (d)). The Co particles are well distributed with the particle size in the range of 5-15 nm for CCC-800 °C. For CCC-900 °C, Co particle size is increased to ~20 nm and the number of particles is significantly decreased. Above 1000 °C, no Co particles are observed in the HRTEM images. To figure out the Co concentration in CCCs, ICP-AES analysis was performed. It shows that 10.7 wt. % of Co for CCC-800 °C, 4.5 wt. % of Co for CCC-900 °C, and less than 1 wt. % of Co for CCCs heat-treated above 1000 °C. The difference in Co content in the CCCs is attributed to the protection of Co particles by carbon layers from EDA during pyrolysis. At 800 °C, the carbon formed from EDA can successfully encapsulate the Co particles to protect them from acid leaching. However, the carbon protecting layer is decomposed at temperatures > 1000 °C and most of the Co particles are exposed to acid during leaching. The results of XRD, Raman, BET, and ICP-AES analysis are summarized in Table 2.1.

2.3.4 Electrochemical stability of CCC

To investigate the electrochemical stability of CCCs, potential cycling test was conducted (Figure 2.9) using an RRDE in a three-electrode electrochemical cell. The HSACB, oxidized HSACB, and CCCs were dispersed on a glassy carbon electrode and cycled between 0.05 to 1.20 V vs. RHE for 500 times in 0.1 M $HClO_4$ solution purged with N_2. The oxidized HSACB (Figure 2.9 (b)) shows increase of quinone-hydroquinone peaks (~0.6 V vs. RHE) and double layer capacitance currents when compared with pristine HSACB (Figure 2.9 (a)) due to surface oxygen group formation during HNO_3

acid treatment [167]. Usually, double layer capacitance depends on the surface area of carbons [168]. In this case, however, the pristine HSACB which has higher BET surface area (800 m^2 g^{-1}), shows relatively small double layer capacitance current since it contains relatively small amount of surface oxygen group. In the case of CCCs, as heat treatment temperature increased, double layer capacitance currents were decreased by combined effects of (i) decrease of BET surface area and (ii) decrease of surface oxygen group due to high temperature heat treatment. After 500 cycles, HSACB shows the highest increase of double layer capacitance current which could be translated by the increase of surface oxygen group and the increase of surface roughness due to electrochemical carbon corrosion. The CCCs show relatively small change in double layer capacitance current after cycling test compared with the one of HSACB. The increase of temperature decreased the change of double layer capacitance after cycling test due to higher degree of graphitization and smaller BET surface area of CCCs. According to the results, we could conclude that high temperature treated CCC has high electrochemical stability at high potentials.

2.4 Conclusion

The CCC was synthesized by the modification of HSACB through heat treatment in the presence of Co-chelate complex. The carbon atoms from EDA had an important role on CCC synthesis which kept the Co particles in the CCC structure by protecting them with thin carbon layers through Co-chelate complex formation followed by graphitic carbon layer formation during pyrolysis. Also, Co-chelate complex introduced nitrogen groups on the surface of CCC during pyrolysis resulting in increased ORR activity. The Co source used for the synthesis helped the graphitization of CCC at

relatively low temperature by catalyzing the graphitization process during pyrolysis. CCC-800 °C showed higher activity for ORR and the higher degree of graphitization compared with the ones of HSACB which are beneficial for a support material for PEMFC cathode catalysts. As pyrolysis temperature increased, the degree of graphitization of CCC was also increased, especially in the case of CCC-1500 °C, where complete carbon nanotube and carbon nanofiber structure formation was observed. The Co content in the CCC was studied by ICP-AES and HRTEM analysis. While a significant amount of Co (~10 wt. %) was detected in CCC-800 °C, a negligible amount of Co was found in CCCs heat treated above 1000 °C. It is because that carbon layers from Co-chelate complex successfully protected the Co particles at 800 °C, but they are decomposed at the higher temperature (> 1000 °C) and resulted in Co loss during acid leaching step. For potential cycling test, CCCs showed enhanced electrochemical stability compared with the pristine HSACB. The increase of pyrolysis temperature increased the electrochemical stability by enhancing the graphitization of CCC and reducing BET surface area. Due to the high activity and stability, CCCs could be suggested as a promising support material for Pt/C cathode catalyst for PEMFCs.

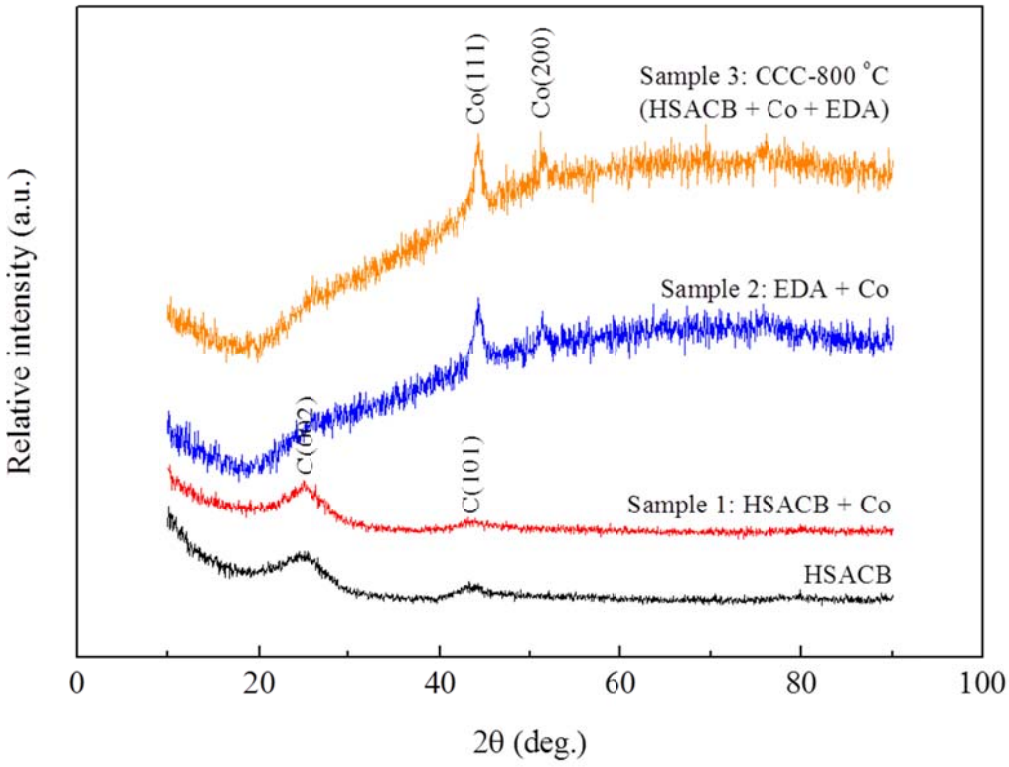

Figure 2.1 XRD patterns of HSACB and CCC samples prepared with differenet combinations of reactants.

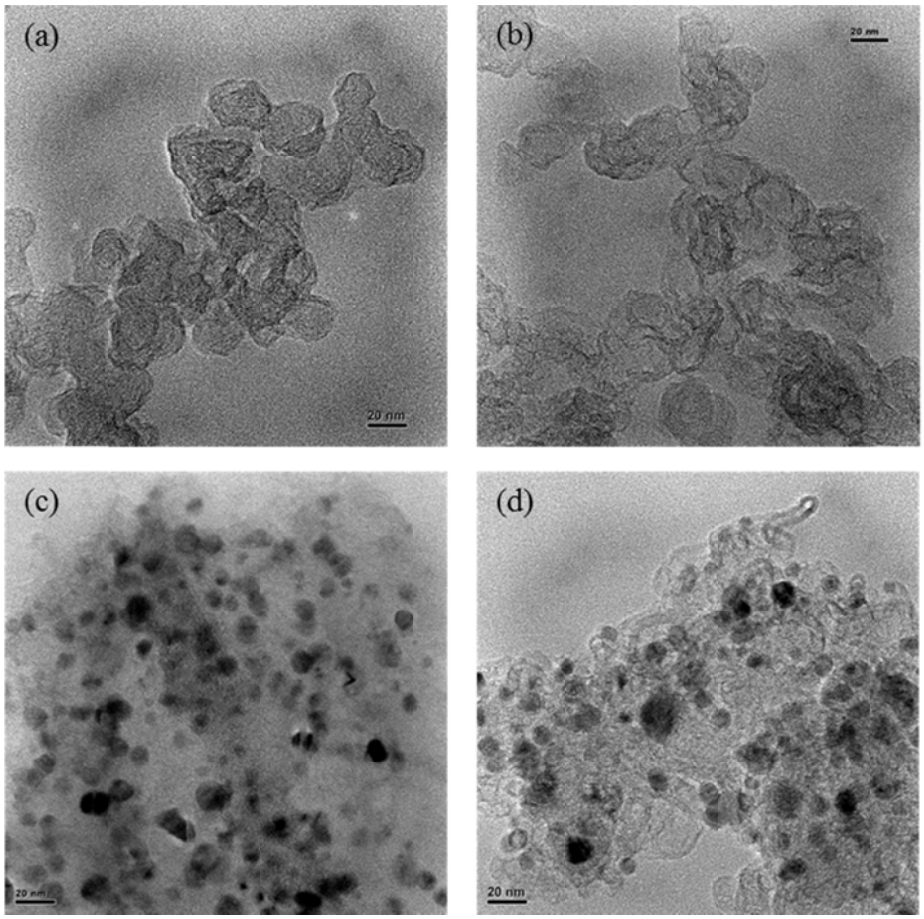

Figure 2.2 HRTEM images of HSACB and CCC samples prepared with different combination of reactants. (a) HSACB, (b) Sample 1: HSACB+Co, (c) Sample 2: EDA+Co, and (d) Sample 3: CCC-800 °C (HSACB+Co+EDA).

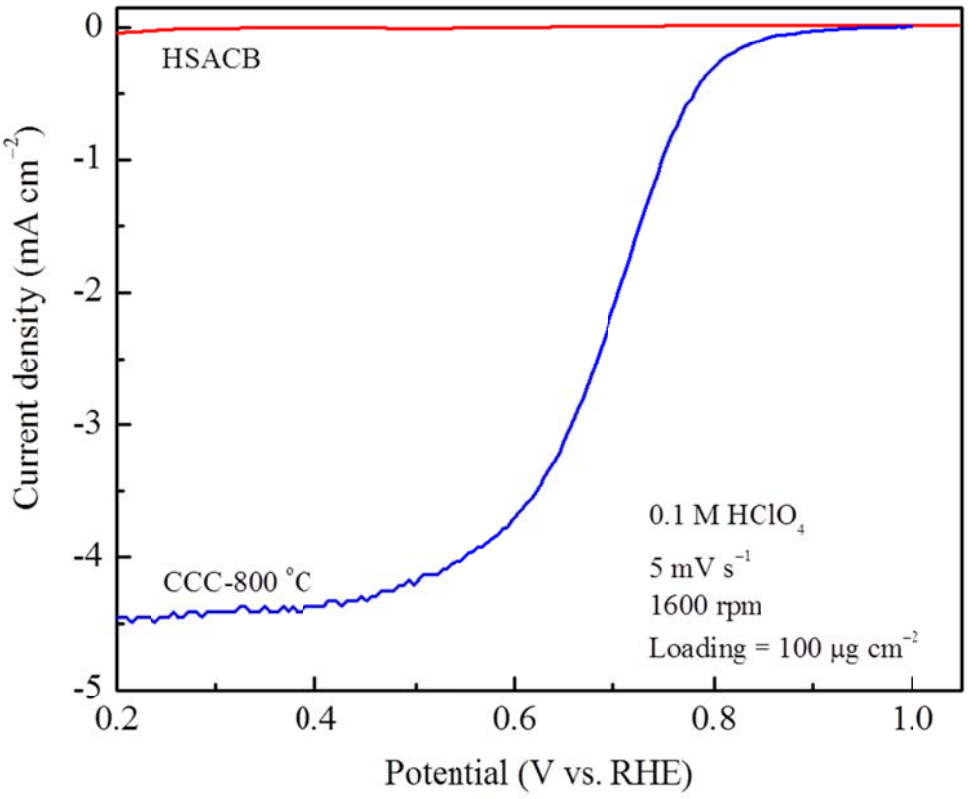

Figure 2.3 Comparison of ORR kinetics of HSACB and CCC-800 °C by linear sweep voltammetry.

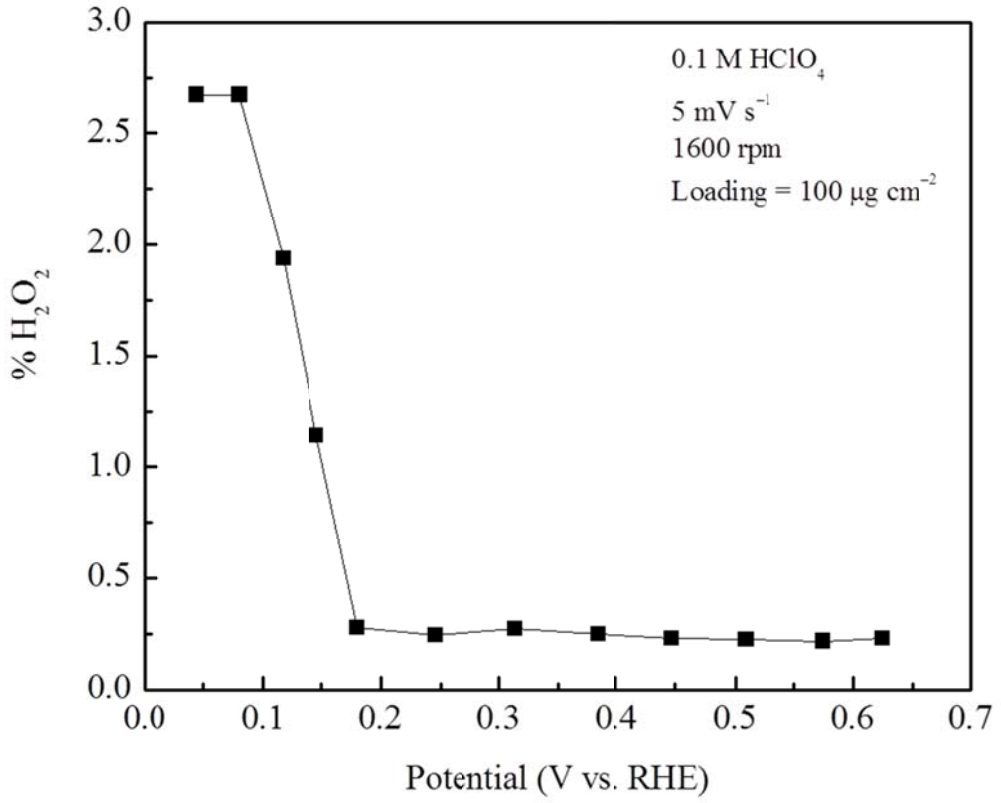

Figure 2.4 H_2O_2 production on CCC-800 °C by linear sweep voltammetry.

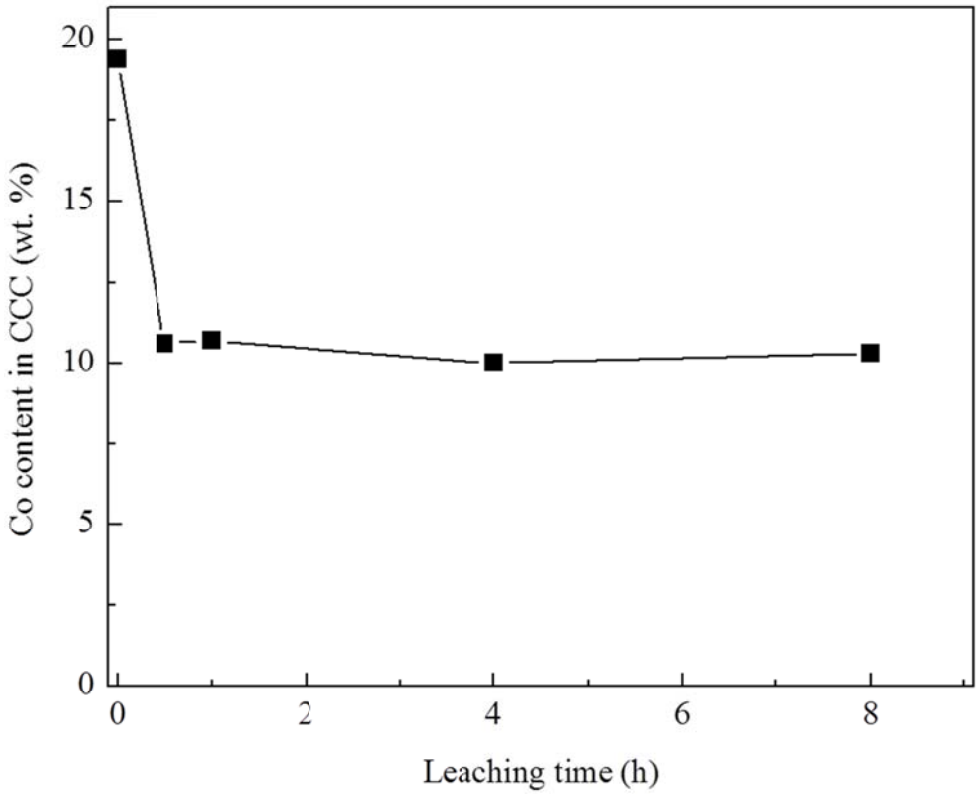

Figure 2.5 Effect of leaching time on the Co content in CCC-800 °C determined by ICP-AES.

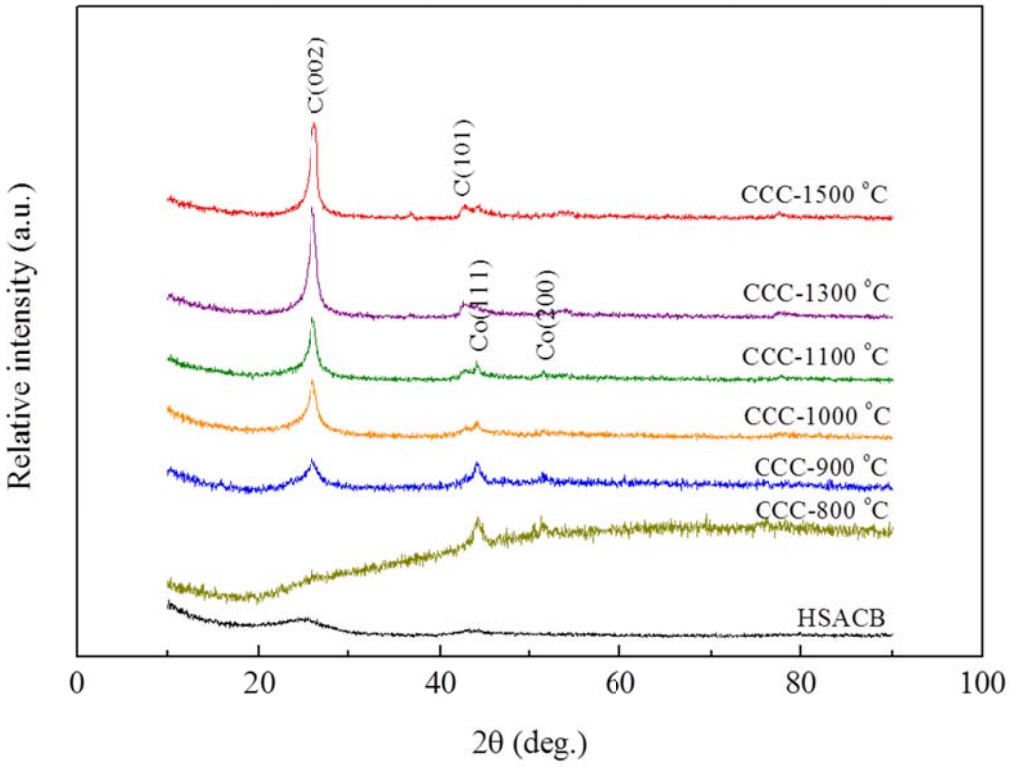

Figure 2.6 Comparison of XRD patterns of HSACB and CCCs.

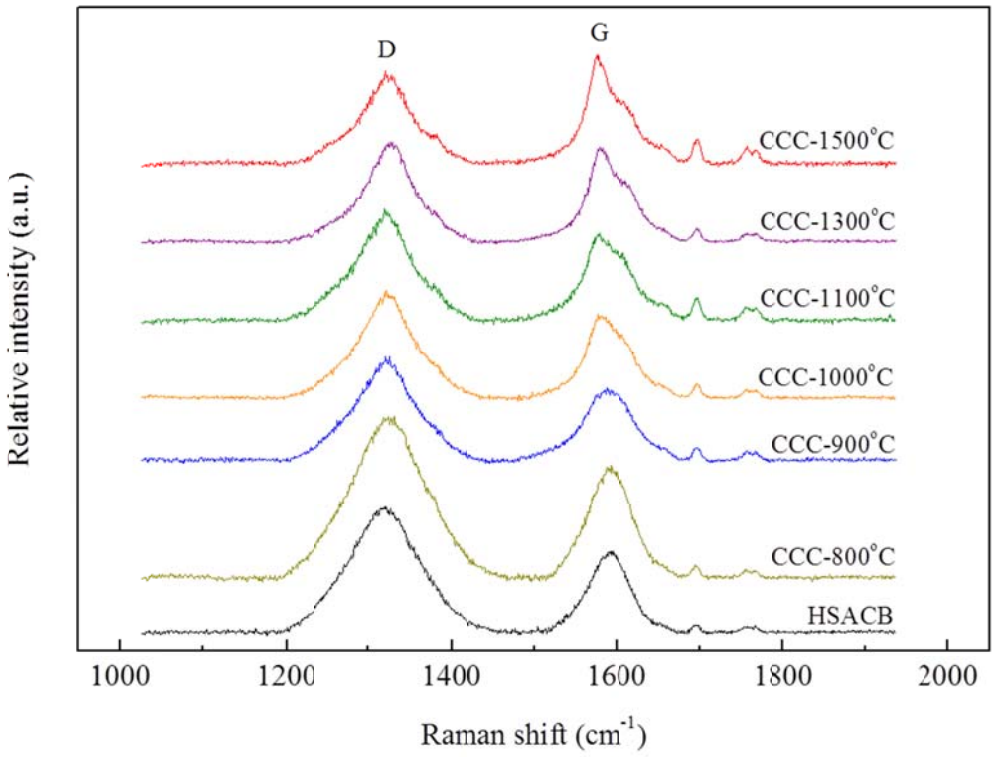

Figure 2.7 Comparison of Raman spectra of HSACB and CCCs.

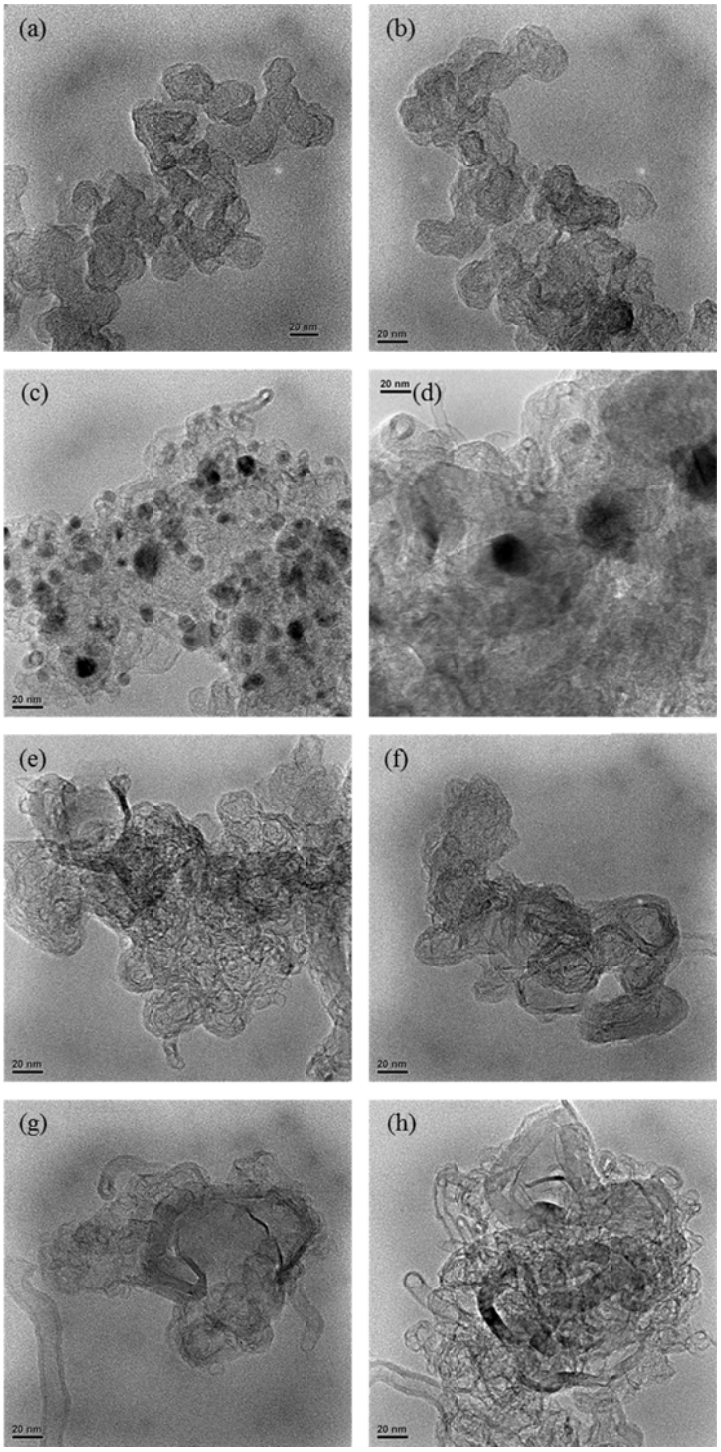

Figure 2.8 HRTEM images of (a) HSACB, (b) oxidized HSACB, (c) CCC-800 °C, (d) CCC-900 °C, (e) CCC-1000 °C, (f) CCC-1100 °C, (g) CCC-1300 °C, and (h) CCC-1500 °C. The scale bar is 20 nm.

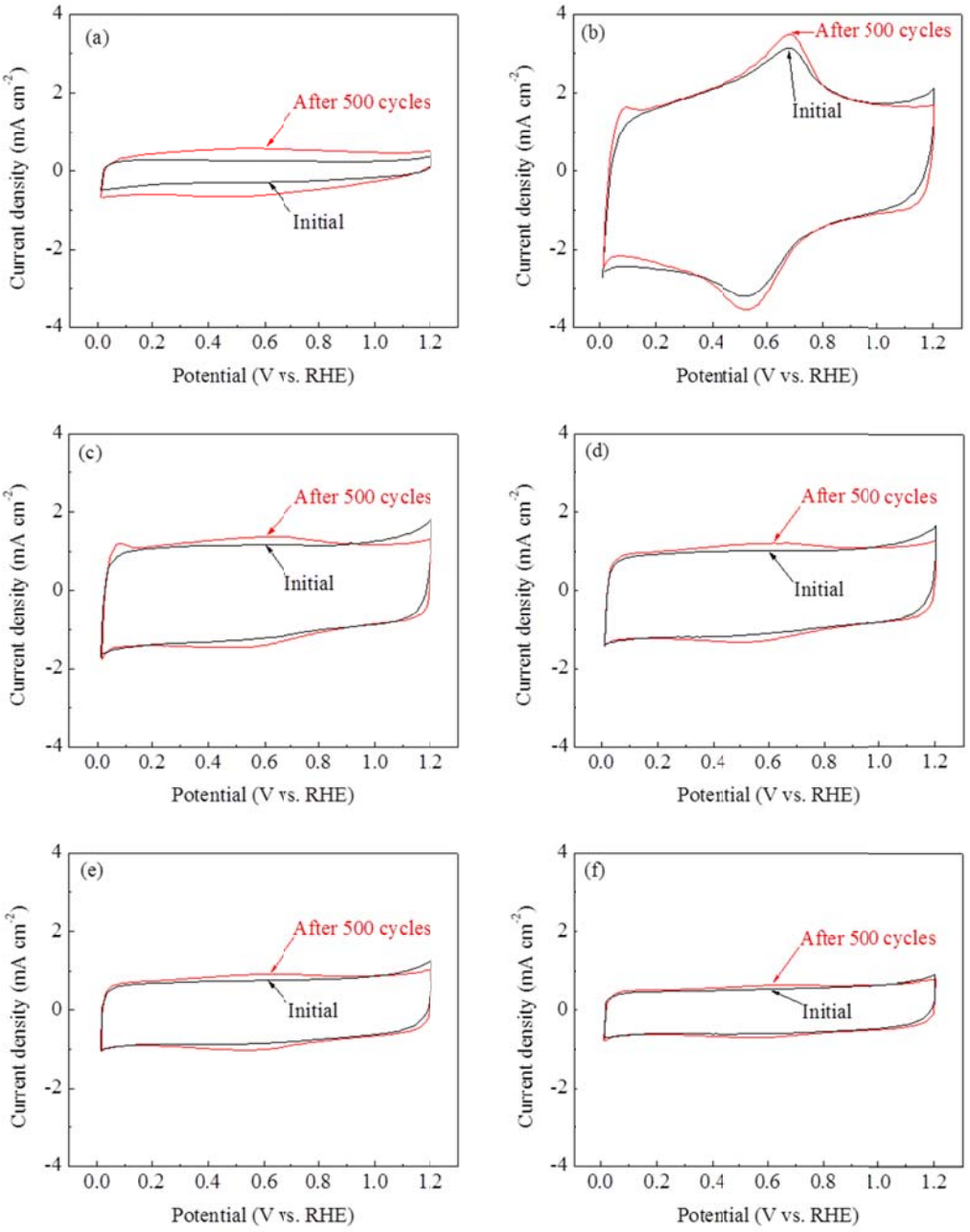

Figure 2.9 Electrochemical stability results of (a) HSACB, (b) oxidized HSACB, (c) CCC-800 °C, (d) CCC-900 °C, (e) CCC-1000 °C, and (f) CCC-1100 °C. Stability test conditions: potential cycling 0.05-1.20 V vs. RHE, 500 cycles, 0.1 M $HClO_4$ with N_2 purging.

Table 2.1 Comparison of physical properties of HSACB and CCCs.

Sample	Pyrolysis temp. (°C)	L_c (nm) (XRD)	d_{002} (nm) (XRD)	I_D/I_G (Raman)	BET surface area ($m^2\ g^{-1}$)	Co conc. (wt. %) (ICP-AES)
HSACB	-	1.1	0.3613	1.60	800	0
CCC-800 °C	800	-	-	1.50	411	10.7
CCC-900 °C	900	3.6	0.3440	1.43	380	4.5
CCC-1000 °C	1000	7.1	0.3433	1.28	255	-
CCC-1100 °C	1100	7.3	0.3431	1.25	241	0.66
CCC-1300 °C	1300	7.8	0.3430	1.07	189	0.69
CCC-1500 °C	1500	7.9	0.3416	0.83	158	0.99

CHAPTER 3

DEVELOPMENT OF Pt/CCC CATHODE CATALYST – EVALUATION OF SUPPORT STABILITY IN THE PRESENCE OF PLATINUM

3.1 Introduction

To investigate the feasibility of the CCC as a cathode catalyst support material for PEMFCs, Pt was deposited and its electrochemical activity and stability was evaluated in 25 cm^2 MEAs. In the previous chapter, the increase of graphitization and the increase of electrochemical stability of CCC by increasing the pyrolysis temperature were observed. In order to use graphitized CCC as a cathode catalyst support material for PEMFCs, it is essential to modify the CCC surface for Pt deposition since the surface of CCC has a hydrophobic character which repels Pt deposition resulting in non-uniform distribution. It is generally accepted that oxygen functional groups transform carbon surfaces from hydrophobic to hydrophilic for better Pt deposition on graphitic carbon supports. There are various methods reported in the literature to modify the carbon surface including treatment with ionic liquids [169, 170], coating with a polymer [171], and oxidative acid treatment [92, 172-178]. Among them, oxidative acid treatment is most widely used and has shown results of uniform dispersion of Pt nanoparticles and improvement of Pt content [92, 173-177]. However, it has been reported that the acid treatment destroys the carbon structure resulting in an increase of carbon corrosion and decrease of Pt/C catalyst stability [176]. To solve these problems, noncovalent functionalization of carbon

as an alternative to oxidative acid treatment has been studied recently [179-181]. Figure 3.1 shows the mechanism of noncovalent functionalization of CNFs with organic compounds like benzyl mercaptan (BM), 1-aminopyrene (AP), and 1-pyrene carboxylic acid (PCA). These materials attach to the carbon surface via nondestructive π-π stacking mechanisms (aromatic interaction) between the pyrene or phenyl moiety resulting in effective functionalization without significant damage to the carbon surface [180]. In the current study, PCA was selected for the surface modification of carbon due to its good functionalization property of graphitic carbon surface thus resulting in improved MEA performance [180]. After surface modification of the CCC, Pt was deposited using a modified polyol method.

Corrosion of HSACB in the presence of Pt is inevitable at high potentials under PEMFC operating conditions such as high oxygen concentration, high water content, and low pH which favor carbon oxidation [42, 182]. During operation, the cathodes of automotive fuel cells often experience very high potentials due to startup/shutdown cycles or due to local fuel starvation at the anode [44, 45, 48]. Reiser et al. [45] have shown that the cathode interfacial potential difference can reach as high as 1.5 V due to the H_2/air front in the anode compartment during startup/shutdown. Carbon corrosion occurs at 0.207 V vs. RHE; however, it is not detected during fuel cell operation due to its sluggish reaction kinetics [44]. In general, carbon corrosion is estimated by measuring the amount of CO_2 produced [32-35] or the corrosion current [44] at high applied potentials in a PEMFC by supplying pure H_2 to the anode and pure N_2 to the cathode. However, the measured current is always coupled with the H_2-oxidation current at the cathode due to H_2 cross-over from the anode through the Nafion® membrane [44]. In the

present investigation, the cathode is subjected to 1.2 V constant potential for 400 h to study the support stability by measuring H_2/air polarization performance, ECSA and mass activity at regular intervals.

3.2 Experimental

3.2.1 Surface modification of CCC and Pt deposition

A surface functionalization process to increase the hydrophilic property of CCC was developed using a bifunctional organic molecule containing aromatic hydrocarbon and acid groups. A surface modification process is necessary in order to obtain a uniform Pt particle size distribution on the CCC. The surface modified CCC was obtained by dispersing the CCC to the concentrated PCA solution. First, the PCA was dissolved in ethanol in a sonication bath for 3 h. After complete dissolution of PCA, the CCC was added to the PCA solution and dispersed in a sonication bath for 12 h. The resulting suspension was filtered and washed with ethanol followed by drying in the vacuum oven at 80 °C. Pt nanoparticle deposition with an initial loading of 30 wt. % was carried out using a modified polyol process to control the particle size and enhance the catalyst-support interaction. In brief, a measured amount of $PtCl_4$ was dissolved in an appropriate volume of ethylene glycol under vigorous stirring for 30 min. 0.5 M NaOH was introduced into the solution to adjust the pH. The pH of the reaction mixture was precisely controlled at every step of the process in order to obtain a uniform Pt deposition. Then, calculated amount of surface modified CCC was added to the solution so that the desired initial Pt loading was achieved in the Pt/CCC catalyst. The resulting suspension was stirred for 1 h at room temperature followed by refluxing at 160 °C for 3 h. The solution was allowed to cool down to room temperature and kept for 12 h under

continuous stirring. 0.1 M H_2SO_4 was then added to the cooled mixture and the solution pH was adjusted to 3. The mixture was kept stirred for 24 h. The Pt/CCC catalysts in the solution were filtered and thoroughly washed with de-ionized (DI) water. The resulting Pt/CCC catalysts were dried in air for 0.5 h at 160 °C and stored for further studies.

3.2.2 Material characterization studies

The physical properties of Pt/CCC catalysts were studied using a variety of physical characterization techniques such as XRD, X-ray fluorescence (XRF), HRTEM, and ICP-AES analysis. XRD patterns were recorded using Rigaku 405S5 to identify the crystalline structure of the synthesized supports and catalysts. XRF was used to confirm the Pt loading on the cathode and anode electrodes. HRTEM (Hitachi H9500) was used to determine the particle size and particle size distribution of Pt/CCC catalysts. ICP-AES (Perkin Elmer) analysis was used to determine the composition of Pt/CCC catalysts.

3.2.3 MEA fabrication and electrochemical measurements

The polarization performances of Pt/CCC catalysts were evaluated in 25 cm^2 MEAs. Commercial Pt/C (TEC10E50E, 46.7 wt. % Pt on Ketjenblack-EC300J, Tanaka Kikinzoku Kogyo K.K., Japan) catalyst was used as a cathode catalyst for Pt/HSACB catalyst since Ketjenblack-EC300J HSACB was used as a support material [162]. The same catalyst was also used as the anode catalyst in all the MEAs. The catalyst inks were prepared by blending the catalysts with a pre-calculated amount of 5% solution of Nafion® in isopropyl alcohol (Alfa Aesar) using an ultrasonic bar. The catalyst inks were directly deposited onto the Nafion® NRE 212 membrane on both cathode and anode. The cathode and anode catalyst loading was fixed at 0.1 mg_{Pt} cm^{-2} and confirmed using XRF. Commercially available carbon paper with a microporous layer (SGL 10 BC) was used as

the GDL for the cathode and anode. The catalyst-coated membrane was hot-pressed with the GDLs on both the cathode and anode side at 140 °C for 3 min using 20 kg cm^{-2} pressure to form the MEA.

Initially, the MEA was activated under a supply of H_2 and O_2 at 80 °C to the anode and cathode compartments, respectively, and the initial polarization performance curves were recorded with a flow rate of 750 ml min^{-1} and 100% RH. The catalyst mass activity was evaluated under H_2/O_2 (2.0/9.5 stoic.) at 80 °C, 100% RH, and 150 kPa_{abs} back pressure. The polarization curves were recorded under H_2/air (2.0/2.0 stoic.) at 80 °C, 50% RH and 170 kPa_{abs} back pressure. The support stability was evaluated using a potentiostatic experiment. The potential holding experiment was performed by applying 1.2 V constant potential to the cathode with respect to the anode for 400 h at a cell temperature of 80 °C. During the experiment, pure hydrogen (200 cc min^{-1}) and nitrogen (75 cc min^{-1}) having 100% RH were supplied to the anode and cathode compartments under 150kPa_{abs} back pressure, respectively. The potential loss under H_2/air, the loss of ECSA and the loss in catalyst mass activity after 400 h potential holding at 1.2 V were used as criteria to evaluate the support stability in Pt/CCC catalysts.

3.3 Results and discussion

3.3.1 Surface modification of CCC for Pt deposition

The hydrophilicity of as-synthesized CCC and surface-modified CCC is evaluated by observing the change in appearance of aqueous dispersions of CCCs. Initially, the CCC samples are uniformly dispersed in DI water using an ultrasonic bath in a glass vial. After 10 h, the as-synthesized CCC that did not undergo functionalization formed large aggregates and settled down completely at the bottom of the vial. The functionalized-

CCC remained as a stable dispersion for 60 h in aqueous media (Figure 3.2). The stability of surface functionalized CCC in water is attributed to the grafting of oxygen-containing groups onto the support surface which endows it with negative charges and provides the electrostatic stability required for a colloidal dispersion. The surface-modified CCC promotes uniform Pt deposition which is essential for achieving high catalyst utilization and stability in PEMFCs [23]. In this study, Pt/CCC-800 °C, Pt/CCC-900 °C, Pt/CCC-1100 °C, Pt/CCC-1300 °C, and Pt/CCC-1500 °C catalysts are synthesized using a modified polyol reduction process. The Pt loading was targeted at 30 wt. % for all the catalysts. The Pt deposition process parameters have been optimized to obtain uniform Pt deposition with an average Pt particle size, d_{Pt}, of 2.3-2.9 nm on various supports used in this study.

The XRD patterns of commercial Pt/C and Pt/CCC catalysts are compared in Figure 3.3. The diffraction patterns represent all the reflections corresponding to the face centered cubic (fcc) lattice of Pt for all the catalysts. The diffraction peaks appearing at 26° can be attributed to C(002) of the supports. Commercial Pt/C shows small and wide C(002) peak which indicates the amorphous character of the supporting carbon. The Pt/CCC catalysts show increased intensity and sharpness of C(002) peaks with an increase in CCC synthesis temperature indicating the increasing graphitization of CCC which is in good agreement with the results presented in Chapter 2 (Table 2.1 / Figure. 2.6 and 2.7). Table 3.1 compares the Pt particle sizes and Pt concentrations of commercial Pt/C and Pt/CCC catalysts. The Pt crystallite size was calculated using the Pt(220) peak appearing at 67.5° by Scherrer equation [183]:

$$D = \frac{k\lambda}{10B\cos\theta} \quad (8)$$

where D is the crystallite size in nm, k is a coefficient (0.9), λ is the wavelength of X-ray (1.5404 Å), B is the line broadening at half the maximum intensity in radians, and θ is the angle at the position of the maximum peak known as Bragg angle. The d_{Pt} values calculated from the XRD analysis are 2.0 nm for the commercial Pt/C and 2.3-2.9 nm for Pt/CCC catalysts, which are confirmed by the HRTEM images shown in Figure 3.4. The Pt loading on CCCs were in the range of 28.2–29.3 wt. % as confirmed by ICP-AES analysis which is in good agreement with the targeted Pt loading of 30 wt. %.

3.3.2 Electrochemical activity and stability of Pt/CCC catalysts

To investigate the electrochemical activity and stability of Pt/CCC catalysts, Pt/CCC-800 °C, Pt/CCC-1100 °C, and Pt/CCC-1500 °C catalysts were selected and tested. The commercial Pt/C catalyst which uses HSACB support was also tested for comparison. The commercial Pt/C catalyst studied in this investigation is deposited on Ketjenblack-EC300J HSACB which is the starting material of CCCs. The support stability results of H_2/air polarization curves (initial and after 400 h at 1.2 V) of commercial Pt/C, Pt/CCC-800 °C, Pt/CCC-1100 °C, and Pt/CCC-1500 °C catalysts are compared in Figure 3.5. The performance decay is evaluated by comparing the cell potential loss at 800 mA cm^{-2}. A very high potential loss (696 mV loss after 400 h) for the commercial Pt/C catalyst (shown in Figure 3.5 (a)) together with high mass activity loss (72%) and ECSA loss (71%) (shown in Table 3.2) confirm the fact that HSACB is prone to electrochemical oxidation when subjected to 1.2 V constant potential for 400 h. The commercial Pt/C catalyst showed very high performance loss under mass-transfer

controlled region due to severe carbon corrosion at high potentials which resulted in detachment of Pt particles from the support that is no longer electrochemically active, increase in hydrophilic property due to carbon corrosion, and in particle agglomeration [31]. Similar studies by Makharia et al. for a 50% Pt/C indicated 30 mV losses at 1500 mA cm^{-2} after 20 h of operation and drastic performance degradation after 30 h due to the onset of mass-transport losses induced by carbon corrosion [44]. Electrochemical carbon corrosion is one of the most important issues that affect the long-term stability of PEMFCs.

Figure 3.5 (b) shows the initial and final (after 400 h) H_2/air fuel cell polarization curves for the Pt/CCC-800 °C catalyst subjected to a potential holding experiment for 400 h. At the beginning of the test, the Pt/CCC-800 °C catalyst showed an iR-corrected cell potential of 699 mV at 800 mA cm^{-2} which decreased to 498 mV after 400 h potential holding at 1.2 V resulting in a potential loss of 201 mV. The mass activity and ECSA losses after 400 h testing are 50% and 60%, respectively (Table 3.2). The high cell potential loss is due to the corrosion of relatively high surface area for the CCC-800 °C (411 m^2 g^{-1}) which could be attributed to the oxidation of non-graphitic carbon initiated by the surface defects on the partially graphitized CCC-800 °C. The broader C(002) peak for CCC-800 °C in Figure 3.3 than for the other CCCs (CCC-1100 °C or CCC-1500 °C) indicates the presence of amorphous and partially graphitized carbons which is confirmed by the Raman spectroscopy results shown in Table 2.1. Due to the heterogeneous nature of CCC-800 °C and the method used for the synthesis, we assume that the primary particles exhibit the high density of surface defects [182]. The edges of these defect sites and corners of basal planes present in CCC-800 °C are susceptible to electrochemical

oxidation and the presence of Pt can propagate the carbon corrosion under 1.2 V potential holding experimental conditions.

The degree of graphitization of the CCC was further increased by increasing the heat treatment temperature to 1100 °C. The high temperature heat treatment resulted in a high degree of graphitization, with a significant decrease in the BET surface area. The support stability results shown in Figure 3.5 (c) clearly indicate the enhancement in stability for the Pt/CCC-1100 °C at 1.2 V potential holding experiment. At 800 mA cm^{-2} current density, the Pt/CCC-1100 °C catalyst showed an initial iR-corrected cell potential of 671 mV and 543 mV after 400 h. The support stability test results indicated a cell potential loss of 128 mV which is much smaller than that for Pt/CCC-800 °C and commercial Pt/C catalysts. Furthermore, the mass activity loss (47%) and ECSA loss (58%) are lower than those for the commercial Pt/C and Pt/CCC-800 °C catalysts. The improved support stability is solely attributed to the high degree of graphitization of the CCC-1100 °C. It has been reported that the extent of graphitization of carbon supports plays an important role on the support stability, with more graphitic carbons being more thermally and electrochemically stable [21, 129].

The H_2/air polarization curves obtained before and after 400 h potential holding at 1.2 V for the Pt/CCC-1500 °C catalyst are compared in Figure 3.5 (d). It shows an initial iR-corrected cell potential of 686 mV and 622 mV after 400 h potential holding with a potential loss of 64 mV. The Pt/CCC-1500 °C catalyst showed mass activity loss of 39% and ECSA loss of 18% after 400 h. Figure 3.6 compare the ECSA loss in the fuel cell for the commercial Pt/C and the Pt/CCC-1500 °C catalysts. The commercial Pt/C showed an initial ECSA of 52 m^2 g_{Pt}^{-1} which drastically decreased to 15 m^2 g_{Pt}^{-1} (71% loss) after

400 h due to severe carbon corrosion. In contrast, the Pt/ CCC-1500 °C showed an ECSA loss of 18% with initial and final ECSA values of 27 and 22 $m^2 g_{Pt}^{-1}$, respectively.

Figure 3.7 and Table 3.2 compare the electrochemical properties in a fuel cell (initially and after 400 h) including potential loss at 800 mA cm^{-2} in H_2/air, ECSA loss and mass activity loss at 0.9 $V_{iR\text{-}corr}$ for commercial Pt/C, Pt/CCC-800 °C, Pt/CCC-1100 °C and Pt/CCC-1500 °C catalysts. All the fuel cell polarization results together with mass activity loss and ECSA loss data clearly indicate that the graphitic carbon support offers better resistance to corrosion during 1.2 V potential holding. With the enhanced support stability for the Pt/CCC-1500 °C, better catalyst stability is anticipated when subjected to potential cycling conditions between 0.6 and 1.0 V where the Pt and Pt-based catalysts suffer a loss of activity due to various processes including metal dissolution, loss in ECSA etc.

3.4 Conclusion

In this chapter, the feasibility of CCC as a cathode catalyst support material for PEMFCs was investigated. After using noncovalent functionalization of the CCCs, Pt nanoparticles could be successfully deposited on the CCC support with particle sizes in the range of 2.3-2.9 nm. The Pt loading on CCCs were in the range of 28.2–29.3 wt. % as confirmed by ICP-AES analysis which is in good agreement with the targeted Pt loading (30 wt. %). The potential holding test was conducted at 1.2 V for 400 h to examine the support stability of commercial Pt/C, Pt/CCC-800 °C, Pt/CCC-1100 °C, and Pt/CCC-1500 °C catalysts. The commercial Pt/C catalyst which used HSACB as a support material showed complete loss of potential at 800 mA cm^{-1} in H_2/air fuel cell polarization performance after 400 h testing. Also, the commercial Pt/C catalyst showed 71% loss of

ECSA and 72% loss of mass activity. On the other hand, the Pt/CCC-1500 °C catalyst showed 64 mV potential loss (at 800 mA cm^{-2}) in H_2/air fuel cell polarization performance, 18% ECSA loss, and 39% mass activity loss after 400 h testing. The enhanced support stability of Pt/CCC-1500 °C catalyst is attributed to the increased graphitic character of CCC-1500 °C support when compared to the commercial HSACB

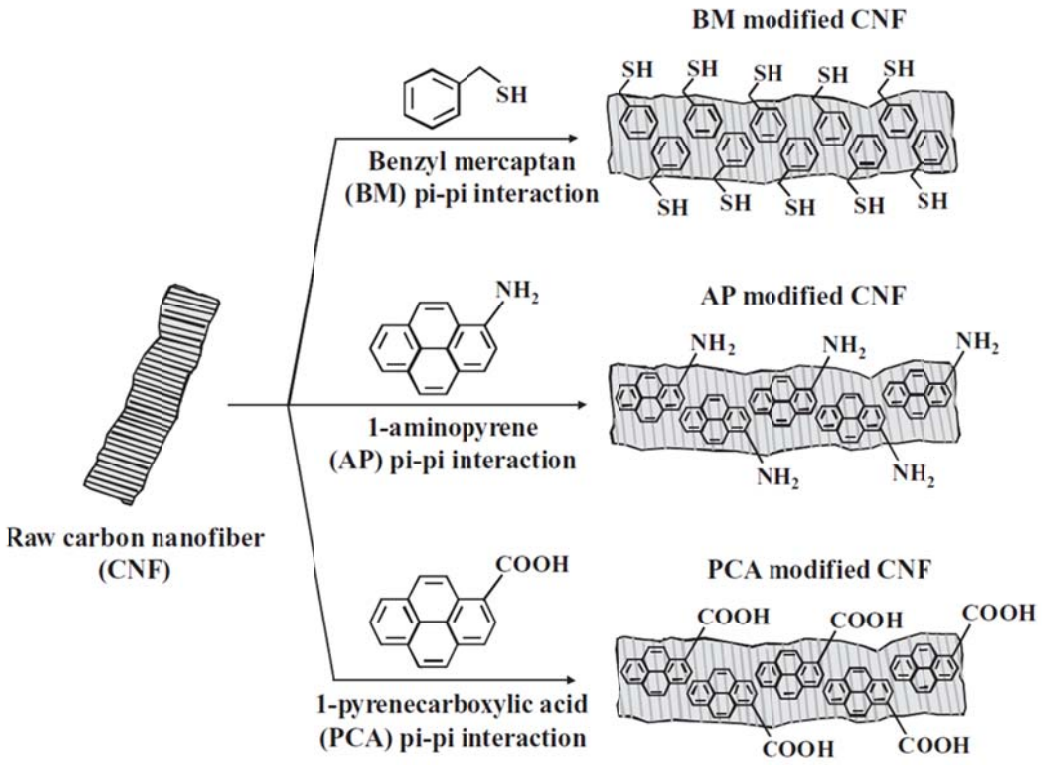

Figure 3.1 Schematic diagram of the functionalization of CNFs with benzyl mercaptan (BM), 1-aminopyrene (AP) and 1-pyrenecarboxylic acid (PCA) [180].

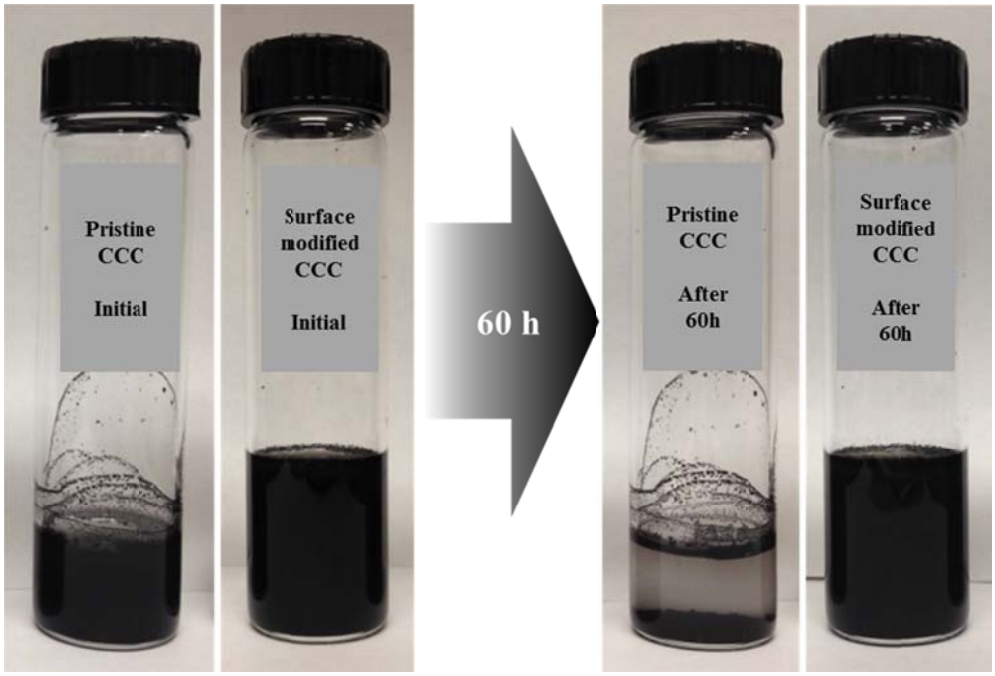

Figure 3.2 Comparison of hydrophilic characters of pristine CCC and surface-modified CCC by precipitation test during 60 h.

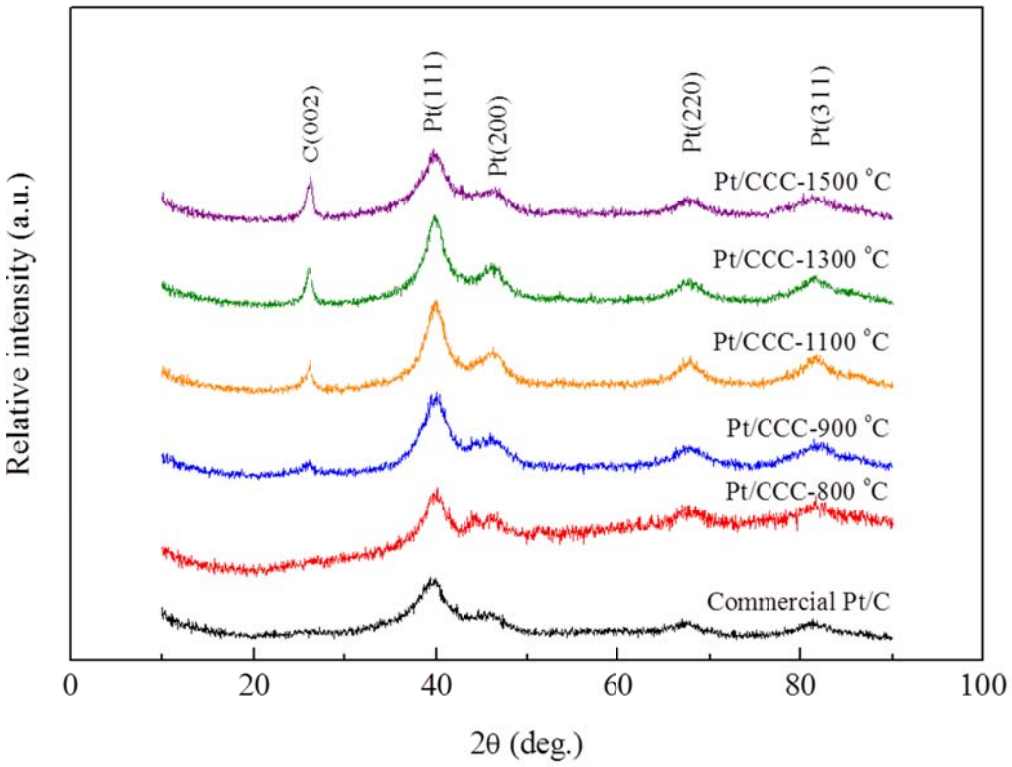

Figure 3.3 XRD patterns of commercial Pt/C and Pt/CCC catalysts.

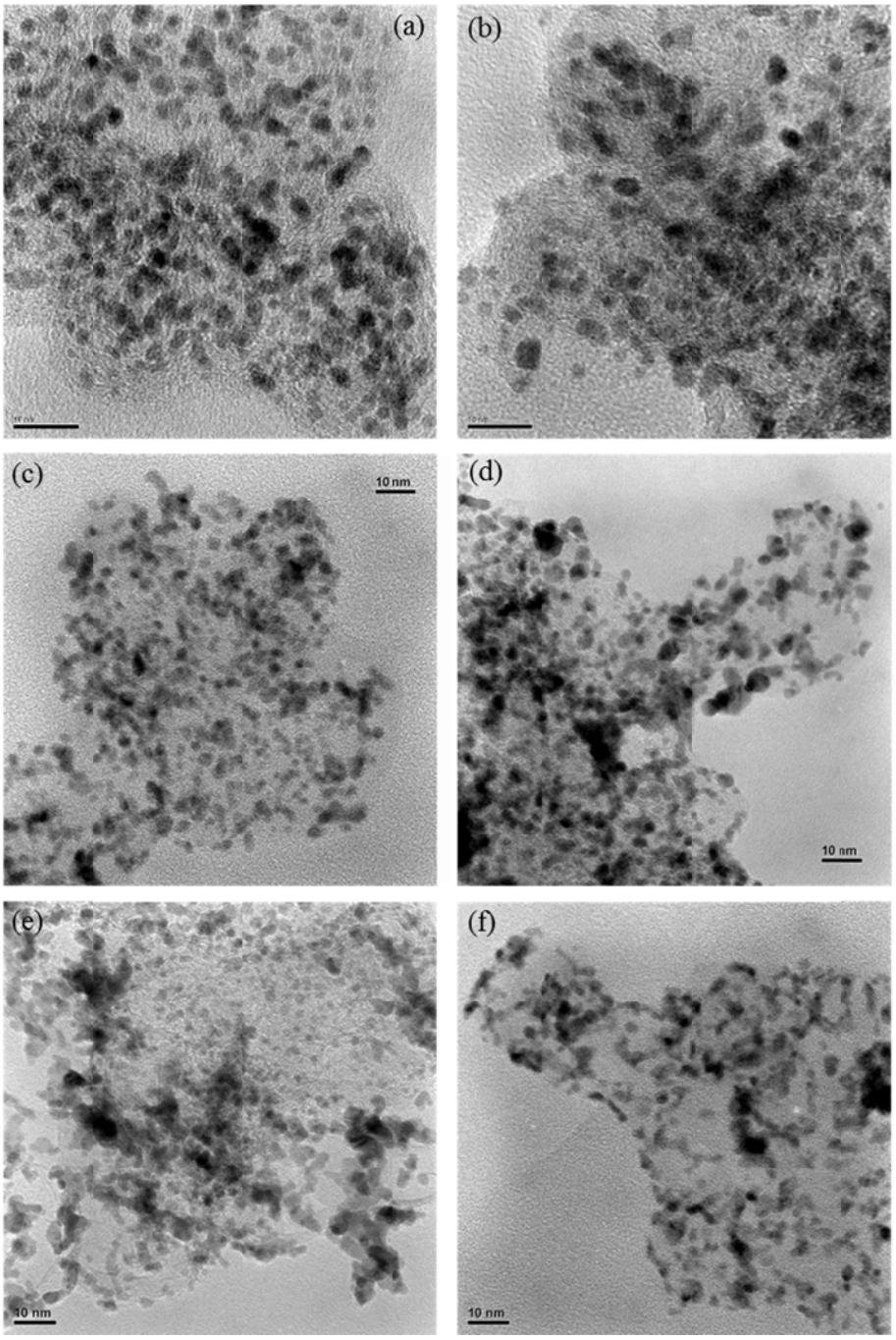

Figure 3.4 HRTEM images of (a) commercial Pt/C, (b) Pt/CCC-800 °C, (c) Pt/CCC-900 °C, (d) Pt/CCC-1100 °C, (e) Pt/CCC-1300 °C, and (f) Pt/CCC-1500 °C. The scale bar is 10 nm.

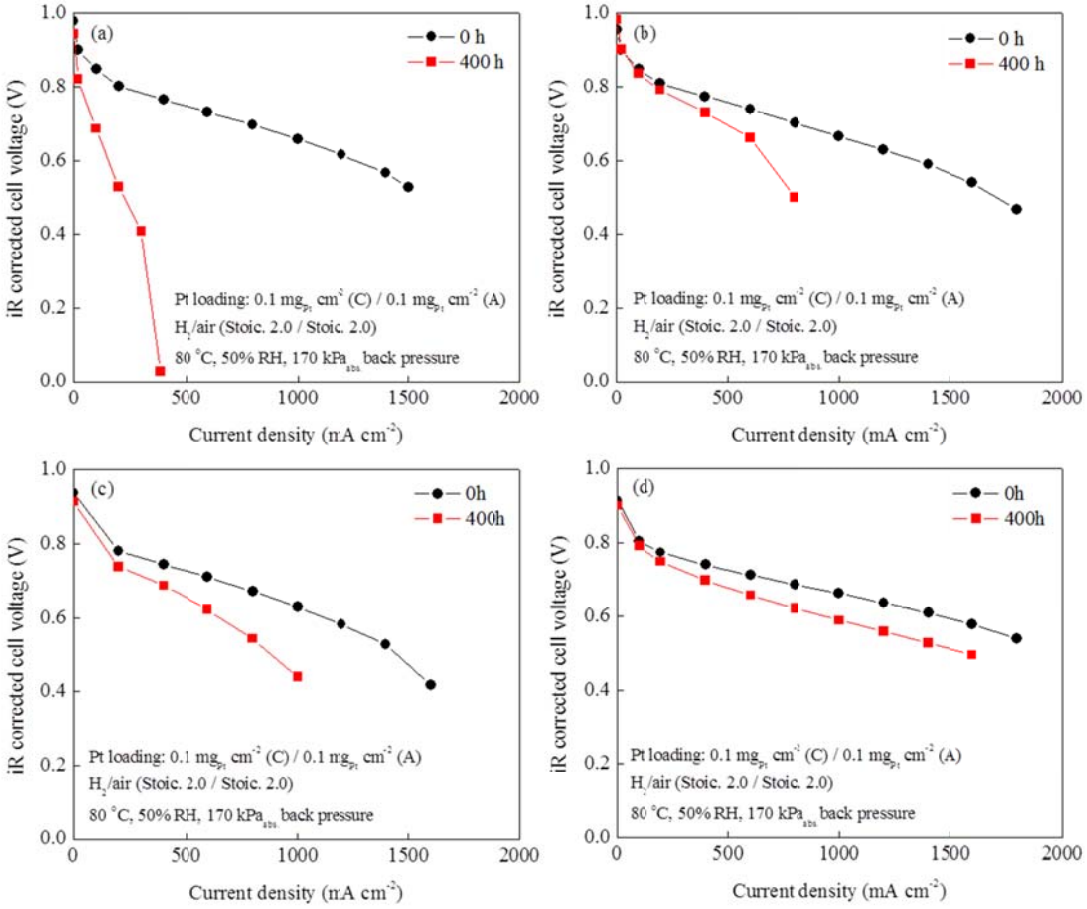

Figure 3.5 H_2/air fuel cell plarization curves of (a) commercial Pt/C, (b) Pt/CCC-800 °C, (c) Pt/CCC-1100 °C, and (d) Pt/CCC-1500 °C catalysts before and after the support stability test (1.2 V potential holding for 400 h).

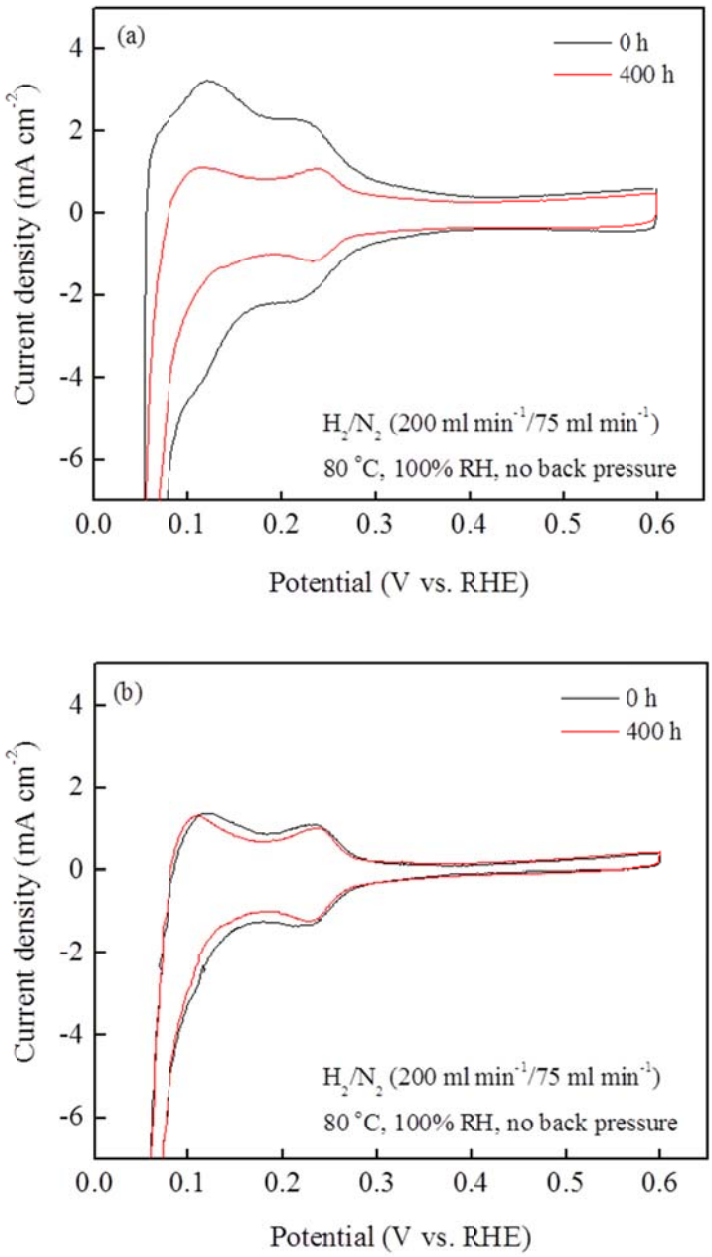

Figure 3.6 Comparison of cyclic voltamograms in MEA for (a) commercial Pt/C and (b) Pt/CCC-1500 °C catalysts before and after the support stability test.

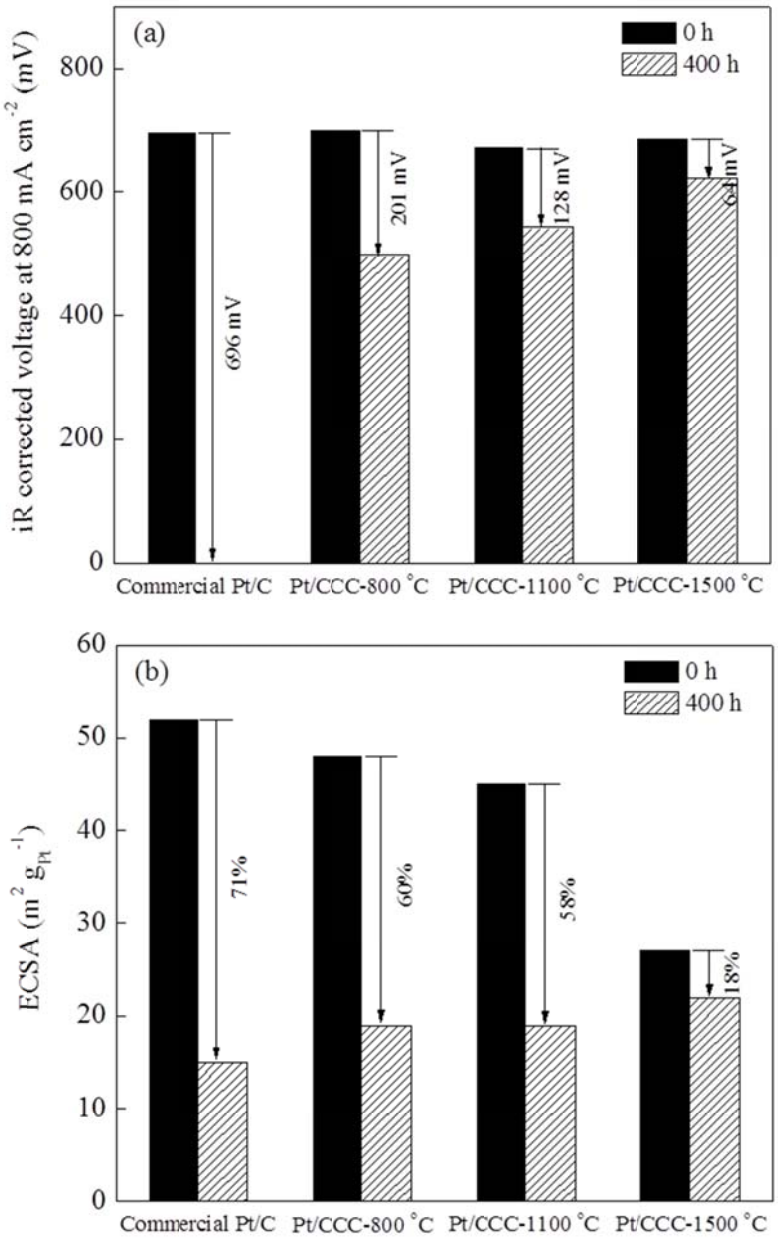

Figure 3.7 Comparison of (a) iR corrected voltage and (b) ECSA of commercial Pt/C, Pt/CCC-800 °C, Pt/CCC-1100 °C, and Pt/CCC-1500 °C catalysts before and after the support stability test.

Table 3.1 Physical properties of commercial Pt/C and Pt/CCC catalysts.

Sample	Support pyrolysis temp. (°C)	d_{Pt} (nm) (XRD)	Pt conc. (wt. %) (ICP-AES)
Commercial Pt/C	-	2.0	44.3
Pt/CCC-800 °C	800	2.4	28.7
Pt/CCC-900 °C	900	2.3	29.3
Pt/CCC-1100 °C	1100	2.9	28.4
Pt/CCC-1300 °C	1300	2.7	28.8
Pt/CCC-1500 °C	1500	2.7	28.2

Table 3.2 Comparison of electrochemical performance before and after the support stability test for commercial Pt/C, Pt/CCC-800 °C, Pt/CCC-1100 °C, and Pt/CCC-1500 °C catalysts.

Sample	iR corrected cell potential (H_2/air) at 800 mA cm^{-2} (mV)			ECSA (m^2 g_{Pt}^{-1})			Mass activity loss at 0.9 $V_{iR\text{-}corr}$ (%)
	0 h	400 h	Loss (mV)	0 h	400 h	Loss (%)	
Commercial Pt/C	696	0	696	52	15	71	72
Pt/CCC-800 °C	699	498	201	48	19	60	50
Pt/CCC-1100 °C	671	543	128	45	19	58	47
Pt/CCC-1500 °C	686	622	64	27	22	18	39

CHAPTER 4

A NOVEL METHOD FOR THE SYNTHESIS OF Pt-Co/CCC CATALYST USING THE CCC AS A CATALYST SUPPORT AND A SOURCE OF COBALT

4.1 Introduction

In chapter 2, significant amount of Co content (10.7%) in the CCC-800 °C sample was observed after subjecting to 0.5 h leaching in 0.5 M H_2SO_4. The CCC-800 °C also showed improved electrochemical stability than of the conventionally used HSASB and good feasibility as a support material for PEMFC applications. By using these unique characteristics of CCC-800 °C, a novel method to synthesize Pt-Co/C catalyst was developed. Various procedures have been reported in the literature to obtain Pt alloy catalyst. The most common procedure to synthesize Pt alloy catalyst is the impregnation of the Co metal precursor on Pt/C followed by heat treatment at high temperature (above 600 °C) to produce Pt-Co alloy [2, 184, 185]. In another method, Pt and transition metal are co-deposited on carbon supports using various reducing agents like sodium formate, formaldehyde, sodium borohydride etc. [186-188]. Other procedures such as precipitation, sol-gel and polyol methods have also been carried out for making Pt-alloy catalysts [189-191]. While a variety of methods has been investigated, in most of the cases, chemical leaching step is necessary to remove excess transition metal on the surface after alloy formation step which hinders active sites of the catalyst. This chemical

leaching step not only helps to clean the surface of the catalyst but it also makes adverse effects on the catalyst by weakening the Pt support interaction which results in poor stability.

In this work, a new approach to synthesize Pt-Co catalyst is developed by using Co-containing CCC-800 °C to improve the catalytic activity and stability of Pt-Co/CCC. Figure 4.1 compares the schematic diagrams of the conventionally used impregnation method and the novel method developed in this study. The strategy is the synthesis of Pt-Co/CCC catalyst by using the Co metal encapsulated within the CCC-800 °C as a catalyst support as well as a Co source for making Pt-Co alloy. The goal is to study the synergistic effect of ORR activity originated from CCC support (non-precious metal catalyst) and Pt. This novel procedure of synthesizing Pt-Co catalyst does not need a chemical leaching step after the alloy formation thus avoiding the overall fuel cell performance loss since the Co is diffused from the interior of CCC to Pt deposited on the surface which minimizes the interference with the Pt activity.

4.2 Experimental

4.2.1 Synthesis of Pt-Co/CCC catalyst

A chloroplatinic acid (H_2PtCl_6, Sigma-Aldrich) was used as the Pt-precursor for the deposition of 30 wt. % Pt on CCC-800 °C support. The desired amount of chloroplatinic acid solution and CCC were mixed in DI water and heated up to 70 °C. Then 2.0 M sodium formate (HCOONa, Sigma-Aldrich) was slowly added to the reaction mixture, followed by refluxing at 70 °C for 12 hr. The resulting Pt/CCC-800 °C sample was washed with DI water, dried under vacuum at 80 °C and finally heat-treated in nitrogen at 800 °C for a different time for Pt-Co/CCC formation.

4.2.2 Material characterization studies

The physical and chemical properties of the materials were characterized using XRD and HRTEM techniques. XRD (Rigaku 405S5) patterns were recorded to identify the crystalline structure of catalyst and measure Pt particle size. HRTEM (Hitachi H9500) was carried out to determine the particle size and dispersion of Pt on support.

4.2.3 RRDE measurements

All the RRDE studies were performed in 0.1 M $HClO_4$ using a Pine bipotentiostat (Model AFCBP1), a Pt-wire counter electrode, and an Ag/AgCl reference electrode. An RRDE with a Pt ring and a glassy carbon disk was used as the working electrode. The catalyst ink was prepared by blending catalyst powder with ethanol in an ultrasonic bath. Then 20 μg_{Pt} cm^{-2} of the ink was deposited onto the glassy carbon. After the deposition, 5 µL of a 0.25 wt% Nafion® solution was applied onto the catalyst layer. Cyclic voltammograms (CV) recorded in nitrogen were used to obtain the background capacitive currents and ECSA of the Pt catalysts. Linear sweep voltammograms in O_2-saturated electrolyte were measured at 900 rpm. The oxygen reduction current was determined as the difference between currents measured in the N_2- and O_2-saturated electrolytes.

The ECSA of Pt was determined by charge integration under the hydrogen desorption peaks appearing between 0 and 0.35 V, by assuming a charge of 210 µC cm^{-2} for the electroactive Pt surface. Then, the specific ECSA was calculated based on the following relation:

$$Specific\ ECSA = \frac{Q_H}{m \times q_H} \tag{9}$$

where Q_H (μC) is the charge for hydrogen desorption, m (μg cm^{-2}) is the Pt metal loading, and q_H (μC cm^{-2}) is the charge required for desorbing a monolayer of hydrogen on Pt surface. The electrolyte was purged with oxygen for 30 min prior to the oxygen reduction measurement. The oxygen reduction current was calculated from the difference between currents measured in the N_2- and O_2-saturated electrolytes.

The mass transfer corrected Tafel plot was calculated by using the diffusion limited current density (j_D) at 0.2 V and the following expression based on the Levich equation [192]:

$$j_k = \frac{j \times j_D}{j + j_D} \tag{10}$$

where j is the measured cell current density (A cm^{-2}).

4.2.4 MEA fabrication and electrochemical measurements

The anode and cathode catalysts were directly deposited on to the Nafion® NRE 212 (DuPont) membrane. The anode and cathode catalyst loading were fixed at 0.1 mg_{Pt} cm^{-2} and confirmed using XRF analysis. The catalyst coated membrane and GDLs were hot-pressed at 140 °C under a pressure of 20 kg cm^{-2} for 3 min. Catalyst mass activity was measured at 0.9 $V_{iR\text{-}corr}$ under H_2/O_2 (2.0/9.5 stoic.) at 80 °C, 100% RH. Polarization studies were performed under H_2/O_2 (750 mL min^{-1}/750 mL min^{-1}) at 80 °C, 100 % RH, no back pressure and H_2/air (1.5/1.8 stoic.) at 80 °C, 40% RH, 150 kPa_{abs} back pressure.

4.3 Results and discussion

4.3.1 Effect of heat treatment time on Pt-Co/CCC formation

To synthesize the Pt-Co alloy catalyst, Pt/CCC catalyst were heat-treated at 800 °C for different duration (0.5-4.0 h) under nitrogen atmosphere. Figure 4.2 shows HRTEM images of Pt/CCC (before heat treatment) and Pt-Co/CCC (after heat treatment at 800 °C for 2 h). Figure 4.2 (a) shows homogeneous dispersion of Pt particles on the CCC support with the particle size in the range of 2-3 nm. The arrow indicates the embedded Co particle within the CCC which will be the Co source for Pt-Co alloy formation. After heat treatment, increase of Pt particle sizes from 2-3 nm to a range of 3-8 nm due to sintering effect at high temperature was observed (Figure 4.2 (b)).

To investigate the effect of heat treatment duration on crystalline structure of Pt-Co/CCC catalysts, XRD patterns for Pt/CCC and different heat treated Pt-Co/CCC catalysts (heat treated for 0.5-4.0 h) are compared (Figure 4.3). The degree of alloying increases as the heat treatment duration increases, which can be seen from the shift in the 2θ to higher values. It is noticeable that a splitting of the Pt lattice peaks occurred for the 0.5 h and 1 h heat treated Pt-Co/CCC catalysts while single peaks were observed for the Pt/CCC, 2 h heat treated Pt-Co/CCC, and 4 h heat treated Pt-Co/CCC catalysts. For more detailed analysis, the deconvolution of Pt(220) lattice peaks between 63-77° for Pt/CCC, 0.5 h heat treated Pt-Co/CCC, 1 h heat treated Pt-Co/CCC, and 2 h heat treated Pt-Co/CCC were carried out (Figure 4.4). The deconvolution of Pt/CCC shows a single peak at 67.3° which indicates the presence of only pristine Pt. On the other hand, the 0.5 h heat treated Pt-Co/CCC shows both Pt (67.9°) and Pt-Co (69.4°) peaks due to presence of mixed structure of Pt and Pt-Co. For 1 h heat treated Pt-Co/CCC, the deconvolution of

peak shows a similar pattern with that of 0.5 h heat treated Pt-Co/CCC which indicates the presence of both Pt and Pt-Co in the catalyst. However, the Pt-Co peak intensity is increased when compared with that of 0.5 h Pt-Co/CCC due to an increase in Pt-Co alloy formation. For 2 h heat treated Pt-Co/CCC, only a single peak for Pt-Co was observed at 69.5° which indicates the completion of Pt-Co alloy formation in the catalyst. The 2θ values for Pt and Pt-Co peaks and particle sizes are summarized in Table 4.1. These results indicate that Co particle present in the CCC support was gradually diffused to the Pt particles and the content of Pt-Co alloy was increased as a function of heat treatment duration. After 2 h heat treatment, the Co was completely diffused to Pt particles and uniform Pt-Co/CCC catalyst was formed.

4.3.2 Electrochemical studies of Pt-Co/CCC catalysts

The CV test was performed for the fresh Pt/CCC and Pt-Co/CCC catalysts pyrolyzed at 800 °C for 0.5, 1, 2, and 4 h to examine their electrochemical performance including ECSA in RRDE test conditions (Figure 4.5). It is noticed that the longer heating time decreased the capacitive current, hydrogen adsorption, and oxide layer formation on the catalyst. The decrease of hydrogen adsorption region was more pronounced than the decrease in the capacitive region indicating that the carbon support surface area was not changed significantly in the presence of Pt during heat treatment.

The ECSA decreased from 96.3 $m^2\ g_{Pt}^{-1}$ to 42.8 $m^2\ g_{Pt}^{-1}$ when the heat treatment time was increased from 0 (no heat treatment) to 2 h due to particle size increase and the Pt-Co alloy formation. The theoretical ECSA was calculated from the average particle size by using the following formula [193]:

$$ECSA_{theoretical} = \frac{6}{\rho_{Pt} \times d} \quad (11)$$

where ρ_{Pt} is the density of Pt (21.6 g cm^{-3}) and d is the average particle diameter, measured using XRD analysis.

Figure 4.6 (a) shows the variation of theoretical and measured ECSA vs. the heat treatment time. The theoretical ECSA is inversely proportional to the particle size, as expected from Eq. 11. The measured ECSAs have a minimum value for the 2 h heat treated Pt-Co/CCC. Simultaneously the difference between the measured and the theoretical value increases as the heat treatment time increases from 0 to 2 h and decreases for 4 h heat treated Pt-Co/CCC catalyst. This effect is probably due to the result of decreased adsorption energy of hydrogen on well-formed Pt-Co alloys and consequently the lower coverage of the H(ads) monolayer. The alloying affects the surface charge and the value of 210 μC cm^{-2} for the adsorption of one monolayer of hydrogen on polycrystalline Pt which was used for the calculation of the ECSA is no longer valid. The uncertainty of exact number of the surface charge of the H monolayer partly caused the discrepancy from Eq. 11. It can be concluded that at 2 h heat treatment, the H adsorption is the smallest and not the specific surface area of Pt caused by the increased particle size.

The specific oxide formation charge (C mg_{Pt}^{-1}) has been calculated by integrating the current from 0.45 V to 1.0 V and normalized to the Pt content:

$$Q_{ox} = \frac{\int_{0.45}^{1}(I - I_{dl})dV/sweeprate}{1000 \times m \times A} \quad (12)$$

where I_{dl} is the capacitive current (A), the sweep rate is equal to 0.05 V s^{-1}, m is the Pt metal loading on the ring disk (20 μg cm^{-2}), and A is the disk area (0.248 cm^2). The specific oxide formation charge result in Figure 4.6 (b) shows the same trend with ECSA, which is in agreement with the expected lower surface O(ads) bonding energy for the Pt-Co alloy surfaces. Among all the catalysts, the 2 h heat treated Pt-Co/CCC showed the lowest oxide coverage.

Figure 4.7 shows the mass transfer corrected ORR activities for Pt/CCC and Pt-Co/CCC catalysts. The specific activity of the catalyst at 0.9 V increased from 0.063 mA cm^{-2} to 0.165 mA cm^{-2} for the non-heat treated (Pt/CCC) and 2 h heat treated Pt-Co/CCC catalysts, respectively. The specific activity at 0.9 V decreased for the 4 h heat treated Pt-Co/CCC catalyst (0.138 mA cm^{-2}). The maximum specific activity was observed for the 2 h heat treated Pt-Co/CCC catalyst, which is in agreement with the minimum oxide coverage observed in Fig 4.6(b). The ECSAs, specific oxide formation charges, and specific activities at 0.9 V for Pt/CCC and Pt-Co/CCC catalysts are summarized in Table 4.2.

From the electrochemical study results, it can be concluded that by applying the innovative Pt-Co/CCC preparation methodology, highly-active Pt-Co/CCC catalyst can be synthesized. This methodology is cost-effective and easy to scale up. Furthermore, no post acid leaching step is necessary to remove unreacted Co from the catalyst. A high catalytic activity has been achieved without the leaching or electrochemical de-alloying steps, which may cause weakening of support-Pt particle interaction and increase the support corrosion leading to poor stability.

4.3.3 Fuel cell studies of Pt-Co/CCC catalysts

The OCV and the kinetic region performance were studied for the elucidation of the synergetic effects of CCC support and Pt-Co catalyst. Figure 4.8 shows H_2/O_2 polarization curves of commercial Pt/C (TEC10E50E, 46.7% Pt, TKK), Pt/CCC, and 2 h heat treated Pt-Co/CCC catalysts. According to these results, the OCV and kinetic region performances increased when Pt was deposited onto CCC support due to the synergistic effect of combined ORR activities of CCC support and Pt/Pt-Co catalysts. The OCV of the ORR on Pt was extensively studied by Damjanovic, Sepa, and Wroblowa by analyzing the effects of oxygen pressure, pH, and contamination on the measurable OCV of ORR on Pt in sulfuric acid [194-196]. The theoretically expected value of 1.23 V was not obtained because of the very low exchange current density for the ORR. They concluded that any small contamination in Pt decreases the OCV and the maximum OCV measured in an extra clean environment was even lower than its thermodynamic value. The oxide formation was found to be independent of the oxygen content and it was accounted for in the following reactions:

$$Pt + H_2O \rightarrow PtO(ads) + 2H^+ + 2e^- \quad (13)$$

$$Pt + H_2O \rightarrow PtOH(ads) + H^+ + e^- \quad (14)$$

$$PtOH(ads) \rightarrow PtO(ads) + H^+ + e^- \quad (15)$$

Consequently a mixed potential [196] is built up in the MEA, in which oxide formation or the contaminants (hydrogen crossover) partly acts as the anodic part and ORR as the cathodic part. Evidently if the ORR is enhanced or the oxide formation is

shifted to a higher mixed potential, higher OCV can be obtained. To sum up, the synergistic effect of CCC support and the Pt-Co catalyst formation enhanced the overall ORR activity of Pt-Co/CCC catalyst resulting in higher measurable OCV than that of the commercial Pt/C catalyst.

Figure 4.9 (a) shows H_2/O_2 fuel cell polarization curves for Pt/CCC and 2 h heat treated Pt-Co/CCC cathode catalysts. The fuel cell performance of 2 h heat treated Pt-Co/CCC is higher than that of the Pt/CCC catalyst in both low and high current regions. The results indicate that the activity of 2 h heat treated Pt-Co/CCC can be improved by achieving complete Pt-Co alloy formation. The current at 0.7 $V_{iR\text{-}corr}$ increased from 1.26 to 2.15 A cm^{-2} when the Pt-Co alloy is formed in the case of 2 h heat treated Pt-Co/CCC catalyst. Mass activity results of Pt/CCC and 2 h heat treated Pt-Co/CCC are shown in Figure 4.9 (b). Mass activity of 2 h heat treated Pt-Co/CCC (0.36 A mg_{Pt}^{-1}) is 2.8 times higher than that of the Pt/CCC (0.13 A mg_{Pt}^{-1}) which shows that mass activity is increased when Pt is alloyed with Co.

H_2/air fuel cell polarizations of Pt/CCC and 2 h heat treated Pt-Co/CCC are presented in Figure 4.10. The 2 h heat treated Pt-Co/CCC shows better fuel cell performance than the Pt/CCC in the same manner as observed in H_2/O_2 polarization studies (Fig. 4.9). Especially at 0.7 $V_{iR\text{-}corr}$, the 2 h heat treated Pt-Co/CCC catalyst generated 1.7 times higher current density than that of Pt/CCC.

4.4 Conclusion

A novel method to synthesize Pt-Co/C was investigated by using Co-containing CCC as the support material to deposit Pt and subsequent heat treatment to obtain Pt-Co/CCC catalysts for PEMFC applications. Series of Pt-Co/CCC catalysts was

synthesized by heat treating the Pt/CCC catalyst at 800 °C for various durations. The Pt-Co alloy formation was confirmed by the observed shift in the 2θ values in the XRD patterns. The effect of alloying on the ORR activity was studied by analyzing the ECSA, the oxide formation charge, and the specific catalytic activity determined by mass transfer corrected Tafel analysis. In the fuel cell studies, 2 h heat treated Pt-Co/CCC showed better H_2/O_2 and H_2/air polarization performance than Pt/CCC. The mass activity of the 2 h heat treated Pt-Co/CCC (0.36 A mg_{Pt}^{-1}) was 2.8 times higher than that of the Pt/CCC (0.13 A mg_{Pt}^{-1}).

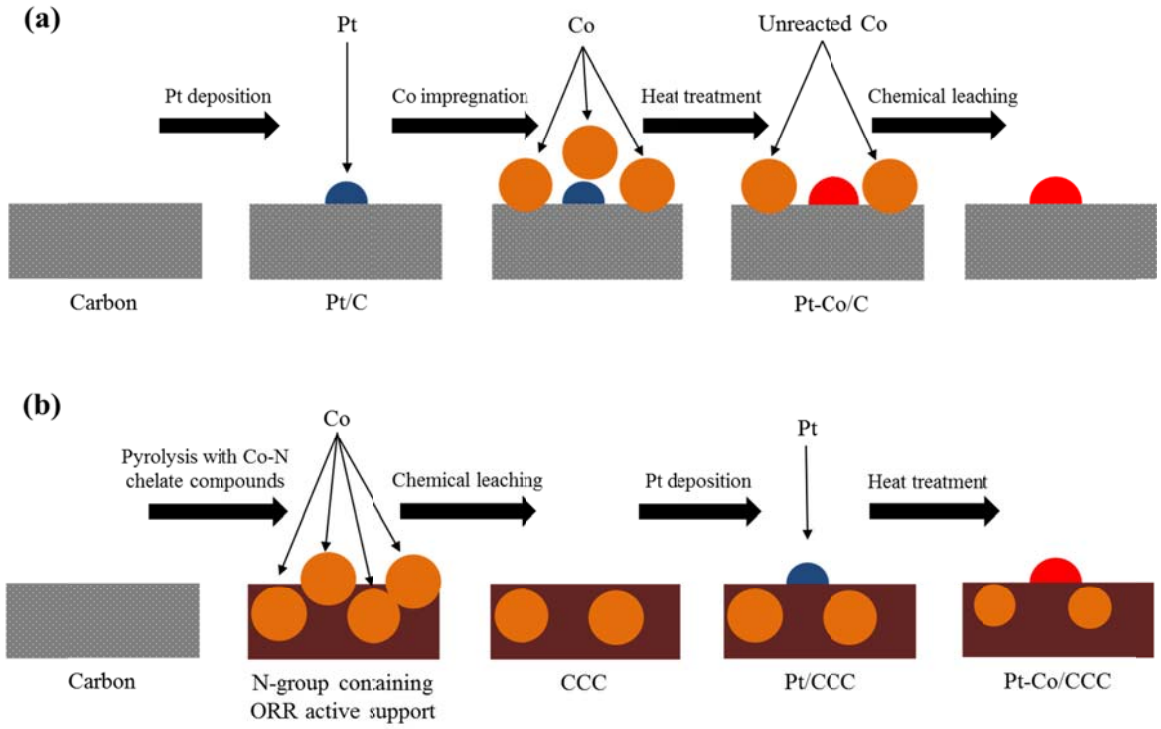

Figure 4.1 Comparison of schematic diagrams for (a) the impregnation method and (b) the USC novel method for Pt-Co/C synthesis.

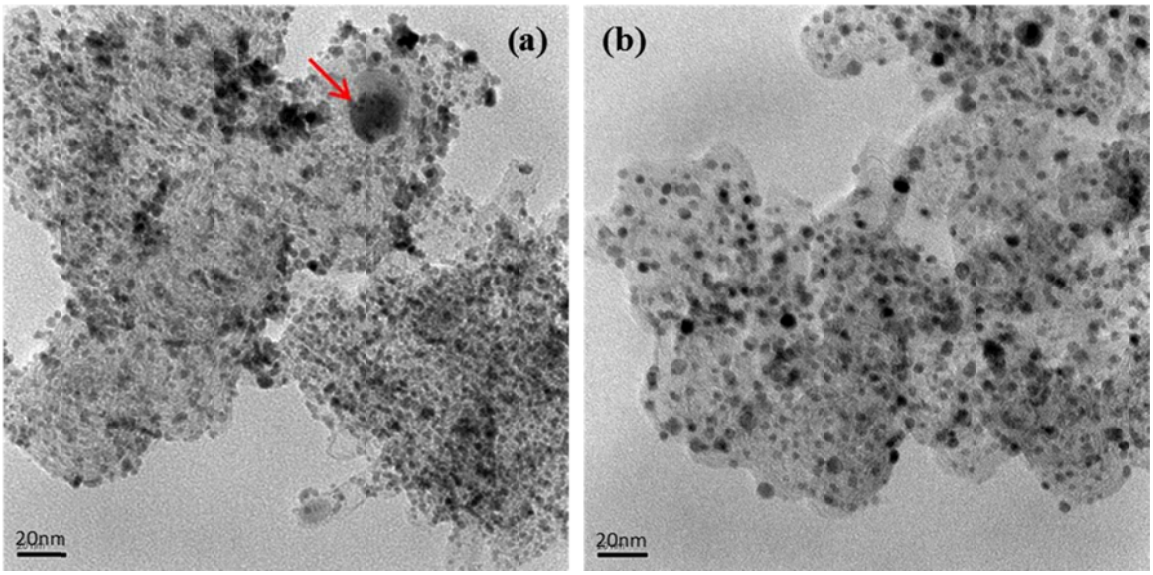

Figure 4.2 HRTEM images of (a) the Pt/CCC catalyst and (b) the Pt-Co/CCC catalyst obtained after 2 h heat treatment at 800 °C.

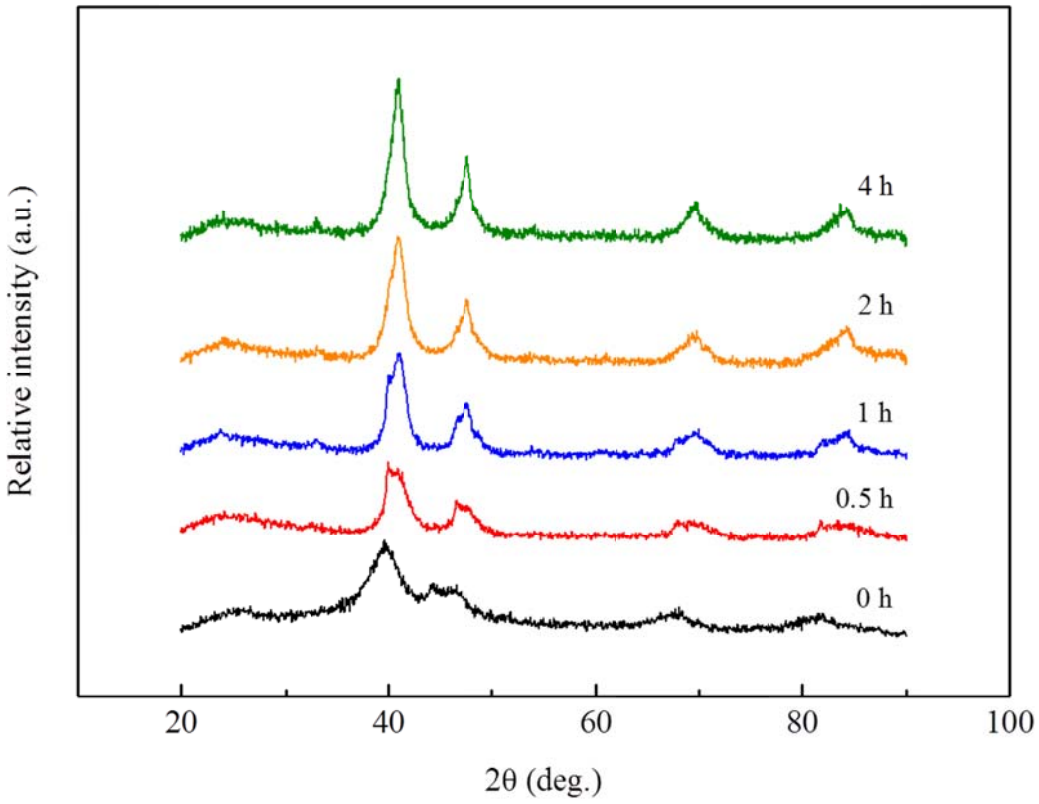

Figure 4.3 XRD patterns of Pt/CCC and Pt-Co/CCC catalysts heat treated at 800 °C for 0.5, 1, 2, and 4 h.

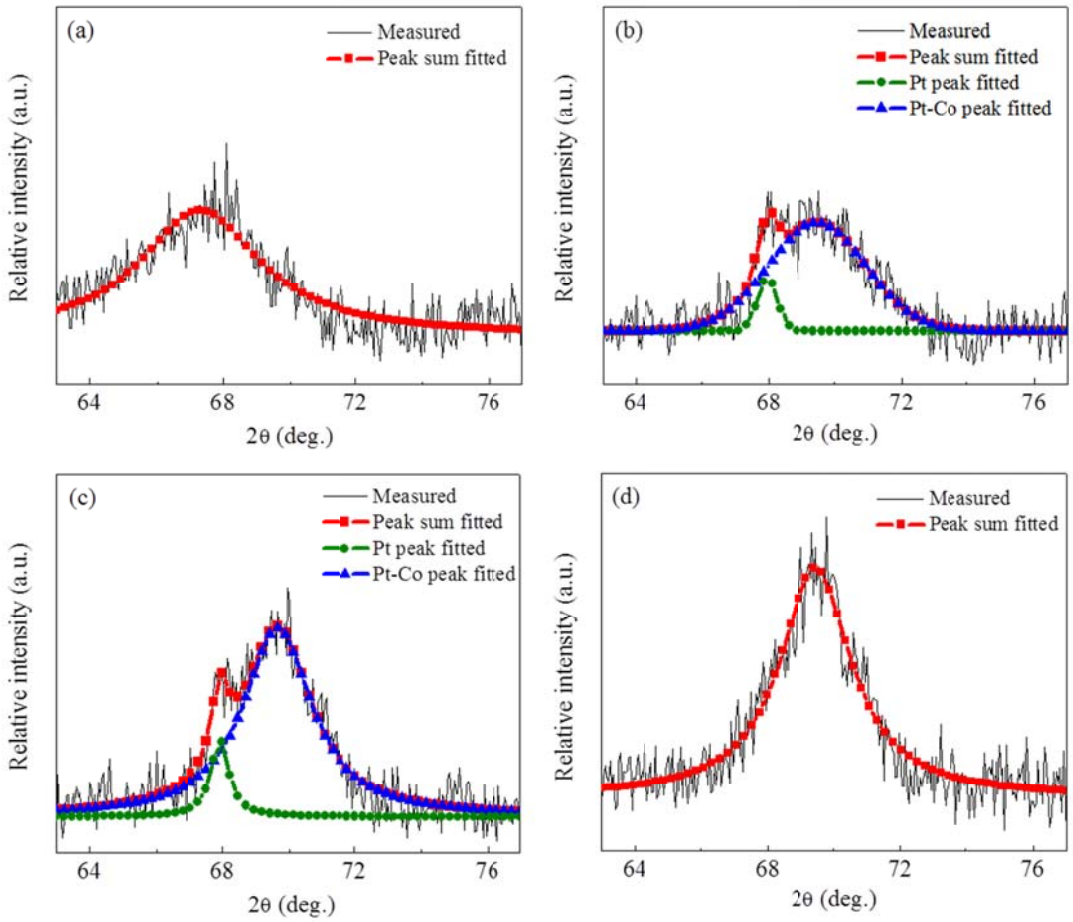

Figure 4.4 The deconvolution of the Pt(220) peaks of (a) Pt/CCC, (b) 0.5 h heat treated Pt-Co/CCC, (c) 1 h heat treated Pt-Co/CCC, and (d) 2 h heat treated Pt-Co/CCC catalysts.

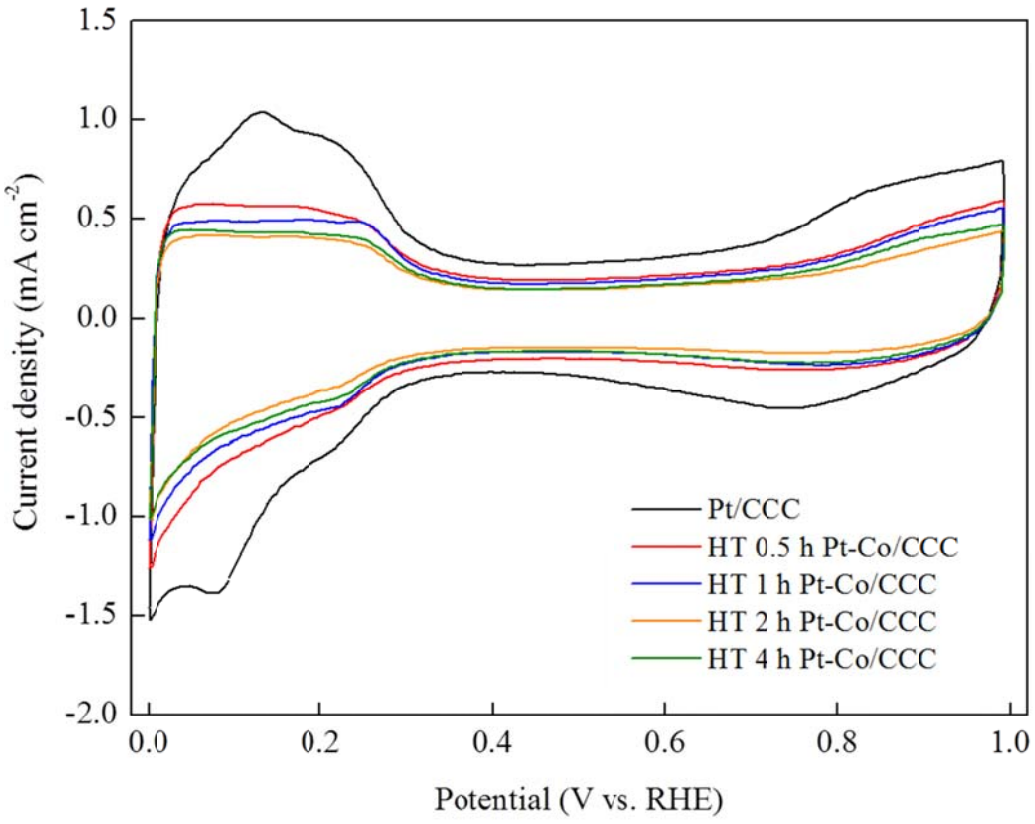

Figure 4.5 CVs of Pt/CCC and Pt-Co/CCC catalysts heat treated for 0.5, 1, 2, and 4 h. CVs were measured in the potential range of 0.0-1.0 V with a scan rate of 50 mV s^{-1} under N_2.

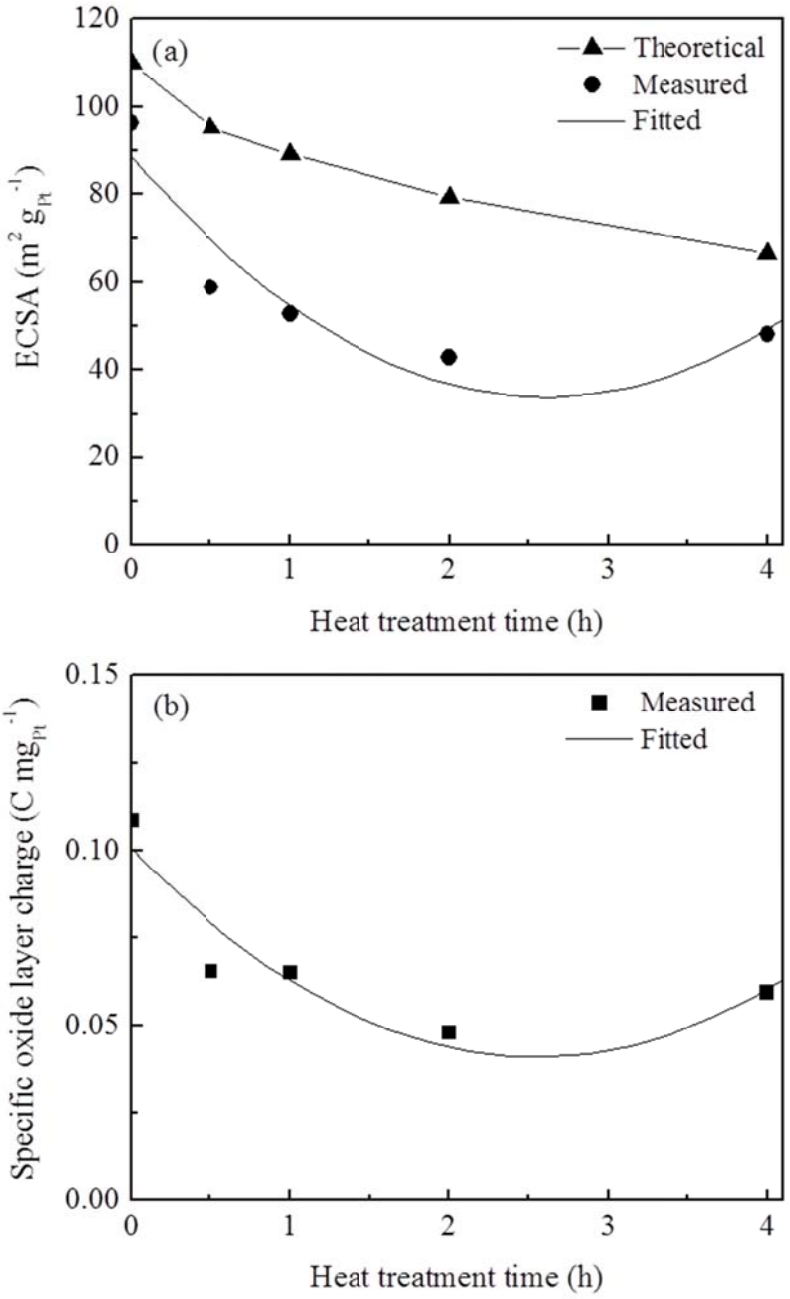

Figure 4.6 Comparison of (a) theoretical and measured ECSA and (b) specific oxide layer charges as a function of heat treatment time for Pt-Co/CCC catalysts.

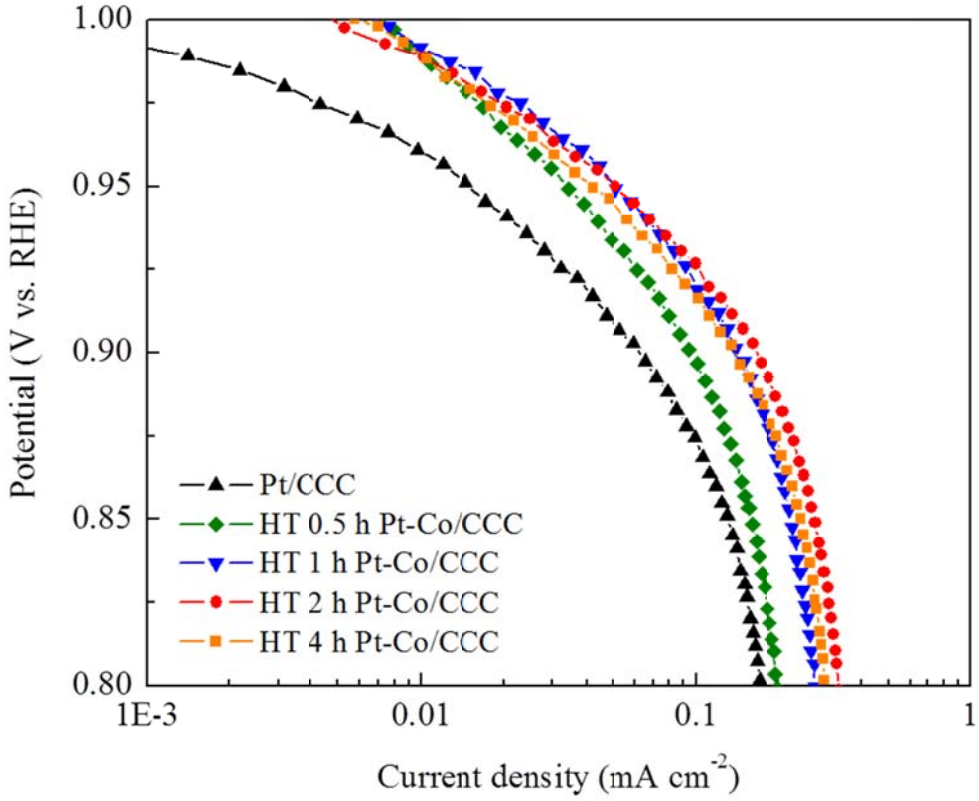

Figure 4.7 The mass transfer corrected ORR activity plots of Pt/CCC and Pt-Co/CCC catalysts heat treated for 0.5, 1, 2, and 4 h.

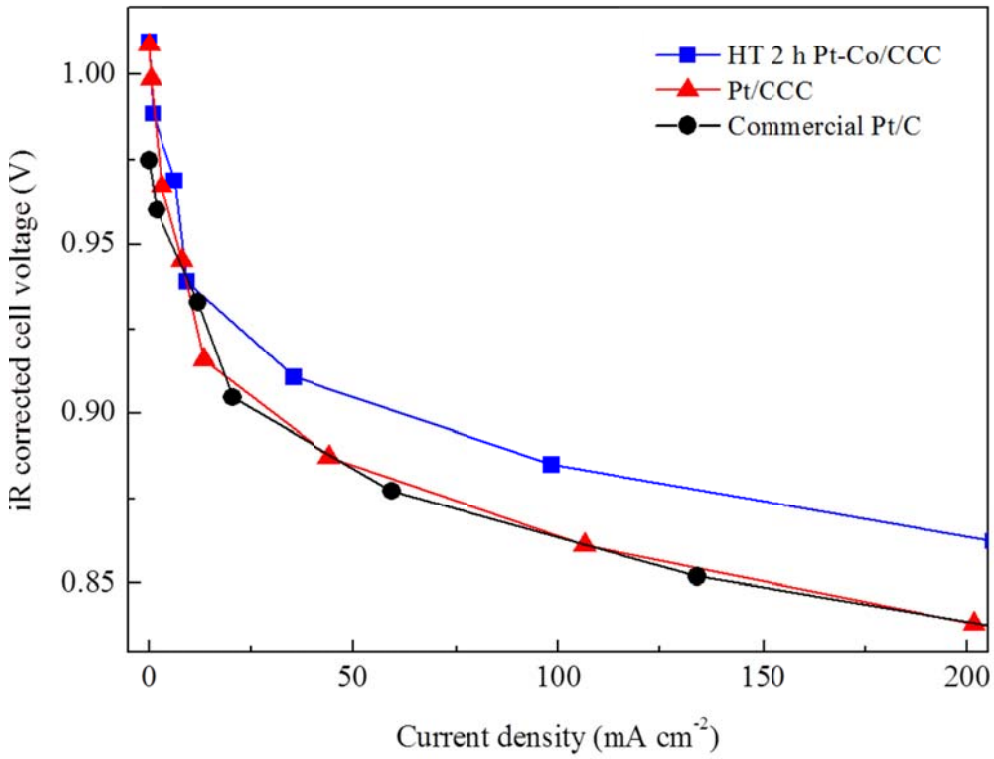

Figure 4.8 Comparison of OCVs on H_2/O_2 polarization curves for commercial Pt/C, Pt/CCC, and 2 h heat treated Pt-Co/CCC.

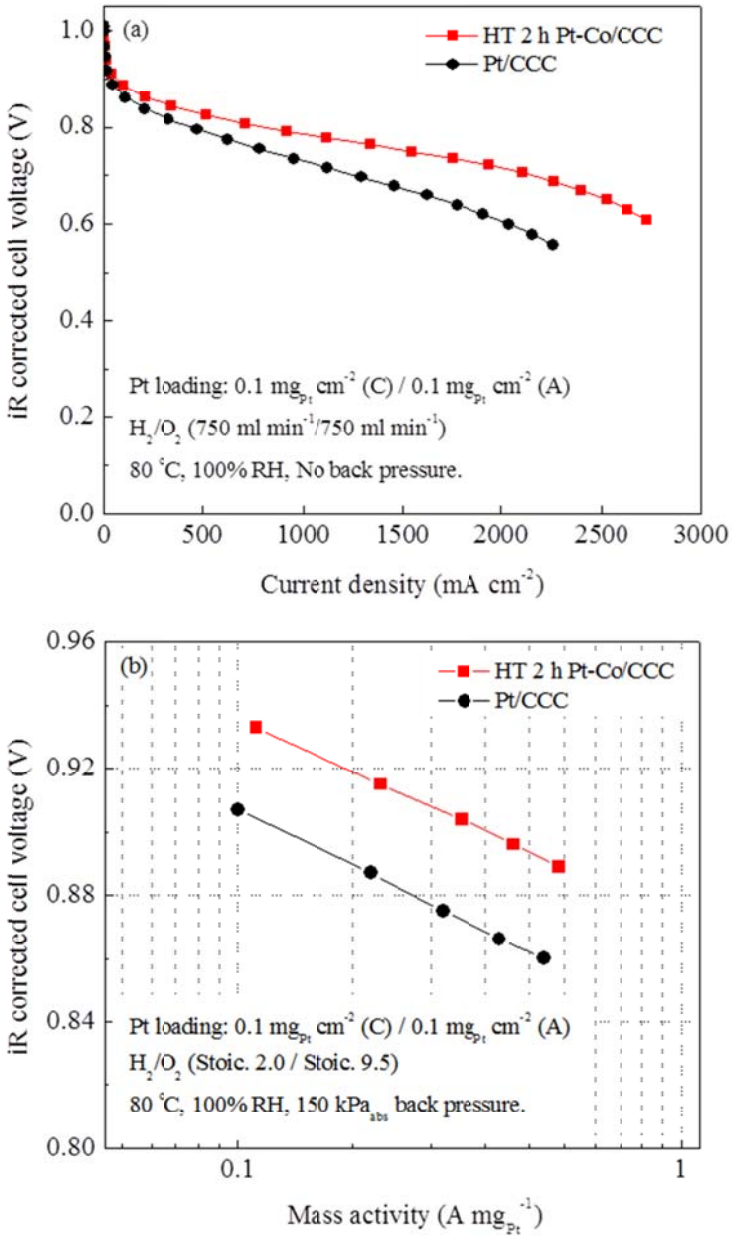

Figure 4.9 Comparison of (a) H_2/O_2 polarization curves and (b) mass activity results for Pt/CCC and 2 h heat treated Pt-Co/CCC catalysts.

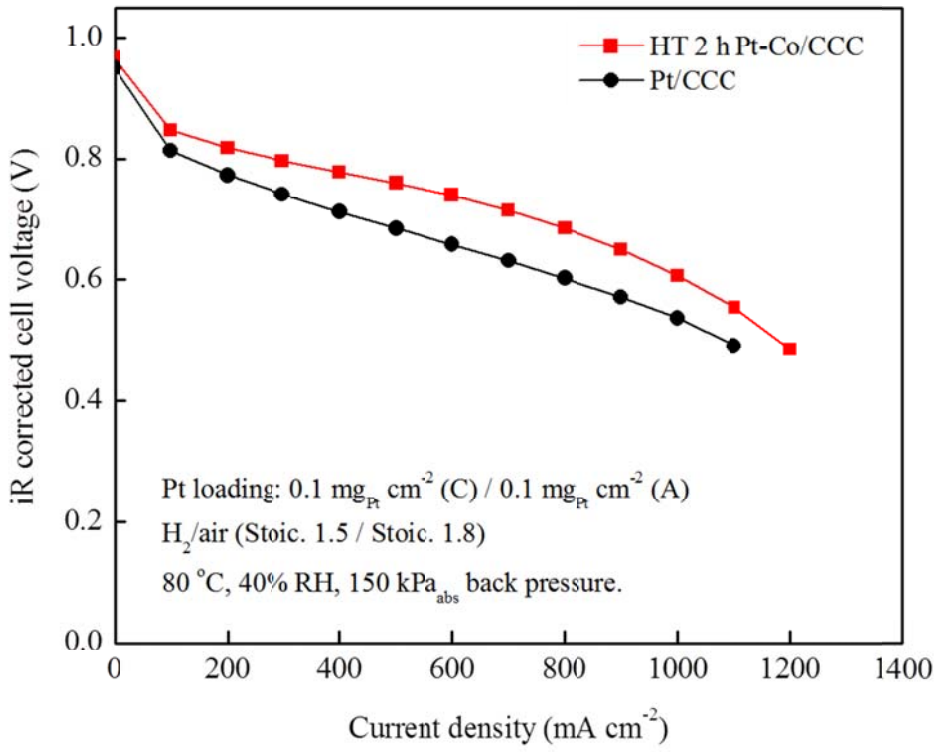

Figure 4.10 Comparison of H_2/air polarization curves for Pt/CCC and 2 h heat treated Pt-Co/CCC.

Table 4.1 Summary of the deconvolution of the Pt(220) peaks and particle sizes for Pt/CCC and Pt-Co/CCC catalysts heat treated at 800 °C for 0.5, 1, 2, and 4 h.

Heat treatment time (h)	Pt peak (deg.)	Pt-Co peak (deg.)	Particle size (nm)
0	67.3	-	2.5
0.5	67.9	69.4	2.8
1	67.8	69.5	3.9
2	-	69.4	3.9
4	-	69.5	4.5

Table 4.2 Summary of electrochemical properties for Pt/CCC and Pt-Co/CCC catalysts heat treated at 800 °C for 0.5, 1, 2, and 4 h.

Heat treatment time (h)	ECSA ($m^2\ g_{Pt}^{-1}$)	Specific oxide formation charge ($C\ mg_{Pt}^{-1}$)	Specific activity at 0.9 V ($mA\ cm^{-2}$)
0	96.3	0.109	0.063
0.5	58.8	0.065	0.095
1	52.8	0.065	0.142
2	42.8	0.048	0.165
4	48.1	0.059	0.138

CHAPTER 5

DEVELOPMENT OF ACTIVATED CARBON COMPOSITE SUPPORT (ACCS) WITH HIGH ACTIVITY AND STABILITY

5.1 Introduction

It is well known that the carbon supported Pt catalysts show improved activity and stability compared to unsupported Pt catalysts due to the high efficiency of well distributed Pt nanoparticles on the carbon support and good interaction of Pt nanoparticles and carbon [197]. Several properties are required for an ideal support material for Pt-based catalysts for PEMFC: (i) good electrical conductivity, (ii) good catalyst-support interaction, (iii) appropriate surface area for catalyst deposition, (iv) mesoporous structure enabling the ionomer to bring the catalyst nanoparticles close to the reactants, i.e. to maximize the triple-phase boundary, (v) good water management capability to avoid flooding, (vi) good corrosion resistance, and (vii) cost-effective for mass production [197]. The choice of support material is vital and highly influential in determining the activity, stability, and cost-effectiveness of the catalyst and the overall PEMFC system.

The HSACB is the most widely used support material in PEMFC due to the high electrical conductivity, high surface area, easy availability, and low cost [197]. However, many studies have shown that HSACB has low resistance towards thermal and electrochemical oxidation because of the HSACB structure containing mainly amorphous

carbon and a small portion of plane graphite carbon, which has an abundance of dangling bonds and defects [43]. The dangling bonds can easily form surface oxides, which results in a higher corrosion rate under electrochemical oxidation. To improve the electrochemical stability of the carbon support and overall Pt/C catalyst, new carbon materials have been tested as support materials for PEMFC, including nano-diamonds [198-200], CNTs [201-203], CNFs [34, 176, 202], CNCs [33, 34], graphene [204, 205], etc. These carbon materials have shown enhanced thermal and electrochemical stability due to higher degree of graphitization of carbon and inert surface structures toward carbon oxidation [201]. However, those properties also act as drawbacks in the preparation of Pt/C catalysts since they do not provide proper active sites for Pt deposition. Furthermore, hydrophobic nature of their surfaces impedes dispersion in a polar solvent thus preventing the Pt deposition on the surfaces [176]. It may cause difficulty in controlling the particle size, uniform distribution of Pt particles, and achieving high metal loading, which results in low activity of catalysts [206]. In order to enhance Pt deposition on these carbons, a surface functionalization is required. However, it makes the preparation more complex and increases the cost. In addition, after attaching the functional groups on carbons, the surface properties are usually influenced, and the stability of functionalized material will be decreased as a result [176]. Relatively high cost of the alternative carbon supports is another huge obstacle although the cost of these materials has fallen continuously in recent years [207].

The activated carbon composite support (ACCS) which was obtained from carbon black has ideal properties for Pt deposition similar to that of carbon blacks. In addition, the preliminary study of thermal stability showed that ACCS has good thermal stability

similar to that of CNFs. From these advantages of ACCS, it was considered as a promising support material for Pt catalyst and was studied extensively in this study. The membrane electrode assembly (MEA) performance and support stability were studied with Pt loading of 0.1 mg cm^{-2} on both cathode and anode electrodes.

To examine the electrochemical stability of carbon support material in PEMFC condition, various methods have been suggested [208]. Generally, it is required to operate more than 5000 h to apply PEMFC to the automotive application [42]. However, it is impractical and inefficient to estimate the stability under practical conditions because of huge testing time and cost. Therefore, various research groups proposed several effective AST methods for testing MEAs and their materials [209-212]. A good AST method should meet several conditions: (i) relatively short testing time, (ii) good selectivity of carbon degradation, and (iii) good degradation behavior of fuel cell performance [213]. To establish appropriate AST protocol to meet all the conditions mentioned above, it is important to understand the mechanism of carbon corrosion at various potential regions and potential profiles (constant potential, triangular cycling, rectangular cycling, etc). Reiser et al. suggested that a cathode interfacial potential difference would be increased up to ~1.5 V due to the "H_2/air front" mechanism in the case of start-up/shut-down process [45]. The same phenomenon also occurs in the case of local hydrogen starvation in the MEA [214]. Furthermore, it has been shown that the cathode potential behavior follows a triangular change with the maximum potential of ~1.5 V when H_2 introduced to the anode compartment [212]. Recently, Hashimasa et al. studied the effects of the potential waveform on carbon corrosion rate by comparing 1.3 V constant potential and 0.9-1.3 V potential cycling [213]. If the carbon corrosion is only affected by high

potential, holding the potential at high value would show high carbon corrosion rate. However, the carbon corrosion rate of 0.9-1.3 V potential cycling was higher than that of 1.3 V constant potential. Park et al. proposed the reason of this phenomenon that de-passivated Pt at the lower potential catalyzes carbon corrosion when potential is increased [215]. The result shows that the potential cycling is more effective than potential holding to test carbon corrosion. But there is still an issue about the lower potential limit of potential cycling; lower potentials than 0.9 V in the potential cycling would also result in Pt degradation through the Pt oxidation and reduction processes [216]. Therefore, the performance loss by carbon corrosion and the one by Pt degradation will be mixed resulting in the poor selectivity of carbon support degradation. Thus, the potential above 1.0 V at which Pt is passivated all the time should be used as the lower potential limit of a potential cycling test to study the carbon support stability without the contribution of Pt degradation. According to all these studies, the potential cycling between 1.0 and 1.5 V would be a good AST protocol to test the carbon support stability in PEMFC. Actually, the FCCJ suggested a potential cycling protocol (1.0-1.5 V, 5000 cycles, 0.5 V s^{-1}) to test the support stability in 2011 [212], and the U.S. DOE revised their previous protocol (1.2 V constant potential for 400 h) with the same potential waveform as the FCCJ in 2013 [217]. The 1.0-1.5 V potential cycling protocol not only correctly simulates the practical startup/shutdown behavior but it also reduces the testing time (2 sec $cycle^{-1}$, < 3 h total). Mukundan reported the comparison of the old protocol (1.2 V constant potential for 400 h) and the new protocol (1.0-1.5 V, 5000 cycles, 0.5 V s^{-1}) of U.S. DOE [218]. It was observed that 200 h constant potential at 1.2 V is equivalent to 2000 cycles at 1.0-1.5 V. According to the result, the author concluded that the new protocol could reduce the

testing time significantly (~100 times) when compared to the old protocol with the same performance decay. Due to the advantages mentioned above, in this study, the 1.0-1.5 V potential cycling protocol has been selected to test the carbon support stability for Pt catalysts deposited on various carbon materials.

5.2 Experimental

5.2.1 Synthesis of activated carbon composite support (ACCS)

The ACCS was synthesized by two-step process - purification and stabilization - from a carbon black.

5.2.2 Carbon thermal stability and thermogravimetric analysis

A variety of carbon supports such as HSACB (Ketjenblack EC-300J, Akzo Nobel), Vulcan XC-72 (Cabot), CCC 1500 °C (In-house), Ensaco 290G (Timcal), ACCS (In-house), CNC (obtained from a collaborating laboratory), and CNF (Sigma-Aldrich) were selected and their thermal stability was measured by heat treatment at 600 °C for 1 h with 10 °C min^{-1} ramping time in a tube furnace with constant air flow (150 ml min^{-1}). The weights before and after heat treatment were measured using a digital balance to calculate the weight loss of each carbon. Complete thermal decomposition of carbons was studied by thermogravimetric analysis (TGA) (Q5000IR, TA Instruments). The experiments were conducted under mixed gas of 10 ml min^{-1} of nitrogen and 25 ml min^{-1} of air. The temperature was increased up to 1000 °C at 10 °C min^{-1} ramping time.

5.2.3 Synthesis of Pt/C catalyst

Platinum nanoparticle deposition with an initial loading of 30 wt. % Pt was carried out using a modified polyol process to control the particle size and to enhance the catalyst-support interaction. In brief, a measured amount of $PtCl_4$ was dissolved in an

appropriate volume of ethylene glycol under vigorous stirring for 30 min. Each carbon was functionalized with PCA solution in order to obtain a uniform Pt particle distribution on the carbon support. Calculated amount of surface modified carbon support was added to the solution so that the desired initial Pt loading was achieved in the final Pt/C catalyst. Then, 0.5 M NaOH was introduced into the solution to adjust the pH in the range between 11 and 12. The resulting suspension was stirred for 1 h at room temperature followed by refluxing at 160 °C for 3 h. The solution was allowed to cool down to room temperature and kept for 12 h under continuous stirring. 0.1 M H_2SO_4 was then added to the cooled mixture and the solution pH was adjusted to 3. The mixture was kept under stirring for 24 h. The catalyst in the solution was filtered and thoroughly washed with DI water. The resulting Pt/C catalyst was dried at 160 °C and stored for further studies.

5.2.4 Material characterization studies

The physical properties of carbon supports and Pt/C catalysts were studied using XRD and HRTEM. XRD patterns were recorded using Rigaku 405S5 to identify the crystalline structure of the supports and catalysts. HRTEM (Hitachi H9500) was used to determine the Pt particle size of Pt/C catalysts.

5.2.5 MEA fabrication and electrochemical measurements

The polarization performances of commercial Pt/C (TEC10E30E, 28.2 wt. % Pt on Ketjenblack EC-300J, Tanaka Kikinzoku Kogyo K.K., Japan), in-house synthesized 30 wt. % Pt/290G (Ensaco 290G carbon support obtained from Timcal), and in-house synthesized 30 wt. % Pt/ACCS catalysts were evaluated in 25 cm^2 MEAs. The 46.7 wt. % commercial Pt/C catalyst (TEC10E50E, 46.7 wt. % Pt on Ketjenblack-EC300J, Tanaka Kikinzoku Kogyo K.K., Japan) was used as the anode catalyst in all the MEAs.

The catalyst inks for the anode and cathode were prepared by blending the catalysts in DI water, isopropyl alcohol, and 5% solution of Nafion® in isopropyl alcohol (Alfa Aesar) in an ultrasonic bath. The catalyst inks were directly deposited onto the Nafion® NRE 212 membrane using a spray gun. The catalyst loadings were fixed at 0.1 mg_{Pt} cm^{-2} and 0.1 mg_{Pt} cm^{-2} confirmed using XRF for cathode and anode, respectively. Commercially available carbon paper (SGL 10 BC) was used as the GDL for both anode and cathode. The catalyst coated membranes were hot-pressed with GDLs at 140 °C for 3 min. under 20 kg cm^{-2} to form MEAs. Initially, the MEA was activated under a supply of H_2 and O_2 at 80 °C to the anode and cathode compartments, respectively, and the initial polarization performance curves were recorded with a flow rate of 750 ml min^{-1} and 100% RH. The catalyst mass activity was evaluated under H_2/O_2 (2.0/9.5 stoic.) at 80 °C, 100% RH, and 150 kPa_{abs} back pressure. The polarization curves were recorded under H_2/air (2/2 stoic.) at 80 °C, 40% RH, and 170 kPa_{abs} back pressure. Electrochemical impedance spectroscopy (EIS) measurement was conducted in the frequency range from 0.025 to 1000 Hz at 10 mA cm^{-2} polarized condition using the in-built EIS analyzer in the Fuel Cell Test System (Model 850e, Scribner Associates, USA) under H_2/air (2/2 stoic.) at 80 °C, 40% RH, and 170 kPa_{abs} back pressure.

Two different DOE suggested AST test protocols are used to evaluate the stability of the catalyst: support stability test under 1.0-1.5 V cycling and catalyst stability test under 0.6-1.0 V cycling. The support stability was evaluated using a simulated start-up/shut-down cycling experiment. The experiment was performed by cycling between 1.0 and 1.5 V for 5000 cycles with 0.5 V s^{-1} scan rate at a cell temperature of 80 °C [217]. The catalyst stability was tested by cycling between 0.6 and 1.0 V for 30000 cycles with

0.05 V s^{-1} scan rate at a cell temperature of 80 °C [217]. During the experiment, pure hydrogen (200 ml min^{-1}) and nitrogen (75 ml min^{-1}) having 100% RH were supplied to the anode and cathode compartments, respectively. The mass activity change under H_2/O_2, the voltage change and the power density change under H_2/air, ECSA under H_2/N_2 after 5000 potential cycles were used to evaluate the support stability.

5.3 Results and discussion

5.3.1 Carbon supports characterization

The thermal stability of various carbons was examined by heat treatment under air flow at 600 °C for 1 h. Figure 5.1 shows the weight retentions after thermal stability test for various carbons. The HSACB, CCC-1500 °C, Vulcan XC-72, Ensaco 290G, ACCS, CNC, and CNF were compared. Two commonly used carbon supports for Pt/C catalyst for PEMFC, namely HSACB (Ketjenblack EC-300J) and Vulcan XC-72, show the lowest weight retention after thermal stability test (1.5% for HSACB and 14.1% for Vulcan XC-72). The CCC-1500 °C obtained from HSACB shows increased thermal retention (24.4%) which agrees with the result of increased degree of graphitization (chapter 2). The Ensaco 290G carbon shows a weight retention of 29.3% which is higher than for HSACB and Vulcan XC-27. The ACCS shows 92.8% retention which is much higher than that of HSACB, Vulcan XC-72, and Ensaco 290G carbons. The high weight retention for ACCS is in similar range of those of CNC and CNF which are highly graphitized carbons. S.M. Andersen et al. [206] claimed that CNF and CNT supports for Pt/C cathode catalyst showed higher thermal stability as well as higher electrochemical stability in MEA test (0 – 1.6 V 15000 cycling) than those of CB support. From the

thermal stability test results, it is expected that the ACCS which showed similar thermal stability as the CNF would show good electrochemical stability in MEA tests.

Among various carbons, HSACB, Ensaco 290G, and ACCS were selected for more detailed thermal decomposition analysis using TGA. Figure 5.2 shows the result of TGA for the three selected carbon supports. The ACCS shows the highest thermal stability by showing highest on-set temperature for decomposition. The HSACB shows the lowest thermal stability and Ensaco 290G shows intermediate thermal stability in between ACCS and HSACB which agrees well with the thermal stability study results presented in Figure 5.1. The starting temperatures of decomposition are 570, 588, and 640 °C for HSACB, Ensaco 290G, and ACCS, respectively.

The XRD patterns of HSACB, Ensaco 290G, and ACCS are shown in Figure 5.3. The crystallite thickness (L_c) calculated by Scherrer's formula and the interlayer spacing (d_{002}) obtained from Bragg's law are used as the factors to determine the degree of graphitization of carbons. It has been reported that higher L_c value of the (002) peak and lower d_{002} number imply a higher degree of graphitization [165, 219]. The ACCS shows L_c value which is almost twice higher than that of HSACB and Enasco 290G, and the lowest d_{002} of 0.349 when compared to the other two supports. From the XRD analysis, a higher degree of graphitization of ACCS compared with the HSACB and Ensaco 290G was observed and it could be attributed to the higher thermal stability of ACCS than HSACB and Ensaco 290G. The weight retentions of various carbons after thermal stability test, the starting temperatures of decomposition on TGA, L_c values, and d_{002} values obtained from XRD analysis are summarized in Table 5.1.

5.3.2 Support stability test (1.0-1.5 V, 5000 cycles)

The 30 wt. % Pt on Ensaco 290G carbon support (Pt/290G) and 30 wt. % Pt on ACCS support (Pt/ACCS) catalysts were synthesized using a modified polyol reduction process. Commercially available 28.2 wt. % Pt/C catalyst (TEC10E30E) was compared with Pt/290G and Pt/ACCS as a cathode catalyst to represent the Pt/HSACB catalyst since Ketjenblack-EC300J HSACB was used as a support material for this commercial catalyst [183]. The XRD patterns of commercial Pt/C, Pt/290G, and Pt/ACCS catalysts are compared in Figure 5.4. The diffraction patterns represent all the reflections corresponding to the face centered cubic (fcc) lattice of Pt supported on various carbon supports. Scherrer's equation was used for calculating the Pt crystallite size using the Pt(220) peak appearing at 67.5° [47, 158]. The d_{Pt} values calculated from the XRD analysis are 1.6, 3.2, and 2.1 nm for the commercial Pt/C, Pt/290G, and Pt/ACCS catalysts, respectively, which are confirmed by the HRTEM images and corresponding particle size distribution shown in Figure 5.5.

The support stability tests were carried out by subjecting the MEAs to a potential cycling test (1.0-1.5 V, 5000 cycles) to simulate the start-up/shut-down conditions of an automotive PEMFC. The corrosion rate of carbon increases drastically at high electrode potentials, and can result in severe degradation of the carbon support via the following reaction [46]:

$$C + 2H_2O \rightarrow CO_2 + 4H^+ + 4e^- \ (E^o = 0.207\ V\ vs.RHE\ at\ 25\ ℃) \qquad (4)$$

Oxidation of the carbon surface increases its hydrophilicity and affects water removal, resulting in an increased mass-transfer resistance. In addition, the oxidation of carbon increases the electrical resistance of the catalysts, leads to the detachment or aggregation of catalyst particles, and damages the cathode catalyst layer structure [51]. Furthermore, the presence of Pt increases the corrosion rate by catalyzing the carbon oxidation [206].

Figure 5.6 shows H_2/air fuel cell polarization curves for the three different cathode catalysts. After 5000 cycles, the Pt/ACCS shows no loss in H_2/air performance indicating good support stability under high potentials (Figure 5.6(c)). On the other hand, commercial Pt/C catalyst shows 69.5% power density loss only after 1000 cycles and a further decrease to 88.7% after 5000 cycles (Figure 5.6(a)). The Pt/290G catalyst shows moderate stability with 22.5% power density loss until 2000 cycles and a rapid decay between 2000 and 5000 cycles resulting in overall power density loss of 84.0% (Figure 5.6(b)). Mass activities under H_2/O_2 operating conditions at 0.9 $V_{iR\text{-}corr}$ were measured before and after support stability test to examine the kinetic performance changes of these three catalysts (Figure 5.7). The Pt/ACCS catalyst shows no loss after the support stability test while commercial Pt/C and Pt/290G catalysts show 57.5% and 66.2% losses, respectively. Similar trends were observed in EIS analysis (Figure 5.8). Commercial Pt/C and Pt/290G catalysts show an increase of charge-transfer resistance after the support stability test, but Pt/ACCS shows a small decrease of resistance which may due to the activation effect. The maximum power densities and mass activities before and after stability test for commercial Pt/C, Pt/290G, and Pt/ACCS catalysts are summarized in Table 5.2.

The good support stability of ACCS was attributed to the higher degree of graphitization of ACCS than HSACB and Ensaco 290G supports which was confirmed by XRD analysis. Also, it could be elucidated by the hydrophobic character of ACCS since carbon corrosion occurs in the presence of water [35]. In order to determine the hydrophilic/hydrophobic nature, the carbon supports were dispersed in water/hexane mixture (Figure 5.9). The HSACB and Ensaco 290G carbons are mainly dispersed in the water phase which indicates the hydrophilicity of these carbons. On the other hand, ACCS shows dispersion mainly in the hexane phase while only a small amount of carbon is dispersed in the water phase which shows good hydrophobic property for ACCS when compared with the other two carbons. The enhanced hydrophobic property of ACCS is also confirmed by the contact angle measurement. As shown in Fig. 5.10, ACCS shows a contact angle of 132° which is much greater than that for HSACB (38°) and Ensaco 290G (32°) carbons. The enhanced hydrophobic property of ACCS can minimize water adsorption on the carbon surface resulting in less carbon corrosion. Furthermore, the difference in hydrophobicity affects the H_2/air fuel cell performance in the mass-transport region. While commercial Pt/C and Pt/290G show current densities of 950 mA cm^{-2} and 1250 mA cm^{-2} at 0.6 $V_{iR\text{-}corr}$, respectively, Pt/ACCS shows 1700 mA cm^{-2} at 0.6 $V_{iR\text{-}corr}$. The higher H_2/air fuel cell performance of Pt/ACCS is due to (i) optimized support properties such as BET surface area which resulted in thin catalyst layer thus favoring effective mass-transfer to the Pt catalytic sites and (ii) hydrophobicity of the ACCS support which results in better water removal during high current operation.

5.3.3 Catalyst stability test (0.6-1.0 V, 30000 cycles)

The DOE suggested catalyst stability test method was used (potential cycling between 0.6 to 1.0 V for 30000 cycles) for the catalyst stability test. Figure 5.11 shows the H_2/air polarization performance of catalyst stability test result for Pt/ACCS and commercial Pt/C cathode catalyst. The Pt/ACCS catalyst shows an initial power density of 0.173 g_{Pt} kW^{-1} with a potential loss of 73 mV (iR-corr) at 0.8 A cm^{-2} after 30000 potential cycles between 0.6 and 1.0 V. The commercial Pt/C shows the initial power density of 0.268 g_{Pt} kW^{-1} and no activity at 0.8 A cm^{-2} after 30000 cycles. Figure 5.12 shows initial mass activity of 0.193 A mg_{Pt}^{-1} and the stability of mass activity for the Pt/ACCS catalyst subjected to potential cycling between 0.6 and 1.0 V. The catalyst stability test resulted in 52% mass activity loss after 30000 cycles for Pt/ACCS catalyst. The commercial 46% Pt/C catalyst shows 0.184 A mg_{Pt}^{-1} initial mass activity and 60% loss after 30000 cycles. The cell voltages, rated power densities, mass activities and ECSAs before and after stability test for Pt/ACCS and commercial Pt/C are summarized in Table 5.3.

5.4 Conclusion

The ACCS was employed as a support material for Pt/C cathode catalyst to improve the catalytic activity and stability under PEMFC operating conditions. Pyrolysis at 600 °C result showed similar thermal stability for ACCS and CNF supports. Also, complete decomposition study by TGA confirmed the good thermal stability of ACCS. Potential cycling between 1.0 and 1.5 V for 5000 cycles showed no loss in both H_2/air fuel cell performance and mass activity for the Pt/ACCS catalyst while commercial Pt/C and Pt/290G showed drastic performance losses after the stability test. The good stability

of ACCS at high potentials is attributed to the higher degree of graphitization which was confirmed by XRD analysis and better hydrophobic nature of ACCS when compared to HSACB and Ensaco 290G carbons. Catalyst stability under 0.6-1.0 V cycling test of Pt/ACCS catalyst showed improved stability than commercial Pt/C catalyst too.

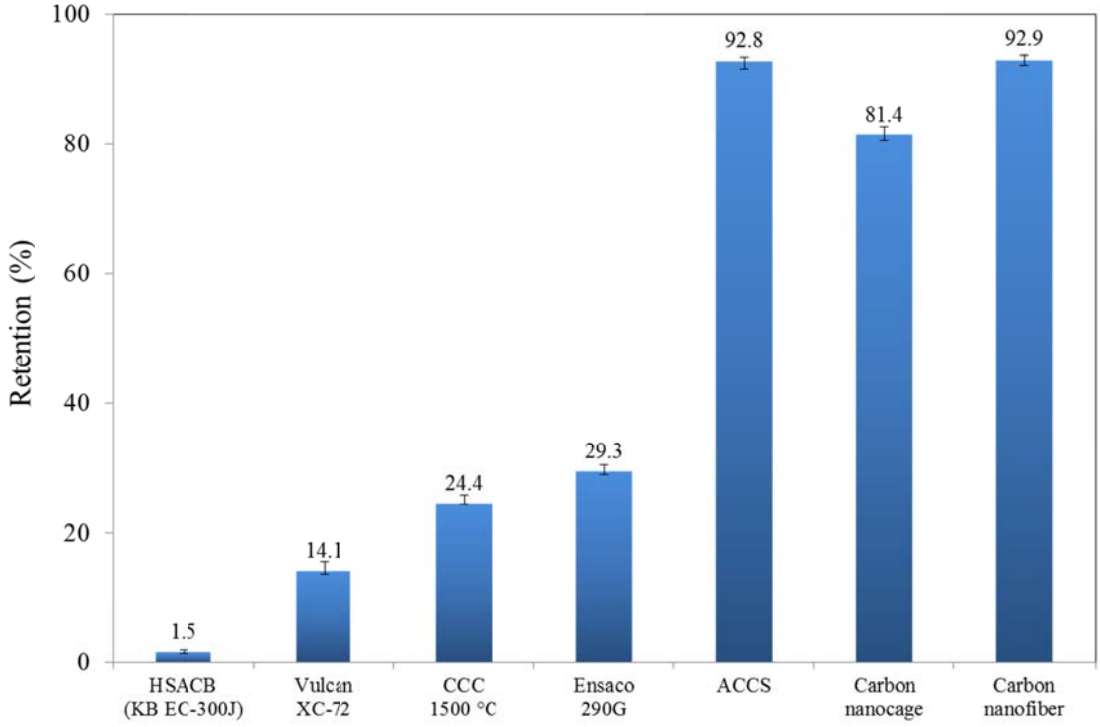

Figure 5.1 The weight retentions of various carbons after thermal stability test at 600 °C.

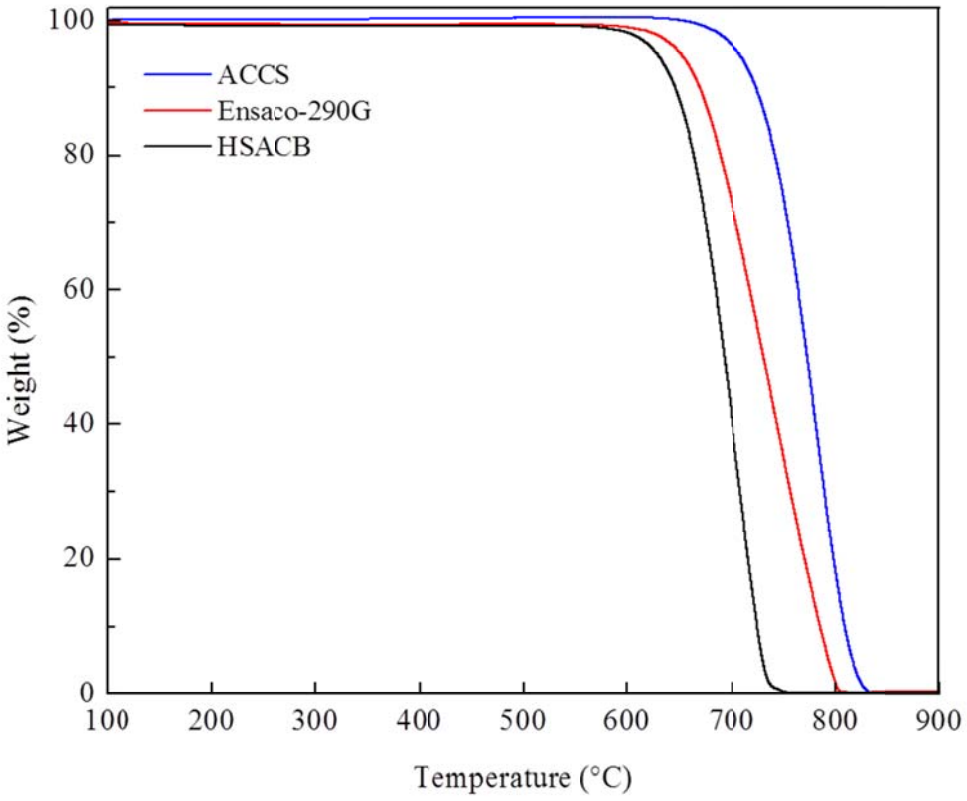

Figure 5.2 Comparison of TGA profiles for HSACB, Ensaco 290G, and ACCS.

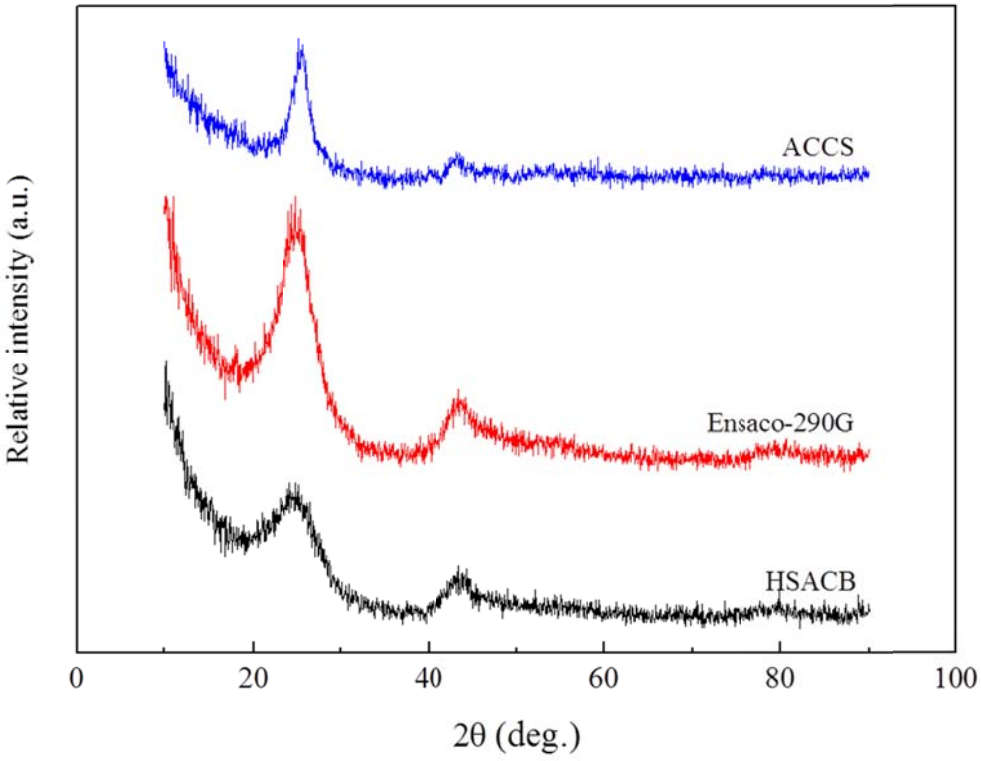

Figure 5.3 Comparison of XRD patterns for HSACB, Ensaco 290G, and ACCS.

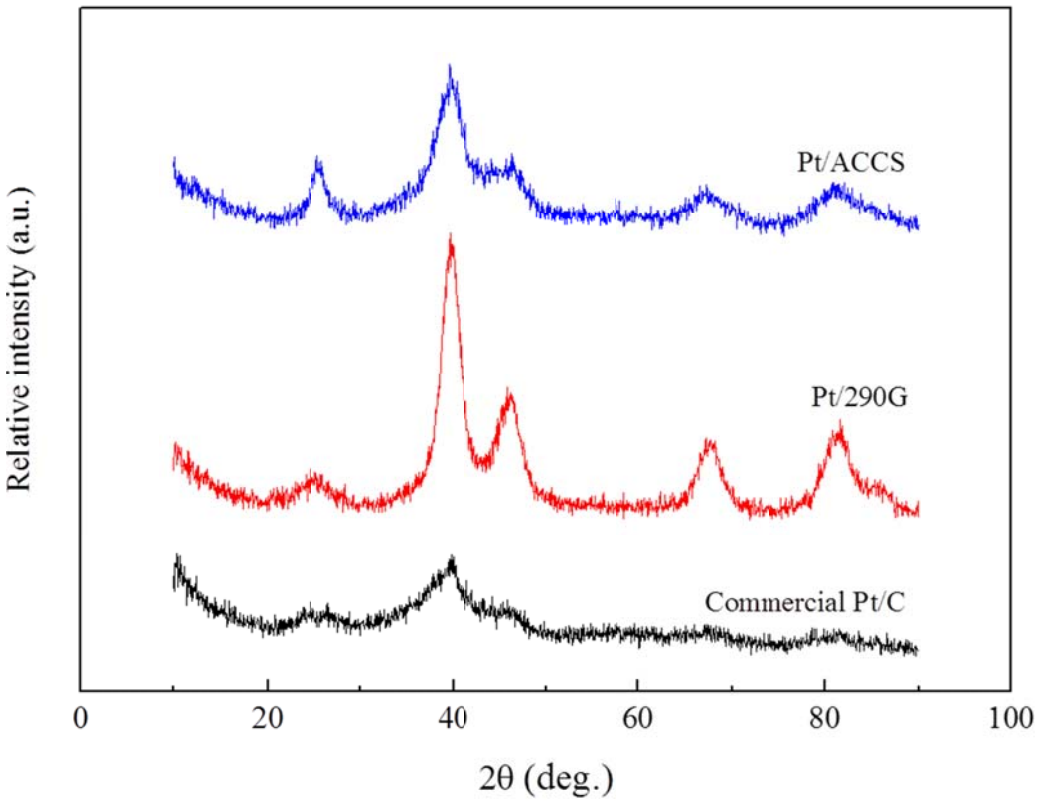

Figure 5.4 Comparison of XRD patterns for commercial Pt/C, Pt/290G, and Pt/ACCS.

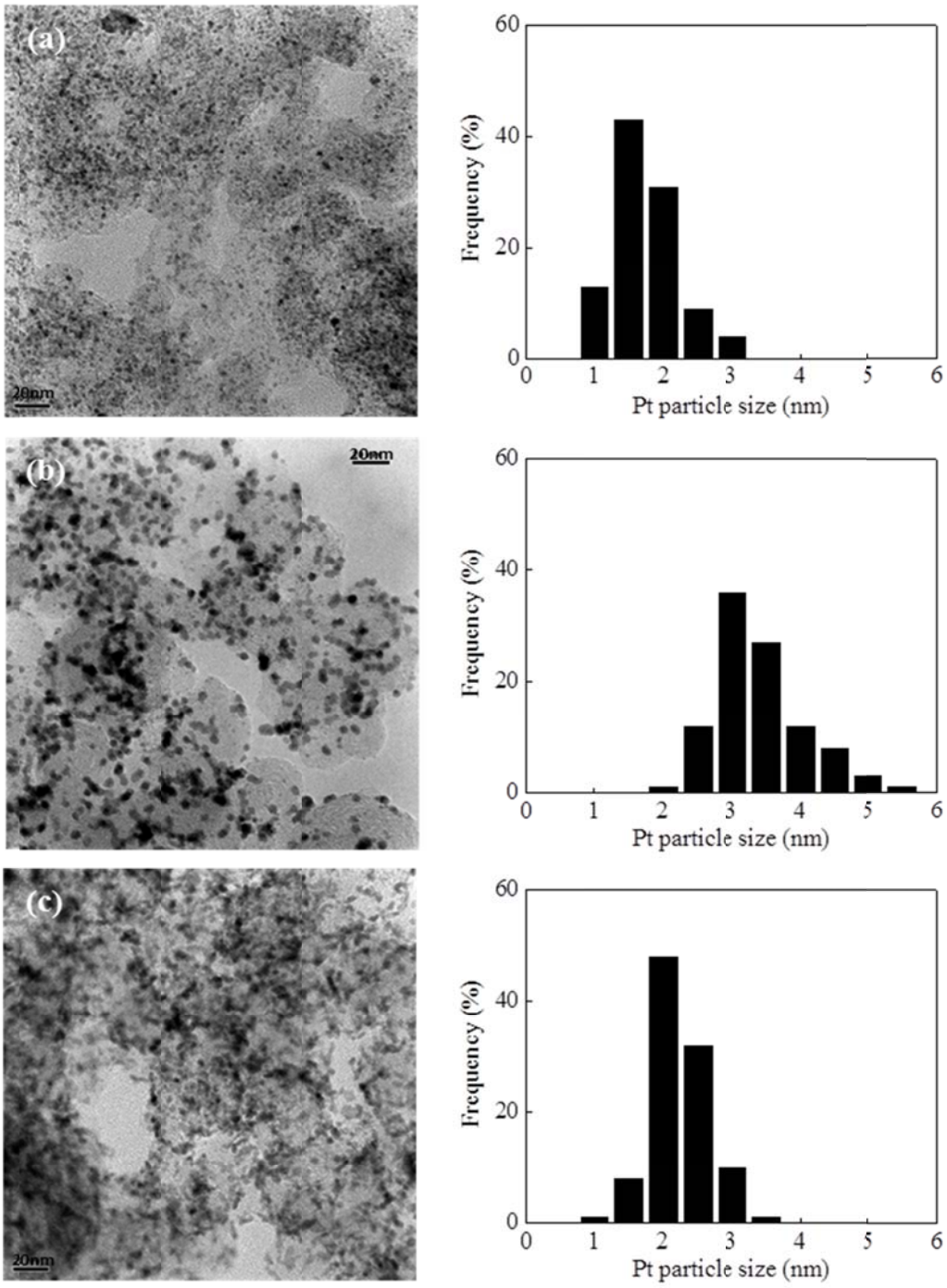

Figure 5.5 HRTEM images and Pt particle size distributions of (a) commercial Pt/C, (b) Pt/290G, and (c) Pt/ACCS. The scale bar is 20 nm.

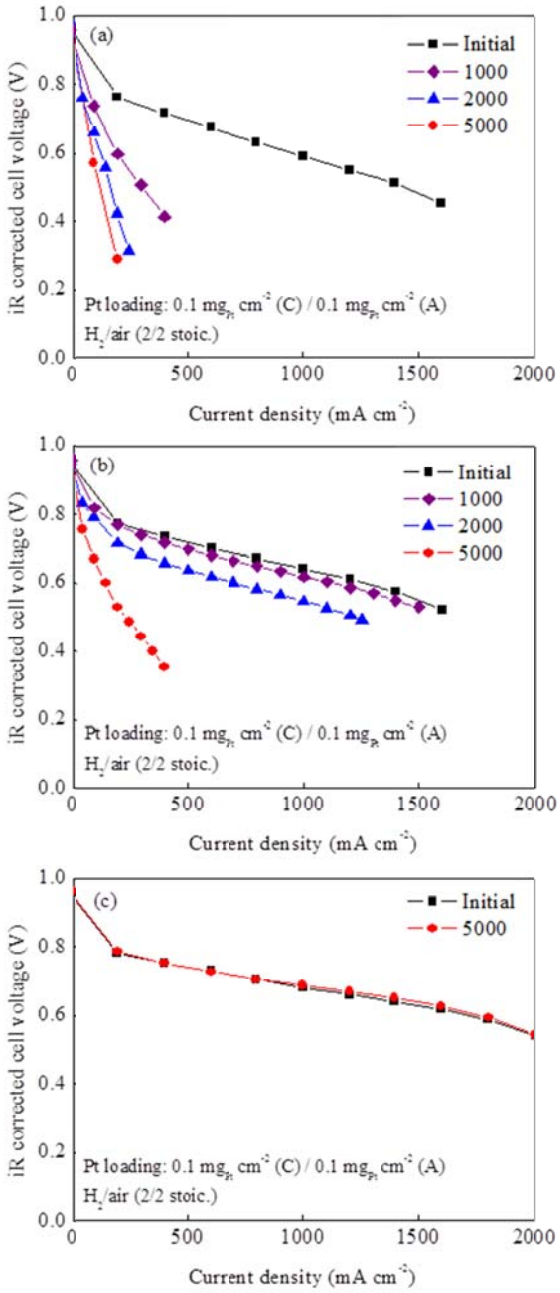

Figure 5.6 H_2/air polarization curves of (a) commercial Pt/C, (b) Pt/290G, and (c) Pt/ACCS cathode catalysts before and after the support stability test (1.0-1.5 V potential cycling for 5000 cycles).

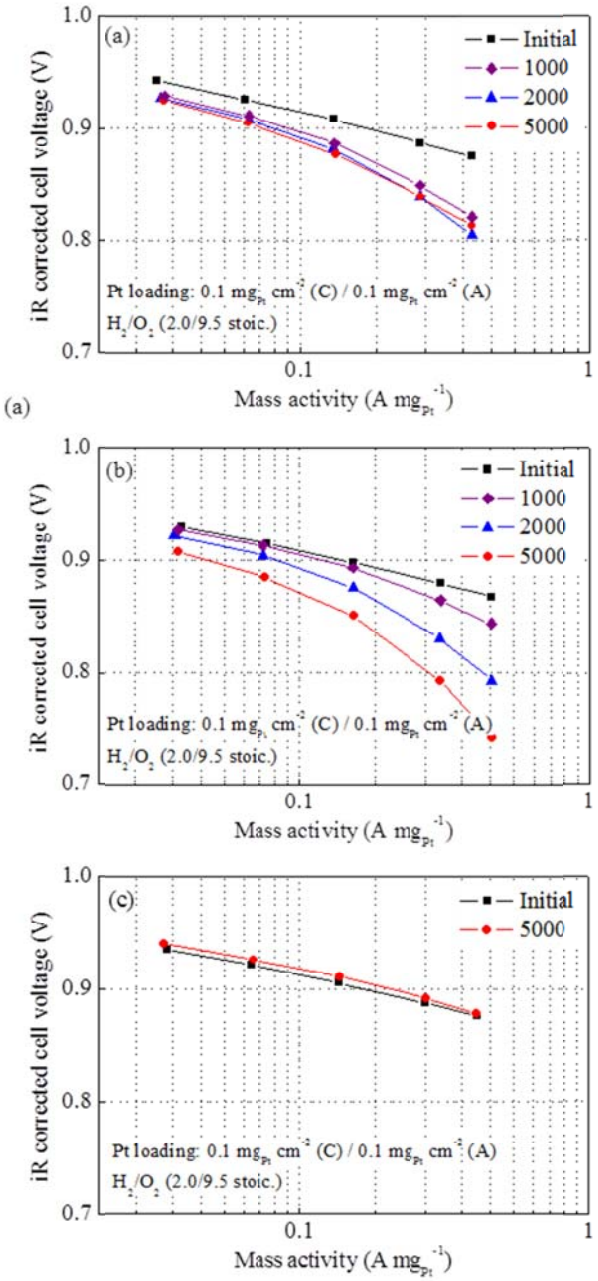

Figure 5.7 Mass activities under the H_2/O_2 condition of (a) commercial Pt/C, (b) Pt/290G, and (c) Pt/ACCS cathode catalysts before and after the support stability test (1.0-1.5 V potential cycling for 5000 cycles).

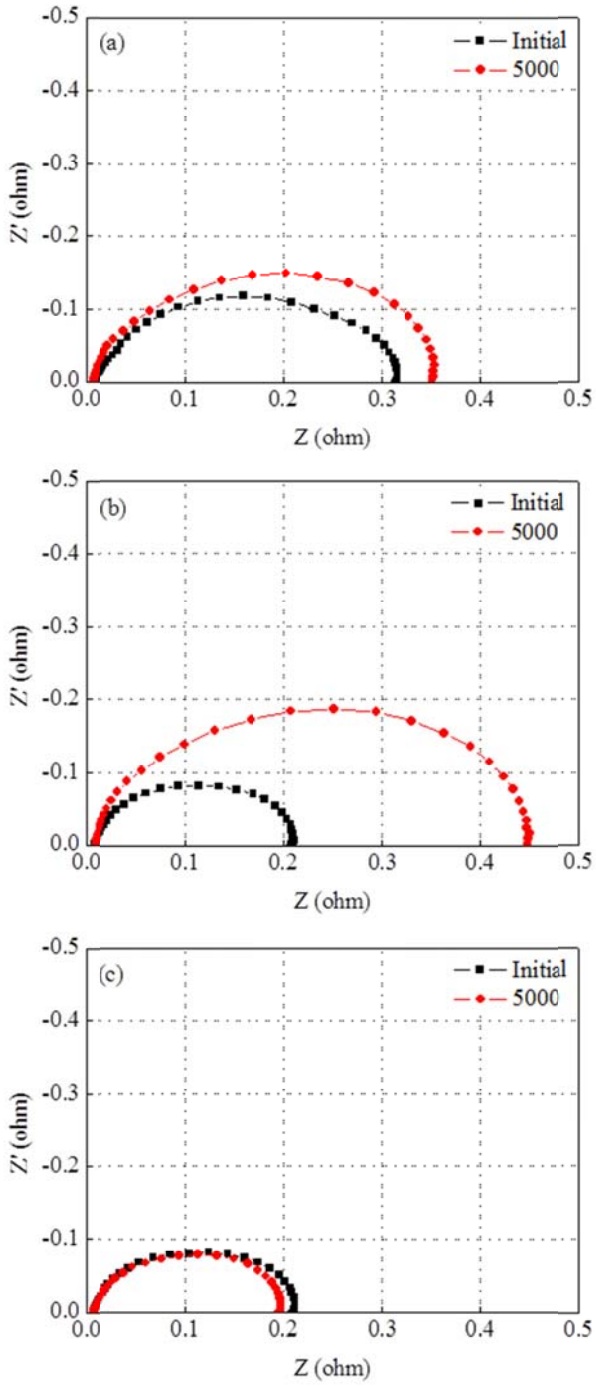

Figure 5.8 EIS plots under the H_2/air condition of (a) commercial Pt/C, (b) Pt/290G, and (c) Pt/ACCS cathode catalysts before and after the support stability test (1.0-1.5 V potential cycling for 5000 cycles).

Figure 5.9 Dispersion of HSACB, Ensaco 290G, and ACCS in water/hexane mixture.

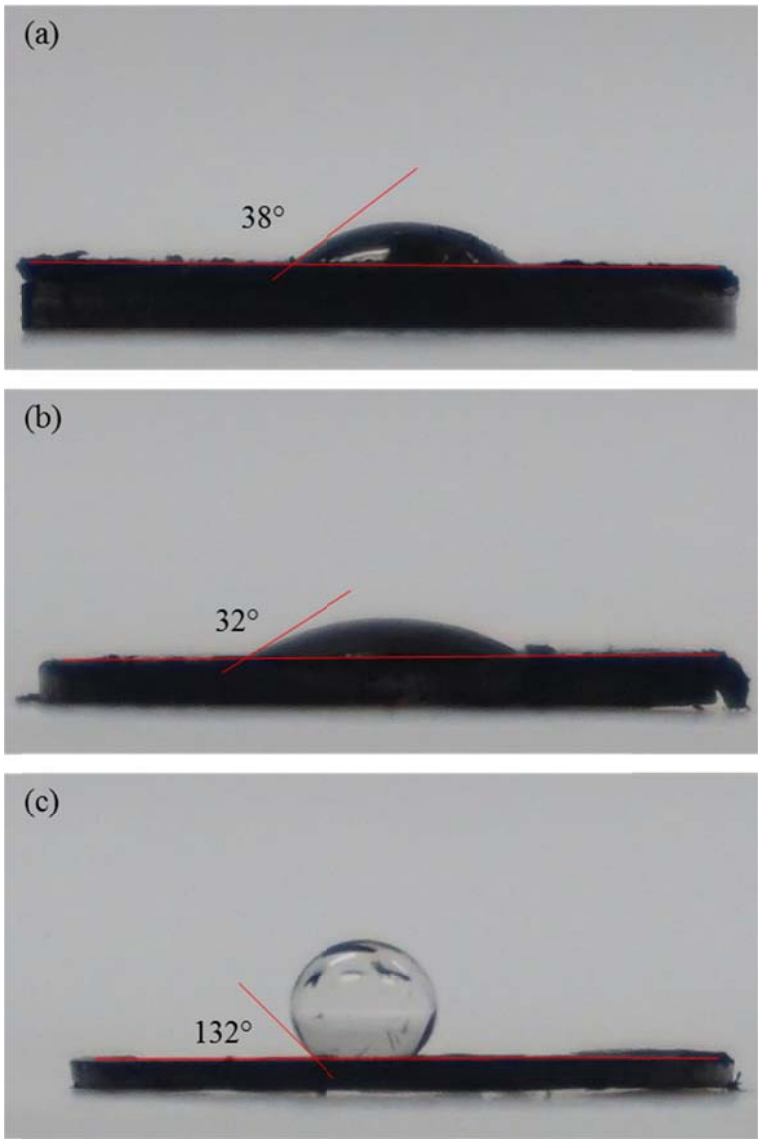

Figure 5.10 Contact angle measurements on (a) HSACB, (b) Ensaco 290G, and (c) ACCS.

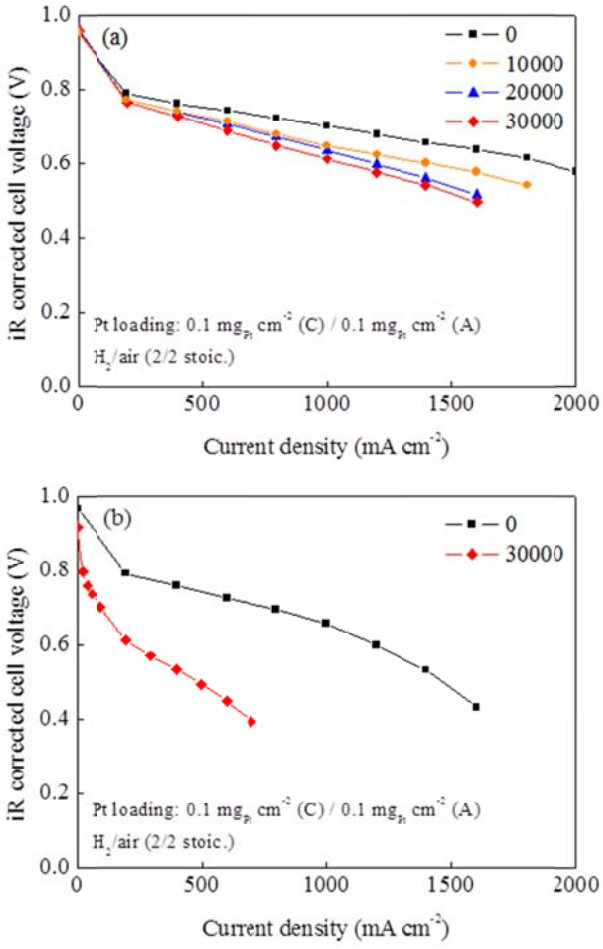

Figure 5.11 H_2/air polarization curves of (a) Pt/ACCS and (b) commercial Pt/C cathode catalysts before and after the catalyst stability test (0.6-1.0 V potential cycling for 30000 cycles).

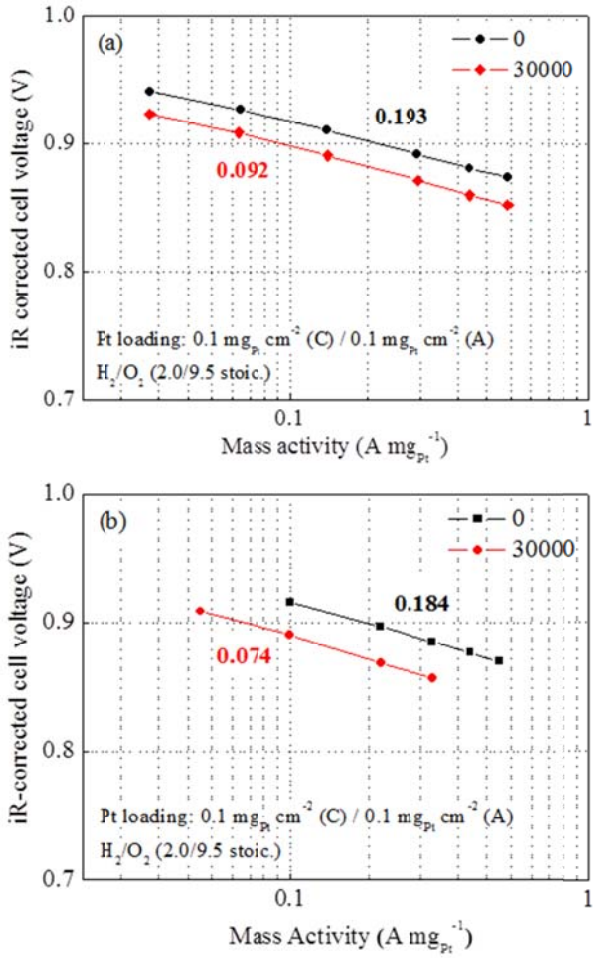

Figure 5.12 Mass activities under the H_2/O_2 condition of (a) Pt/ACCS and (b) commercial Pt/C cathode catalysts before and after the catalyst stability test (0.6-1.0 V potential cycling for 30000 cycles).

Table 5.1 List of carbons and physical properties of various carbons.

Sample	Weight retention after heat treatment at 600 °C (%)	Starting temp. of decomposition (°C) (TGA)	L_c (nm) (XRD)	d_{002} (nm) (XRD)
HSACB	1.5	570	1.8	0.361
Vulcan XC-72	14.1	-	-	-
CCC 1500 °C	24.4	-	-	-
Ensaco 290G	29.3	588	2.0	0.358
ACCS	92.8	640	4.0	0.349
CNC	81.4	-	-	-
CNF	92.9	-	-	-

Table 5.2 Comparison of fuel cell performances of commercial Pt/C, Pt/290G, and Pt/ACCS catalysts before and after the support stability test (1.0-1.5 V potential cycling for 5000 cycles).

Sample	Max. power density (mW cm^{-2})			Mass activity (A mg_{Pt}^{-1})		
	Initial	After 5k cycles	Change (%)	Initial	After 5k cycles	Change (%)
Commercial Pt/C	495	56	−88.7	0.167	0.071	−57.5
Pt/290G	530	85	−84.0	0.139	0.047	−66.2
Pt/ACCS	722	793	9.8	0.165	0.167	1.0

Table 5.3 Comparison of fuel cell performances of Pt/ACCS and commercial Pt/C catalysts before and after the catalyst stability test (0.6-1.0 V potential cycling for 30000 cycles).

Catalyst/Test	Cell voltage (mV) @ 1.5 A/cm^2 for support stability @ 0.8 A/cm^2 for catalyst stability		Rated power density (g_{Pt} kW^{-1})		Mass activity (A mg_{Pt}^{-1})		ECSA (m^2 g_{Pt}^{-1})	
	Initial	Final	Initial	Final	Initial	Final	Initial	Final
Pt/ACCS								
Support stability (1.0-1.5 V, 5k)	629	638 (No loss)	0.186	0.174	0.165	0.167 (No loss)	50.0	27.5 (−45%)
Catalyst stability (0.6-1.0 V, 30k)	723	650 (−73)	0.173	0.252	0.193	0.092 (−52%)	41.0	14.0 (−66%)
Commercial Pt/C								
Support stability (1.0-1.5 V, 5k)	481	0 (−481)	0.278	3.460	0.167	0.071 (−58%)	59.8	11.0 (−82%)
Catalyst stability (0.6-1.0 V, 30k)	696	0 (−696)	0.268	0.730	0.184	0.074 (−60%)	62.0	13.6 (−78%)

CHAPTER 6

DEVELOPMENT OF COMPRESSIVE Pt LATTICE CATALYST ON ACCS SUPPORT (Pt*/ACCS) TO IMPROVE ACTIVITY AND STABILITY UNDER 0.6-1.0 V CYCLING

6.1 Introduction

As discussed previously, it is essential to decrease the Pt loading in the MEA by increasing the catalyst activity and stability to meet the cost targets of automotive PEMFC commercialization. One of the promising pathways to achieve a high activity of the catalyst is through the modification of the intrinsic catalyst activity of Pt by doping the catalyst with transition metal that results in the formation of bimetallic surfaces. In the past decades, great progress has been made in developing more active and durable Pt-M catalysts and in understating the factors contributing to their activity enhancements. In the literature, usually two to three-fold specific activity enhancements for the Pt-M catalysts have been reported [4, 12, 220-222]. There have been several attempts made to hypothesize the relationship between the higher activities of Pt-M alloy catalysts over Pt catalysts: a surface roughening effect due to leaching of the alloying metal [223, 224]; decreased lattice spacing of Pt atom [225, 226]; electronic effects of the neighboring atoms on Pt, such as increased Pt d-band vacancy [220, 227] or depressed d-band center energy [228-230]; and decreased Pt oxide/hydroxide formation at high potentials [220, 231]. Some mechanisms are partly coupled with each other, for instance, the decreased

lattice spacing may affect the electronic structure of Pt atoms, which in turn may inhibit the Pt oxide/hydroxide formation.

In the early 1980s, Jalan and Taylor suggested that the nearest-neighbor distance between Pt atoms played an important role in the ORR, the rate determining step being the rupture of O-O bond via various dual-site mechanisms [225]. They proposed that the original distance between the nearest-neighbor atoms on the surface of pure Pt is not ideal for the dual site adsorption of O_2. The introduction of foreign atoms which reduce the Pt nearest-neighbor spacing would result in a higher ORR activity. Mukerjee et al. have reported extensive set of values for five Pt-M alloys (PtCr/C, PtMn/C, PtFe/C, PtCo/C, and PtNi/C) supported on the high surface area carbon supports [220]. The results indicated that 20-30 mV activity gains over Pt/C could be obtained or a 1.2-5.0-fold increase in specific activity and similar increase in mass activity of the Pt-M alloys over Pt. By employing extended X-ray absorption fine structure (EXAFS) and X-ray diffraction (XRD) analysis, contractions in the Pt-Pt bond distances were observed. Also, they found that the Pt-alloys possess higher Pt d-band vacancies than Pt/C in the double-layer potential region (0.54 V vs. RHE), while Pt/C shows higher d-band vacancy relative to alloys in the high potential region (0.84 V vs. RHE) which could be interpreted as a result of the significant adsorption of OH species at high potential on Pt/C, but to a lesser extent on Pt-M alloys.

Various synthesis techniques have been used to develop Pt-M alloy catalysts on carbon supports. Xiong and Manthiram synthesized nanostructured Pt-M/C (M = Fe, and Co) alloy catalysts by a micro-emulsion method and high-temperature treatment [232]. They observed 3-4 times higher mass activities for the Pt-M/C alloy catalysts than Pt/C

catalyst, with Pt-Co/C being the best performing catalyst. Yano et al. succeeded to obtain highly-dispersed Pt and Pt-M/C (M = V, Cr, Fe, Co, and Ni) nano-particles on CB support by the simultaneous reduction of $Pt(acac)_2$ and $M(acac)_x$ in organic nano-capsule with good control of both the particle size and uniform alloy composition [233]. It was observed that ORR activities of Pt-M/CB alloys were 1.3-1.8 times higher than that of Pt/CB catalyst. Qian et al. prepared Pt-M/C (M = Cr, Fe, and Co) using a reverse micelle method [234]. They showed that Pt-M/C catalysts obtained by the reverse micelle method had more uniform particles and narrow particle size distribution than that prepared using the impregnation method. Rao and Viswanathan prepared Pt-M/C (M = Cr, Fe, and Co) catalysts by simultaneous polyol reduction and decomposition of metal precursors with 1,2-hexadecanediol in the presence of nonanoic acid and nonylamine protecting agents [235]. The ORR activities of Pt-M/C catalysts are found to be ~1.5 times higher than that of the as-synthesized and commercial Pt/C catalysts.

It has been reported that the topmost atomic layer of an annealed Pt-M alloy catalyst is composed of pure Pt while the second layer is enriched with the transition metal [229, 236, 237]. These Pt-rich surface catalysts are produced during annealing by the displacement of Pt and M atoms in the first several layers to minimize the total free energy. Xu et al. studied the adsorption of O and O_2 and the dissociation of O_2 on the (111) faces of ordered Pt_3Co and Pt_3Fe alloys and on monolayer Pt skins covering these two alloys [238]. The absolute magnitudes of the binding energies of O and O_2 followed the same order in these two alloy systems: Pt skin < compressed Pt(111) < Pt(111) < unsegregated $Pt_3Co(111)$ or unsegregated $Pt_3Fe(111)$ which were caused by the shifting of the d-band center of Pt-skin and compressed Pt(111). The authors proposed that an

alleviation of poisoning by O and enhanced rates for reactions involving O could be some of the reasons why Pt-skins are more active for the ORR.

Stamenkovic et al. employed the ultra-high vacuum (UHV) and in situ electrochemical methods to prepare, characterize, and study the ORR on polycrystalline Pt_3Ni and Pt_3Co bulk alloys in acid electrolytes [237, 239]. It was found that in 0.1 M $HClO_4$, the catalytic enhancement was greater than that in 0.5 M H_2SO_4 for all the catalysts, and the order of activities was Pt skin > Pt_3Co > Pt_3Ni > Pt. The maximum catalytic activity was found on the Pt-skin on Pt_3Co; 3-4 times higher than that for pure Pt. The enhancement of activity was interpreted by the reduced adsorption of oxygenated species from water onto Pt-skin or Pt-M alloy catalysts, that is, a ~20-30 mV shift in the formation potential of OH_{ad} to more positive potentials on the alloy surfaces, leaving more active Pt sites for the ORR. They found that the relationship between the specific activity and the d-band center position on the Pt-skin or Pt-skeleton surfaces exhibits a volcano shape, with the maximum catalytic activity obtained for Pt_3Co (Figure 6.1) [230]. To create better catalysts than Pt for the ORR, the catalysts should counterbalance two opposing effects, that is, relatively strong adsorption energy of O_2 and reaction intermediates and relatively low coverage by spectator oxygenated species and specifically adsorbed anions. For catalysts that bind O_2 too strongly, the rate is limited by the rate of removing surface oxides and anions and for catalysts that bind O_2 too weakly, the rate is limited by the rate of electron and proton transfer to adsorbed O_2.

Chen et al. [236, 240] observed chemical composition variations within individual nanoparticles of acid-treated Pt_3Co catalysts, which is in good agreement with the formation of percolated Pt-rich regions that extend from the surface to the particle center,

analogous to the skeleton structure proposed previously for bulk Pt-alloy surfaces after acid leaching [230, 241]. The acid-treated Pt_3Co nanoparticles showed ~ 2 times higher specific activity than that of pure Pt nanoparticles. They also annealed the acid-treated Pt_3Co catalyst and found direct evidence of Pt sandwich-segregation surfaces of ordered Pt_3Co nanoparticles with the topmost layer of pure Pt atoms. The specific activity of the annealed nanoparticles was ~ 4 times higher than that of pure Pt nanoparticles. The enhanced ORR activity of acid-treated and annealed Pt_3Co nanoparticles relative to Pt nanoparticles was attributed to compressive strains and ligand effects associated with the percolated and sandwich-segregation structures in nanoparticles near-surface regions, respectively.

From extensive researche about Pt-M catalysts, it has been seen that promising results towards enhancement of ORR activity have been achieved, especially for compressive Pt catalyst obtained from Pt-Co interaction. However, most of these exciting approaches have been tested and characterized only using an RRDE which is very different from that of real PEMFC operating conditions. Moreover, in RRDE studies, the transport of oxygen is limited with the dissolved oxygen in acid electrolytes (~10-12 ppm) and the catalyst surface is entirely wet with the electrolyte forming three-phase (solid-liquid-gas) equilibrium. In this respect, the objectives of this research is to develop Pt-Co catalysts using robust carbon-based supports and perform studies in 25 cm^2 MEAs under H_2/O_2 and H_2/air to investigate the activity and stability of compressive Pt catalyst from Pt-Co under real-time PEMFC operating condition.

6.2 Experimental

6.2.1 Synthesis of Pt*/ACCS catalyst

Pt*/ACCS catalyst was synthesized by the annealing of Pt/ACCS catalyst in the presence of Co under 5% H_2 (balanced with N_2) atmosphere. Annealing temperature was studied in the range of 300 to 900 °C. To prevent Pt particle sintering and agglomeration, a protective coating was applied to Pt/ACCS catalyst before annealing. Also, Pt/Co ratio was studied to investigate the formation of Pt*/ACCS and fuel cell performance as a function of Co amount in the Pt*/ACCS.

6.2.2 Material characterization studies

The physical properties of Pt*/ACCS catalysts were studied using XRD and HRTEM. XRD patterns were recorded using Rigaku 405S5 to identify the crystalline structure of the supports and catalysts. HRTEM (Hitachi H9500) was used to determine the Pt particle size of Pt*/ACCS catalysts.

6.2.3 MEA fabrication and electrochemical measurements

The polarization performances of 30 wt. % Pt*/ACCS catalysts were evaluated in 25 cm^2 MEAs. The 46.7 wt. % commercial Pt/C catalyst (TEC10E50E, 46.7 wt. % Pt on Ketjenblack-EC300J, Tanaka Kikinzoku Kogyo K.K., Japan) was used as the anode catalyst in all the MEAs. The catalyst inks for the anode and cathode were prepared by blending the catalysts in DI water, isopropyl alcohol, and 5% solution of Nafion® in isopropyl alcohol (Alfa Aesar) in an ultrasonic bath. The catalyst inks were directly deposited onto the Nafion® NRE 212 membrane using a spray gun. The catalyst loadings were fixed at 0.1 mg_{Pt} cm^{-2} and 0.1 mg_{Pt} cm^{-2} confirmed using XRF for cathode and anode, respectively. Commercially available carbon paper (SGL 10 BC) was used as the

GDL for both anode and cathode. The catalyst coated membranes were hot-pressed with GDLs at 140 °C for 3 min. under 20 kg cm^{-2} to form MEAs. Initially, the MEA was activated under a supply of H_2 and O_2 at 80 °C to the anode and cathode compartments, respectively, and the initial polarization performance curves were recorded with a flow rate of 750 ml min^{-1} and 100% RH. The catalyst mass activity was evaluated under H_2/O_2 (2.0/9.5 stoic.) at 80 °C, 100% RH, and 150 kPa_{abs} back pressure. The polarization curves were recorded under H_2/air (2/2 stoic.) at 80 °C, 40% RH and 170 kPa_{abs} back pressure.

Two different DOE suggested AST test protocols are used to evaluate the stability of the catalyst: support stability test under 1.0-1.5 V cycling and catalyst stability test under 0.6-1.0 V cycling. The support stability was evaluated using a simulated start-up/shut-down cycling experiment. The experiment was performed by cycling between 1.0 and 1.5 V for 5000 cycles with 0.5 V s^{-1} scan rate at a cell temperature of 80 °C [217]. The catalyst stability was tested by cycling between 0.6 and 1.0 V for 30000 cycles with 0.05 V s^{-1} scan rate at a cell temperature of 80 °C [217]. During the experiment, pure hydrogen (200 ml min^{-1}) and nitrogen (75 ml min^{-1}) having 100% RH were supplied to the anode and cathode compartments, respectively. The mass activity change under H_2/O_2, the voltage change and the power density change under H_2/air, ECSA under H_2/N_2 after 5000 potential cycles were used to evaluate the support stability.

6.3 Results and discussion

6.3.1 Effect of protective coating

Pt*/ACCS catalyst was prepared using a methodology developed at USC. To introduce Pt* catalyst, Co was used for a doping material with an amount which is relevant to Pt_2Co_1 atomic ratio. Figure 6.2 shows the effect of protective coating on the

particle size of Pt*/ACCS catalyst. To activate the Pt-Co interaction, high-temperature annealing was applied. After annealing at 800 °C for 4 h of Co-doped Pt/ACCS catalyst, the peak positions of Pt increased from 39.81° to 40.6-40.9° which indicates good Pt-Co interaction and formation of compressive Pt lattice. However, the particle size was increased to 6.7 nm when no protective coating was used (d_{Pt} = 2.9 nm before heat treatment). The large Pt particle size results in small ECSA and low fuel cell performance. To maintain the Pt particle size after high-temperature annealing, the protective coating was introduced in the process. As shown in Figure 6.2, the particle size was maintained at 3.2 nm after annealing in cases where the protective coating was used. The HRTEM images of Pt/ACCS catalyst and Pt*/ACCS catalysts which were heat treated with a protective coating and without the protective coating are shown in Figure 6.3. The pristine Pt/ACCS shows uniform Pt dispersion on the ACCS. Without the protective coating, large particles are seen in the range between 8 and 20 nm. However, when the protective coating is present, uniform particle distribution is seen with a particle size in the range between 3 and 5 nm.

6.3.2 Effect of annealing temperature

The effect of annealing temperature on the particle sizes of Pt*/ACCS was studied in the temperature range from 300 to 900 °C. In this study, the protective coating was applied to all the samples and all the samples were annealed for 4 h with same Co amount of Pt_2Co_1 atomic ratio. The corresponding XRD patterns of various temperature annealed Pt*/ACCS catalyst are shown in Figure 6.4. The Pt(111) peak is shifted to a higher 2θ value as the annealing temperature is increased. The peak shift is linearly increased up to around 700 °C and is saturated above 700 °C annealing temperature (Figure 6.5). From

this result, we can conclude that more compressive Pt lattice is formed by increasing temperature and formation of compressive Pt lattice is saturated above 800 °C under this condition. The effect of annealing temperature on the particle size is shown in the HRTEM images (Figure 6.6). Up to 800 °C, no significant Pt agglomeration was observed even though they showed larger Pt particle size than a pristine Pt/ACCS catalyst. However, significant particle agglomeration and particle size growth are observed on the Pt*/ACCS catalyst annealed at 900 °C. From the results above, it is reasonable to conclude that choosing the annealing temperature in the range of 700-800 °C for the synthesis of Pt*/ACCS catalyst to maximize the Pt* formation while maintaining good particle size of Pt.

The effect of annealing temperature on the fuel cell performance of Pt*/ACCS with a composition of Pt_2Co_1 is studied. Figure 6.7 shows ECSAs of Pt/ACCS and various temperature annealed Pt*/ACCS catalysts. While the ECSA of Pt/ACCS showed 41.0 $m^2\ g_{Pt}^{-1}$, Pt*/ACCS catalysts showed ECSAs lower than 35 $m^2\ g_{Pt}^{-1}$ due to its relatively large particle size than Pt/ACCS. As annealing temperature increased, Pt particle size increased and ECSA decreased since the ECSA is directly related with the Pt particle size (Eq. 11). The mass activities of Pt/ACCS and Pt*/ACCS catalysts at 0.9 $V_{iR\text{-}corr}$ under H_2/O_2 condition are shown in Figure 6.8. The mass activities of Pt*/ACCS catalysts showed more than two times higher values (> 0.40 A mg_{Pt}^{-1}) than that of Pt/ACCS catalyst (0.193 A mg_{Pt}^{-1}). The mass activity gradually increased to 0.492 A mg_{Pt}^{-1} until 700 °C annealing temperature. The increase in mass activity can be attributed to an increase of Pt* lattice formation as a function of annealing temperature which was confirmed by XRD analysis. At 900 °C, a decrease of mass activity was observed

because of the agglomeration of Pt particles and large particle size of Pt. The H_2/air fuel cell performance was studied to investigate the performance of Pt*/ACCS in the operating condition of automotive application (Figure 6.9). At 0.7 $V_{iR\text{-}corr}$ which is the ohmic loss region, Pt*/ACCS catalysts showed more 100 mA higher current densities than that of Pt/ACCS catalyst in H_2/air polarization. The current densities of 1186 mA cm^{-2} and 1143 mA cm^{-2} were observed at 0.7 $V_{iR\text{-}corr}$ for 700 °C and 800 °C annealed Pt*/ACCS catalyst respectively compared with 1011 mA cm^{-2} for Pt/ACCS catalyst. However, the H_2/air performance at mass transfer limitation region at 0.6 $V_{iR\text{-}corr}$ did not show significant improvement which was observed in mass activity and H_2/air performance at ohmic loss region. The current densities of 1889 mA cm^{-2} and 1800 mA cm^{-2} were observed at 0.6 $V_{iR\text{-}corr}$ for 700 °C and 800 °C annealed Pt*/ACCS catalysts, respectively. These performances are similar values to the pristine Pt/ACCS catalyst (1884 mA cm^{-2} at 0.6 $V_{iR\text{-}corr}$). Also, lower performances than Pt/ACCS catalyst were observed in the case of catalysts synthesized below 600 °C and over 850 °C. For the catalysts annealed below 600 °C, the low H_2/air performances are due to the residual coating materials on Pt particles which cover the active site of Pt. The low performance of the catalysts annealed over 850 °C is attributed to the large Pt particle size and agglomerations which were shown in the HRTEM images.

The reason for this phenomenon is that the H_2/air performance is mainly controlled by the kinetic performance of catalyst at the low current density region but is mostly controlled by the mass transfer limitation including O_2 concentration and water removal at the high current density region. Furthermore, for both Pt/ACCS and Pt*/ACCS, only pure Pt will be present on the catalyst surface at applied potentials of

0.6-0.7 V due to the electrochemical reduction of Pt oxides at that potential. Thus, the H_2/air performance at low potentials will not be greatly affected as much as in the case of mass activity which is measured at 0.9 $V_{iR\text{-}corr}$. However, the most important achievement of the Pt*/ACCS catalyst is the improvement of catalyst stability under 0.6-1.0 V potential cycling experiment. The result of catalyst stability and the mechanism of improvement of catalyst stability will be discussed in a following section. The effect of annealing temperature of Pt*/ACCS catalyst on physical property and electrochemical property is summarized in Table 6.1.

6.3.3 Effect of Pt/Co ratio

The pristine Pt/ACCS catalyst presents high support stability and enhanced catalyst stability when compared to commercial Pt/C catalysts. In order to further improve the catalyst stability, Pt should be doped with Co to induce Pt lattice contraction which decreases Pt dissolution during potential cycling (0.6-1.0 V). However, doping Pt with excess of Co decreases the ORR activity due to Co coverage on the Pt active sites. On the other hand, our results indicated that a smaller Co to Pt ratio may not be effective to provide the compressed Pt strain. Therefore, the Pt to Co ratio plays a significant role in catalyst development and needs to be optimized to synthesize a highly active and stable catalyst.

To investigate the effect of the Pt/Co ratio on Pt*/ACCS catalyst, various Pt/Co ratio from Pt_4Co_1/ACCS to Pt_1Co_1/ACCS were synthesized using same protective coating process and annealing conditions of 800 °C for 4 h. The effect of the Pt/Co ratio on the particle size and Pt structure is shown in Figure 6.10. All Pt*/ACCS catalysts with various Pt/Co ratios showed peak shifts in XRD. The Pt*/ACCS catalyst synthesized with

a higher amount of Co exhibited a higher shift in the 2θ angle indicating a more compressive Pt lattice formation. Furthermore, Pt particle sizes of the Pt*/ACCS catalysts measured by XRD patterns showed the values in the range of 3-4 nm which were well maintained after annealing due to the controlled annealing with protective coating procedure. The mass activity results for Pt/ACCS and Pt*/ACCS synthesized with various Pt/Co ratios are presented in Figure 6.11. As the Co amount increased in the Pt*/ACCS catalyst, mass activity increased due to the formation of a more compressive Pt lattice. While all the Pt*/ACCS catalysts annealed at various temperatures showed Pt(111) 2θ values higher than 40.50° and mass activities above 0.40 A mg_{Pt}^{-1}, Pt_4Co_1/ACCS and Pt_3Co_1/ACCS catalysts showed 2θ values of 40.29° and 40.46° and mass activities of 0.329 and 0.344 A mg_{Pt}^{-1} which are smaller than those of various temperature annealed catalysts. These results indicate that the Pt/Co ratio is a more sensitive factor than the annealing temperature to form a compressive Pt lattice catalyst. The H_2/air fuel cell performance for Pt/ACCS and Pt*/ACCS synthesized with various Pt/Co ratios are shown in Figure 6.12. The H_2/air fuel cell performance of Pt_2Co_1/ACCS and Pt_3Co_1/ACCS catalysts showed similar performance with that of the Pt/ACCS catalyst. The Pt_1Co_1/ACCS catalyst showed lower H_2/air fuel cell performance (1230 mA cm^{-2}) when compared to that of the pristine Pt/ACCS catalyst (1884 mA cm^{-2}) due to the partially covered Pt active sites by an excess Co amount in the Pt_1Co_1/ACCS catalyst.

Based on the physical and electrochemical properties of various Pt*/ACCS catalysts with different Pt/Co ratios, a catalyst with a composition of Pt_3Co_1/ACCS catalyst annealed at 800 °C for 4 h was selected and subjected to support stability and catalyst stability studies under 1.0-1.5 V and 0.6-1.0 V potential cycling conditions,

respectively. The effect of the Pt/Co ratio of Pt*/ACCS catalyst on physical and electrochemical properties is summarized in Table 6.2.

6.3.4 Support stability test (1.0-1.5 V, 5000 cycles)

Prior to the stability tests, the reproducibility of the Pt*/ACCS catalyst was tested by fabricating five different MEAs and testing their fuel cell performances (Figure 6.13). The MEAs showed good agreement of H_2/air performance and mass activity results within ±4% difference. The H_2/air fuel cell performance and mass activity of the Pt*/ACCS catalyst subjected to 1.0-1.5 V potential cycling test is shown on Figure 6.14. The Pt*/ACCS catalyst showed an initial potential of 633 $mV_{iR\text{-}corr}$ at 1.5 A cm^{-2} and a potential loss of 8 mV at 1.5 A cm^{-2} after 5000 potential cycles between 1.0 and 1.5 V. The commercial Pt/C catalyst showed 481 $mV_{iR\text{-}corr}$ at 1.5 A cm^{-2} for initial performance and no activity after only 1000 cycles between 1.0-1.5 V (Figure 5.6 (a)). The mass activity of the Pt*/ACCS catalyst showed 0.341 A mg_{Pt}^{-1} for initial performance and 50% loss after 5000 cycles at 1.0-1.5 V. The commercial Pt/C catalyst showed 0.167 A mg_{Pt}^{-1} initial mass activity and 58% loss after 5000 cycles at 1.0-1.5 V. The good support stability of Pt*/ACCS is attributed to the stable ACCS support as we discussed in chapter 5. The mass activity of Pt*/ACCS showed higher loss than that of Pt/ACCS since Co dissolution is inevitable at high potential region. The dissolution of Co changes the structure of the compressive Pt catalyst and decreases the mass activity which is closely related with the compressive Pt lattice formation as we observed above.

6.3.5 Catalyst stability test (0.6-1.0 V, 30000 cycles)

Figure 6.15 shows the H_2/air fuel cell performance of Pt*/ACCS catalyst tested in 25 cm^2 MEA subjected to 0.6-1.0 V potential cycling test. The Pt*/ACCS catalyst

showed an initial potential of 729 $mV_{iR\text{-}corr}$ at 0.8 A cm^{-2} with a potential loss of 24 $mV_{iR\text{-}corr}$ at 0.8 A cm^{-2} after 30000 potential cycles between 0.6 and 1.0 V. As shown in Table 6.3, the commercial Pt/C showed an initial potential of 699 $mV_{iR\text{-}corr}$ at 0.8 A cm^{-2} and no activity at 0.8 A cm^{-2} after 30000 cycles. The support stability and catalyst stability test results for the Pt*/ACCS catalyst compared with Pt/ACCS and commercial Pt/C catalysts are summarized in Table 6.3.

The positive potential change of Pt oxide formation on Pt-M catalyst when compared to pure Pt has been reported previously [242, 243]. The CV patterns for Pt*/ACCS and Pt/ACCS catalysts indicate a shift of potential of Pt oxide formation by ~40 mV for Pt*/ACCS when compared to Pt/ACCS. During potential cycling from 0.6 to 1.0 V, Pt oxides are formed according to the following reactions [216]:

$$Pt + H_2O \rightarrow PtO + 2H^+ + 2e^- \quad (16)$$

$$Pt + 2H_2O \rightarrow PtO_2 + 4H^+ + 4e^- \quad (17)$$

$$Pt + H_2O \rightarrow PtO(ads) + 2H^+ + 2e^- \quad (18)$$

In the reverse scan from 1.0 to 0.6 V, Pt oxides are reduced to Pt according to the following reactions:

$$PtO + 2H^+ + 2e^- \rightarrow Pt + H_2O \quad (19)$$

$$PtO_2 + 4H^+ + 4e^- \rightarrow Pt + 2H_2O \quad (20)$$

$$PtO(ads) + 2H^+ + 2e^- \rightarrow Pt + H_2O \quad (21)$$

The potential shift for Pt oxidation to higher values increases the mass activity (from 0.193 to 0.344 A mg_{Pt}^{-1}) due to the suppression of Pt oxide formation which has much lower exchange current density for ORR (i^o =1.7×10^{-10} A cm^{-2}) when compared to pure Pt (i^o = 2.8×10^{-7} A cm^{-2}) [244]. Besides the effect of higher mass activity, the Pt* catalyst also illustrates improved stability when compared to the pure Pt catalyst. Since Pt oxide dissolves during potential cycling conditions according to Eq. 22 and Eq. 23, less Pt oxide formation in the forward scan due to higher Pt oxidation potential in the case of the Pt*/ACCS catalyst alleviates Pt dissolution in the reverse scan and enhances the catalyst stability.

$$PtO + 2H^+ \rightarrow Pt^{2+} + H_2O \quad (22)$$

$$PtO_2 + 4H^+ + 2e^- \rightarrow Pt^{2+} + 2H_2O \quad (23)$$

6.4 Conclusion

The Pt*/ACCS catalyst was synthesized according to the methodology developed at USC. To prevent the Pt particle sintering and agglomeration during annealing, the protective coating was applied to the synthesis process. The synthesis parameters including annealing temperature and Pt/Co ratio were studied to optimize the formation of compressive Pt lattice and its fuel cell performances. The fuel cell performance of the Pt*/ACCS catalyst and its support stability under 1.0-1.5 V potential cycling and catalyst stability under 0.6-1.0 V potential cycling were evaluated using a 25 cm^2 MEA. The Pt*/ACCS catalyst showed an initial mass activity of 0.344 A mg_{Pt}^{-1} at 0.9 $V_{iR\text{-}corr}$ and an initial power density (rated) of 0.174 g_{Pt} kW^{-1}. The support stability under 1.0-1.5 V

potential cycling showed a mass activity loss of 50%, a potential loss of 8 mV at 1.5 A cm^{-2}, and an ECSA loss of 22% after 5000 cycles. The catalyst stability under 0.6-1.0 V potential cycling showed a loss of mass activity of 45%, a potential loss of 24 mV at 0.8 A cm^{-2}, and an ECSA loss of 42% after 30000 cycles which were improved over those of the Pt/ACCS catalyst. The improved catalyst stability of Pt*/ACCS is attributed to a lower formation of Pt oxide in the forward scan of 0.6-1.0 V due to a higher Pt oxide formation potential than Pt/ACCS which leads to less dissolution of Pt in the backward scan of 1.0-0.6 V. The Pt*/ACCS catalyst which showed high initial fuel cell performance, good support stability, and good catalyst stability would be an ideal cathode catalyst candidate for automotive application PEMFC.

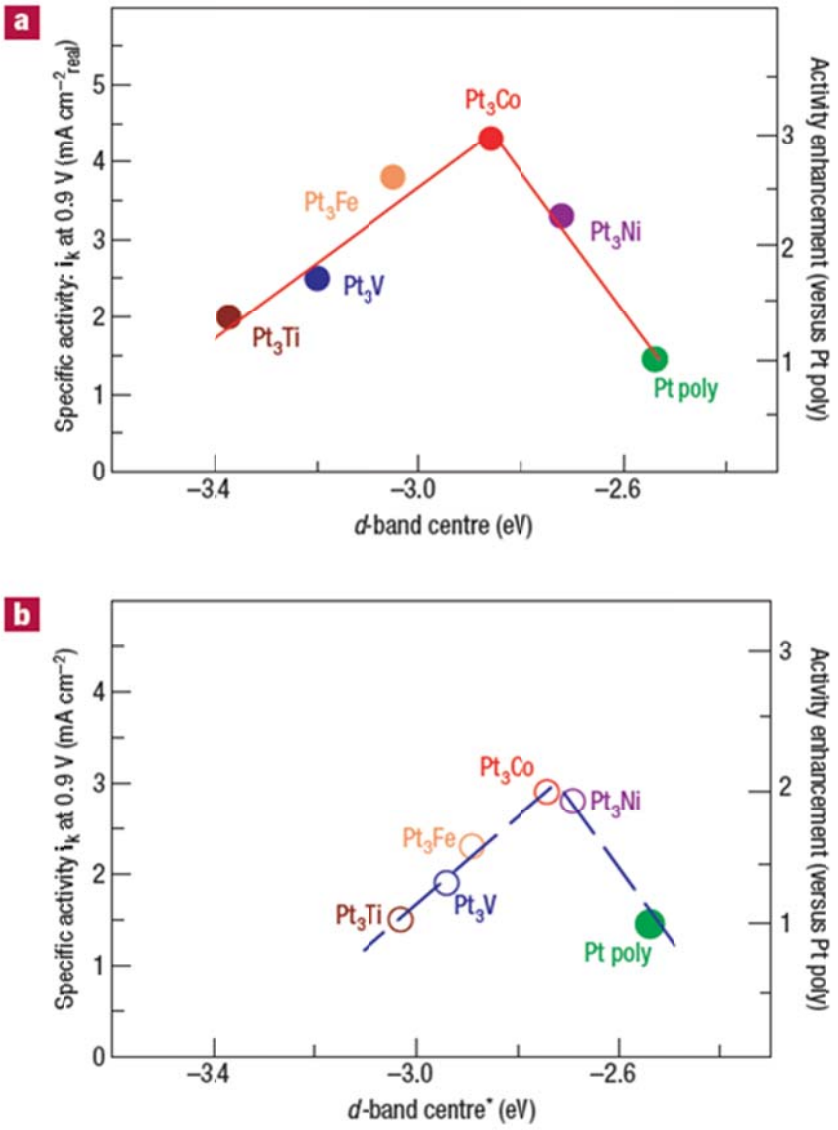

Figure 6.1 Relationships between the catalytic properties and electronic structure of Pt_3M catalysts. Relationships between experimentally measured specific activity for the ORR on Pt_3M surfaces in 0.1M $HClO_4$ at 333 K versus the d-band center position for the Pt-skin (a) and Pt-skeleton (b) surfaces [230].

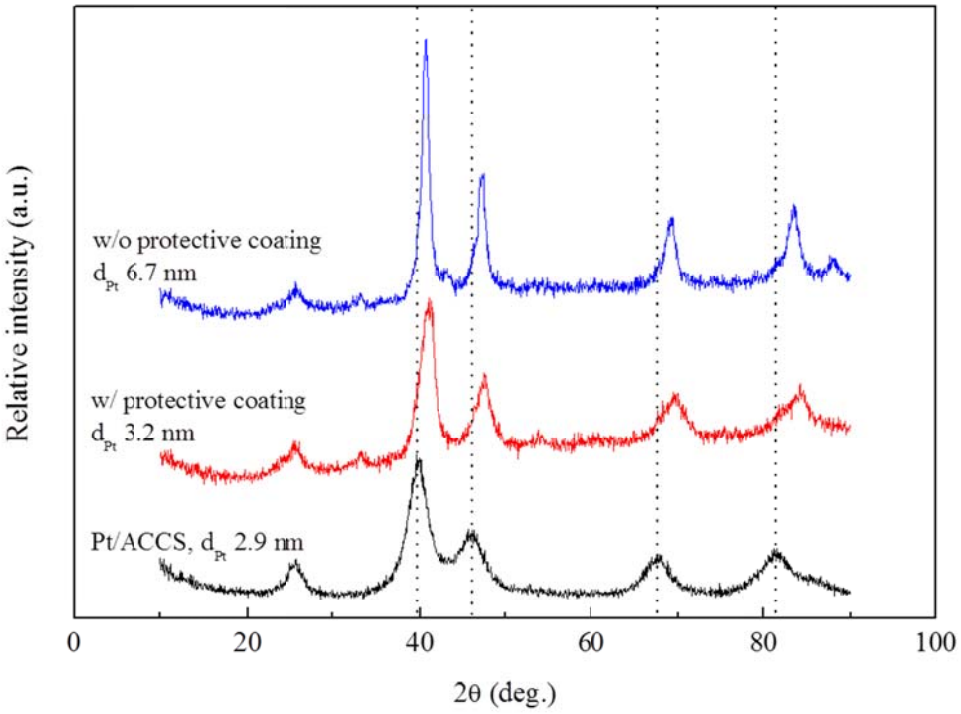

Figure 6.2 Comparison of XRD patterns for Pt/ACCS, Pt*/ACCS catalyst annealed in the presence of protective coating and Pt*/ACCS catalyst annealed without protective coating.

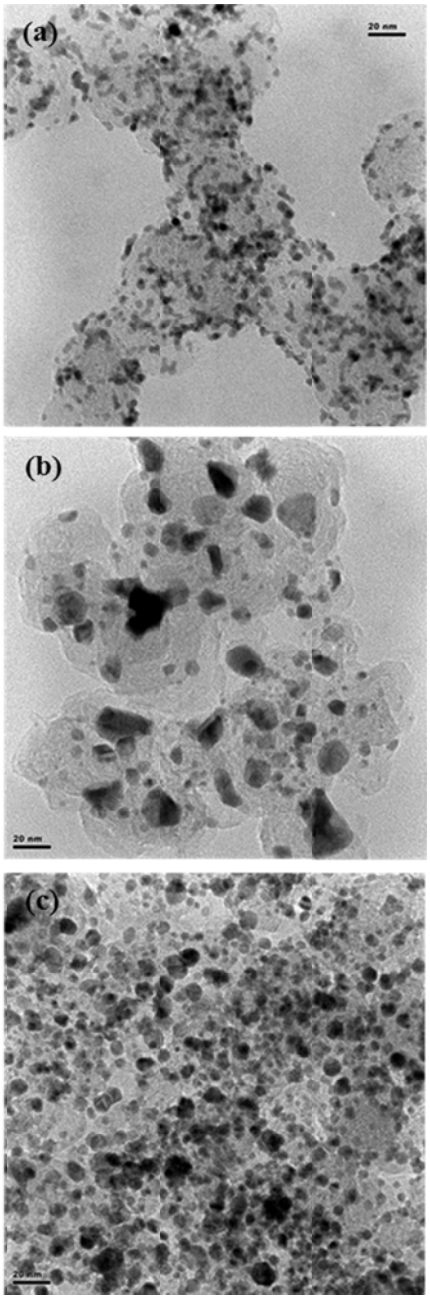

Figure 6.3 HRTEM images of (a) Pt/ACCS, (b) Pt*/ACCS catalyst annealed without protective coating and (c) Pt*/ACCS catalyst annealed in the presence of protective coating.

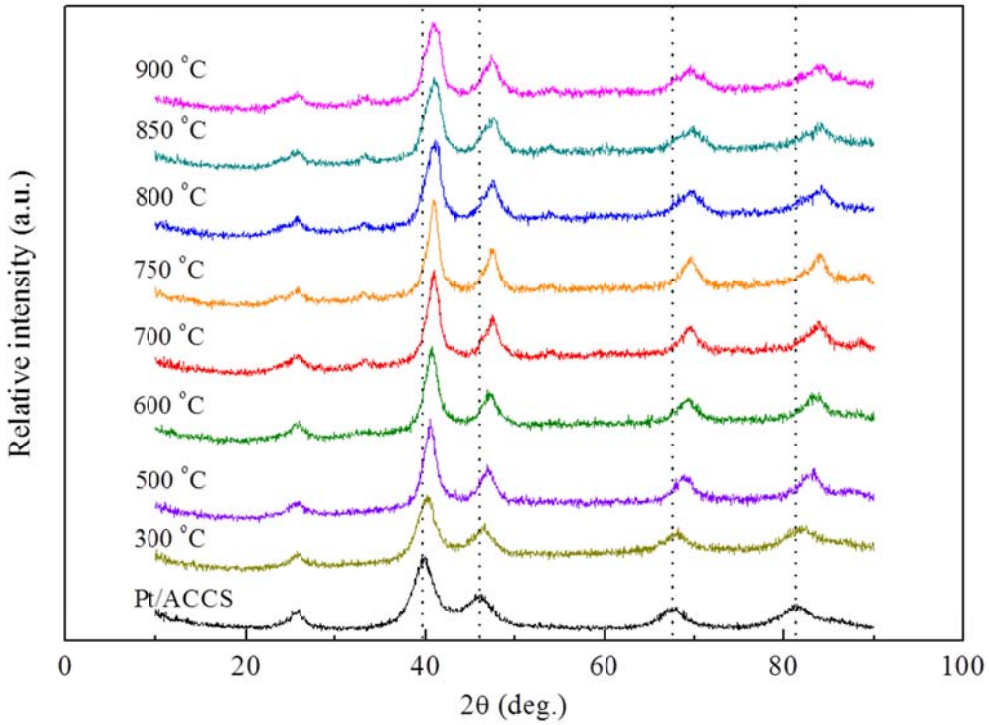

Figure 6.4 XRD patterns for Pt/ACCS and Pt*/ACCS catalysts annealed at various temperatures in the range of 300 to 900 °C.

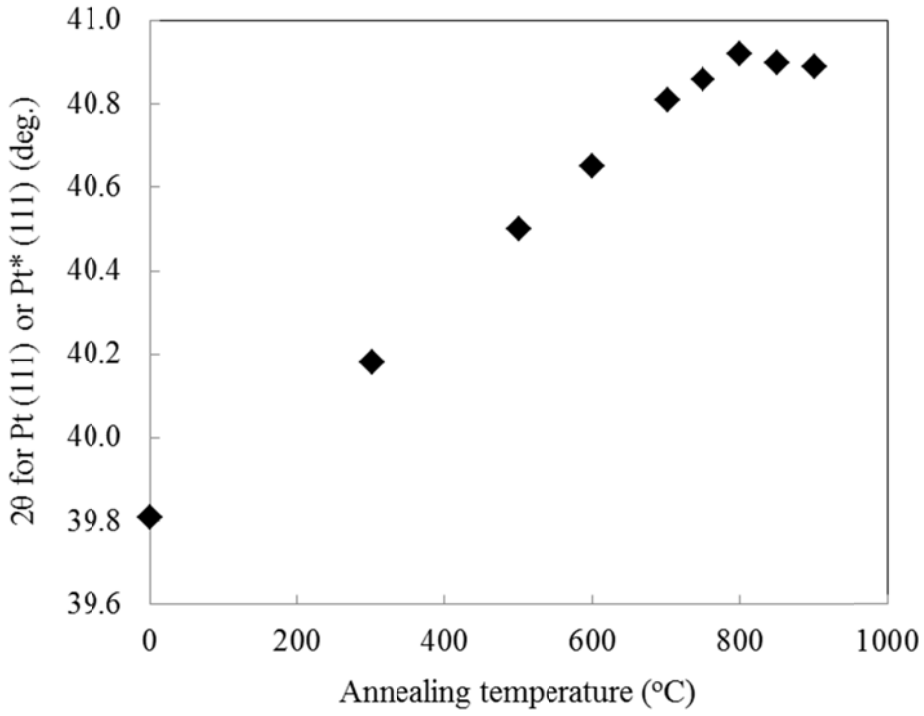

Figure 6.5 Effect of annealing temperature on the change of 2θ values of Pt(111) or Pt*(111) peaks in XRD analysis.

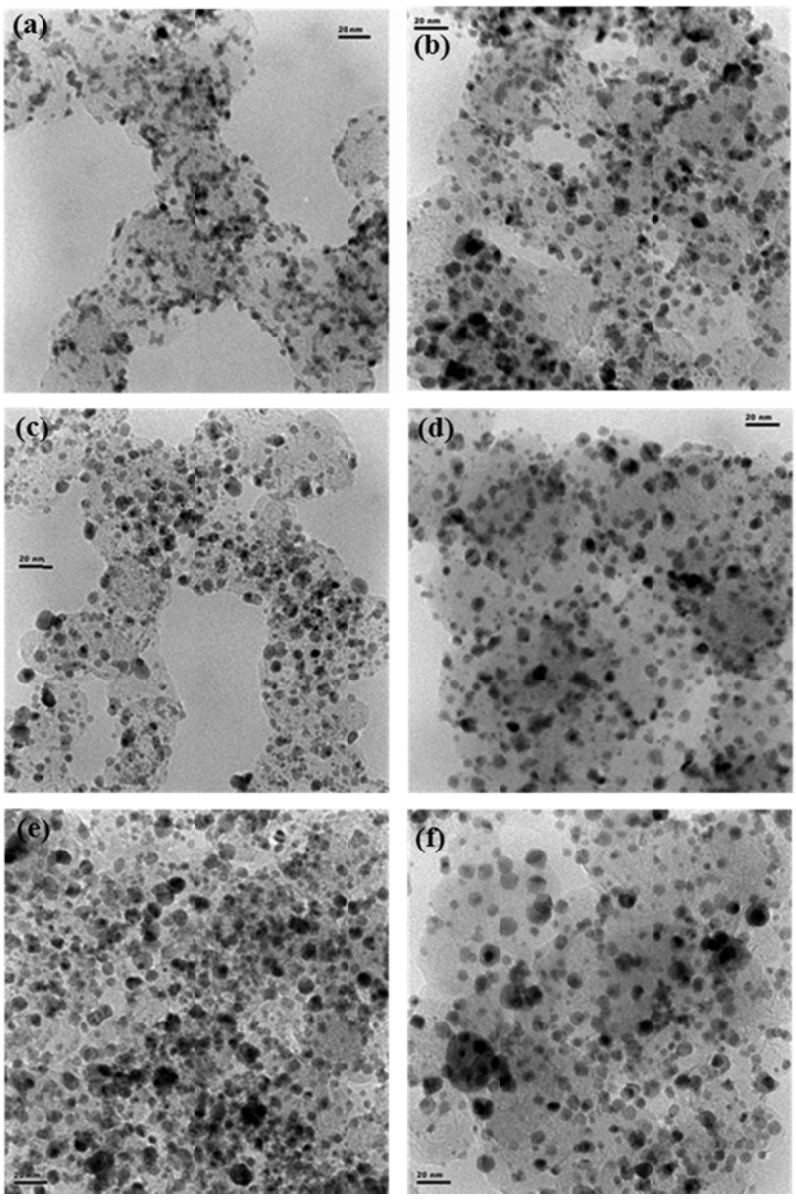

Figure 6.6 HRTEM images of Pt/ACCS and Pt*/ACCS catalysts annealed at various temperature. (a) Pt/ACCS, (b) Pt*/ACCS annealed at 500°C, (c) Pt*/ACCS annealed at 600°C, (d) Pt*/ACCS annealed at 700°C, (e) Pt*/ACCS annealed at 800°C and (f) Pt*/ACCS annealed at 900°C.

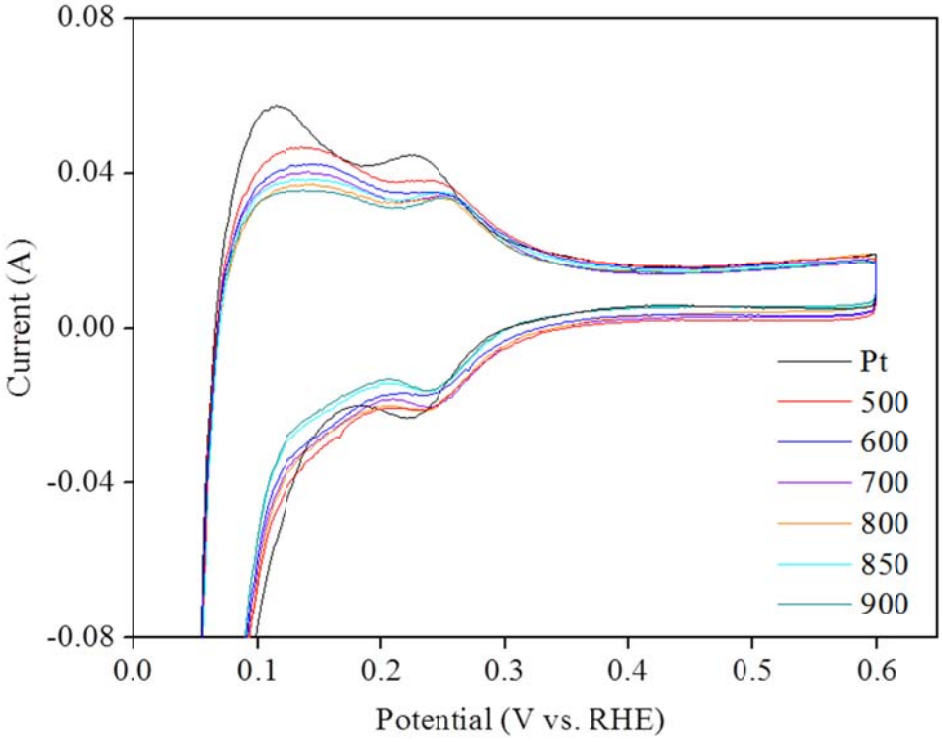

Figure 6.7 Comparison of ECSAs in MEA for Pt/ACCS and Pt*/ACCS catalysts annealed at various temperatures.

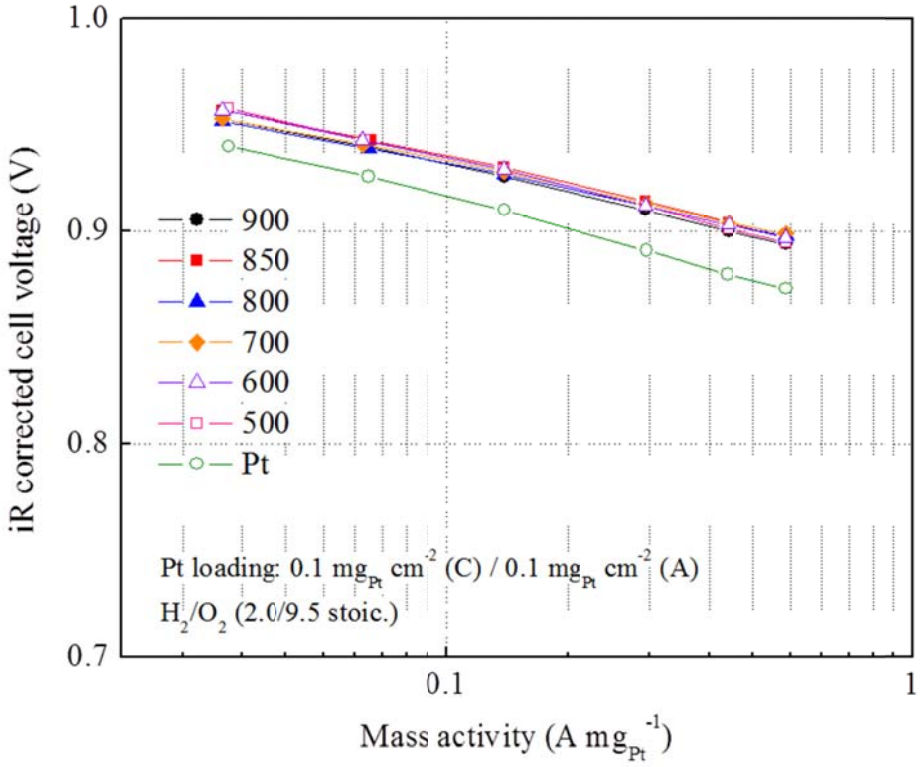

Figure 6.8 Comparison of mass activities for Pt/ACCS and Pt*/ACCS catalysts annealed at various temperatures.

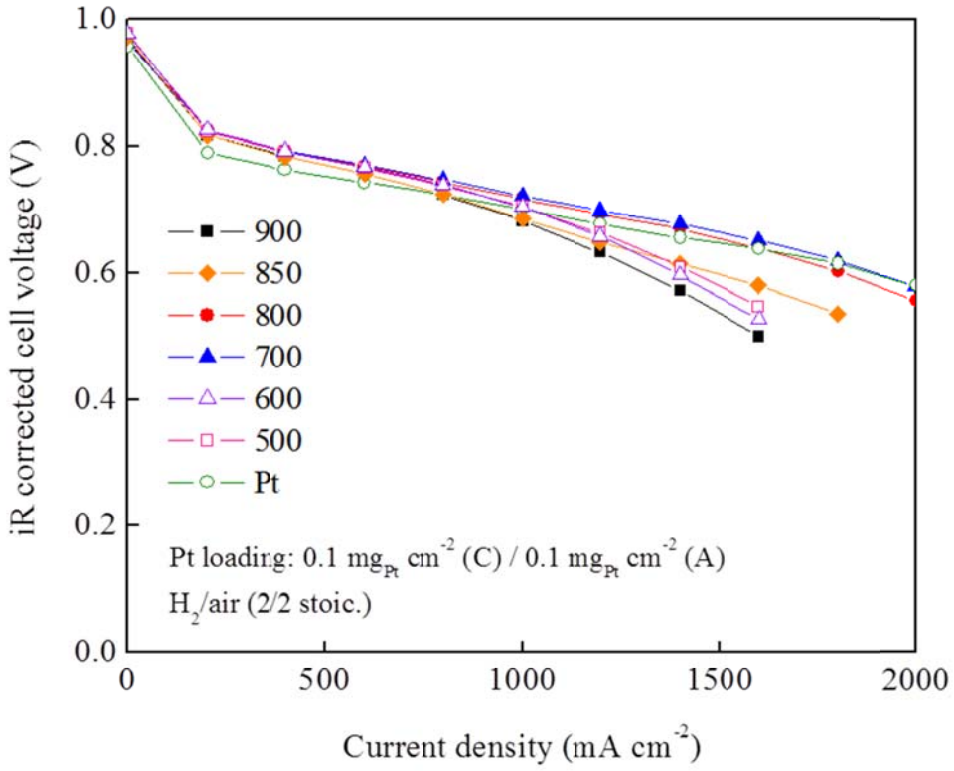

Figure 6.9 Comparison of H_2/air polarization results for Pt/ACCS and Pt*/ACCS catalysts annealed at various temperatures.

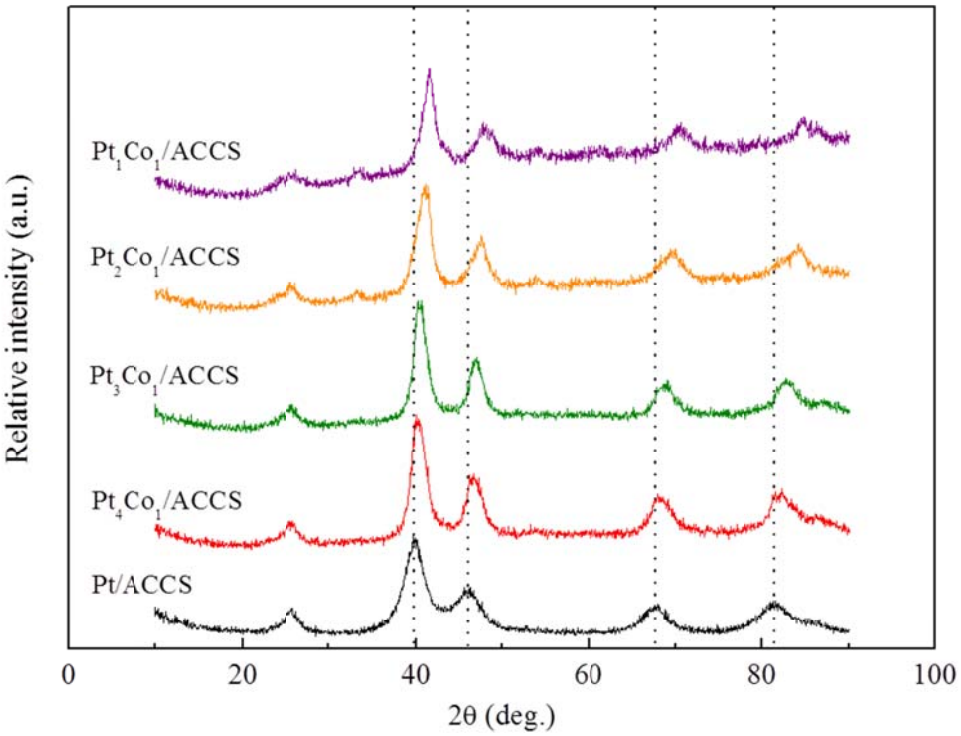

Figure 6.10 XRD patterns for Pt/ACCS and Pt*/ACCS catalysts synthesized with various Pt/Co ratios.

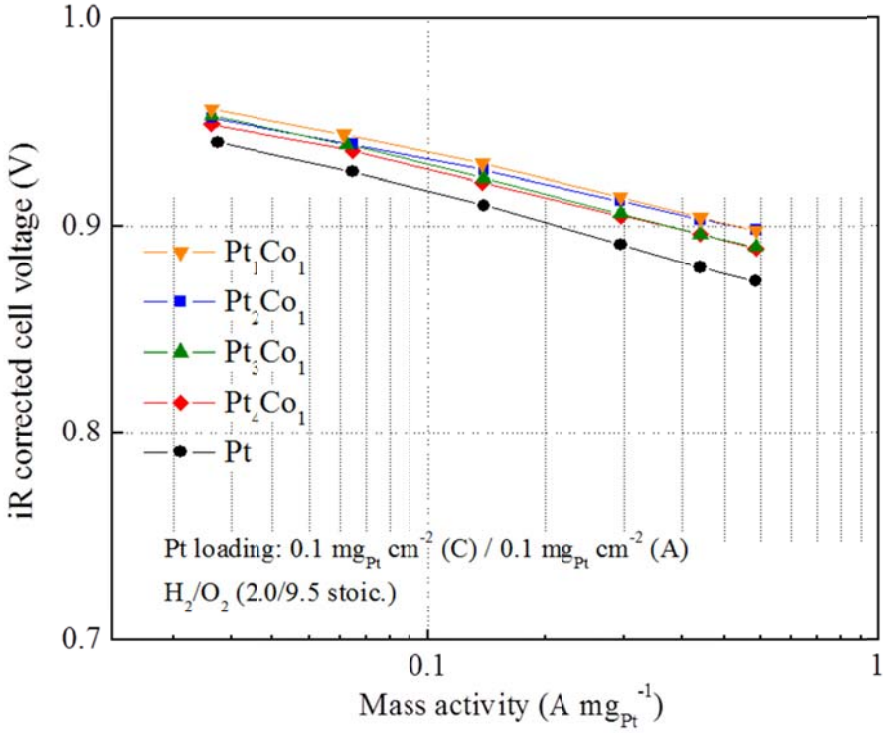

Figure 6.11 Comparison of mass activities for Pt/ACCS and Pt*/ACCS catalysts synthesized with various Pt/Co ratios.

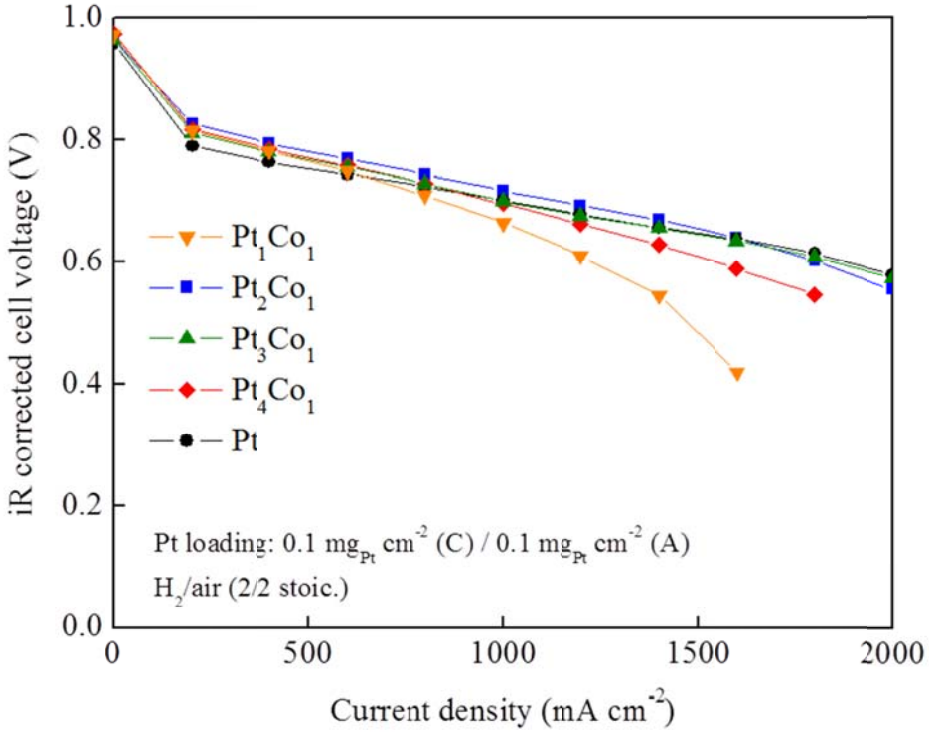

Figure 6.12 Comparison of H_2/air polarization results for Pt/ACCS and Pt*/ACCS catalysts synthesized with various Pt/Co ratios.

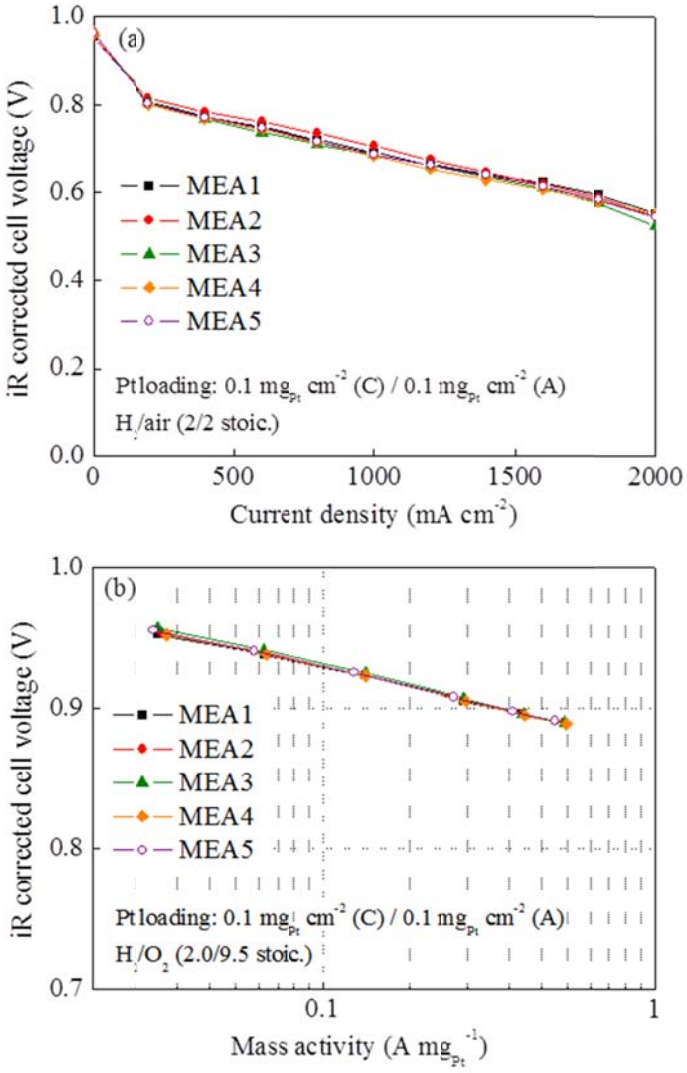

Figure 6.13 H_2/air performance and mass activity reproducibility test results of Pt*/ACCS catalyst (Pt_3Co_1) with five different MEAs.

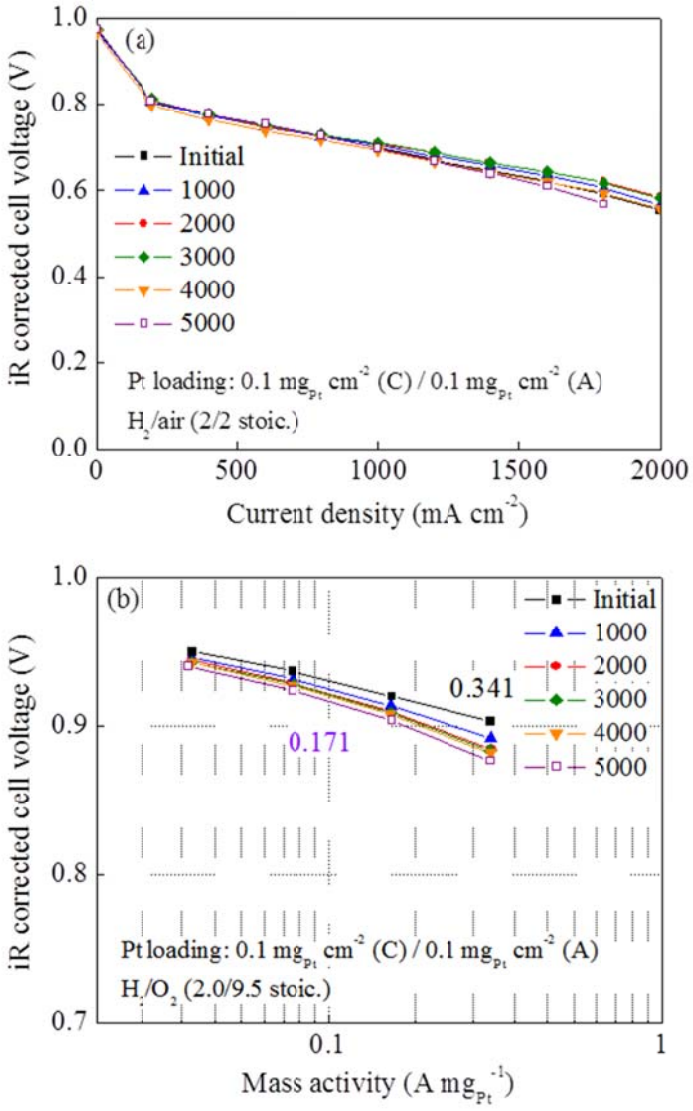

Figure 6.14 The support stability test (1.0-1.5 V potential cycling for 5000 cycles) results on (a) H_2/air performance and (b) mass activity for Pt*/ACCS cathode catalysts.

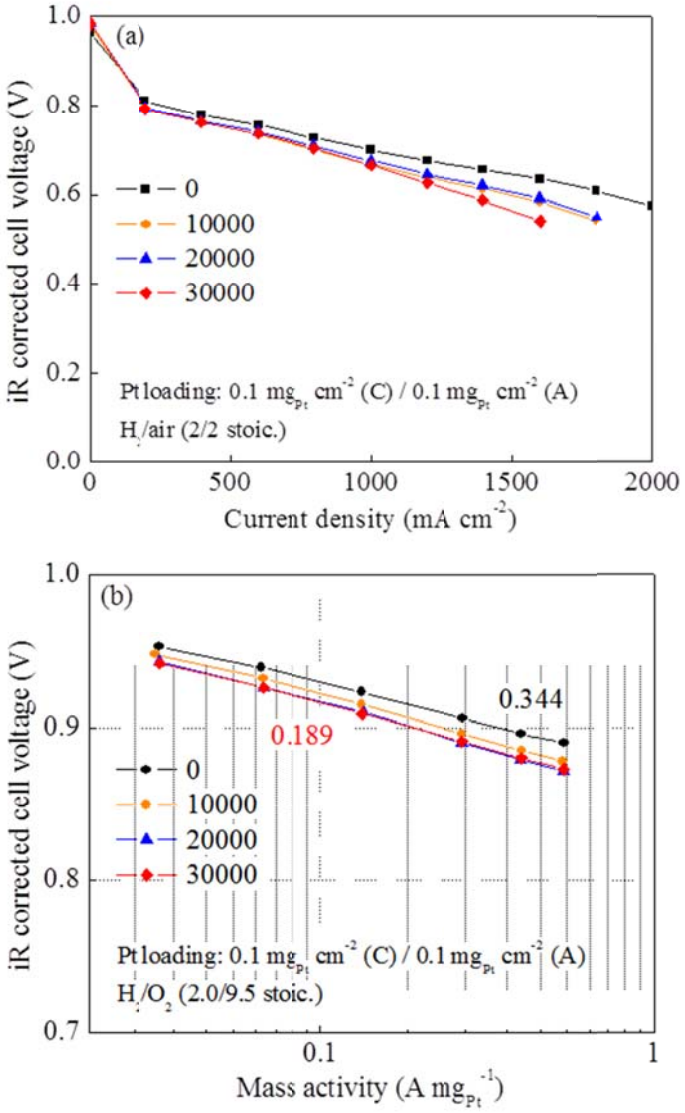

Figure 6.15 The catalyst stability test (0.6-1.0 V potential cycling for 30000 cycles) results on (a) H_2/air performance and (b) mass activity for Pt*/ACCS cathode catalysts.

Table 6.1 Summary of the physical and electrochemical properties for Pt/ACCS and Pt*/ACCS catalysts annealed at various temperatures.

Annealing temp. (°C)	d_{Pt} (XRD) (nm)	2θ for Pt (111) (°)	ECSA ($m^2\ g_{Pt}^{-1}$)	Mass activity ($A\ mg_{Pt}^{-1}$)	Current density at 0.7 $V_{iR\text{-}corr}$ ($mA\ cm^{-2}$)	Current density at 0.6 $V_{iR\text{-}corr}$ ($mA\ cm^{-2}$)	Rated power density ($g_{Pt}\ kW^{-1}$)
Pt	2.9	39.81	41.0	0.193	1011	1884	0.174
300	3.0	40.18	-	-	-	-	-
500	4.1	40.50	34.2	0.425	1028	1418	0.229
600	4.1	40.65	30.5	0.458	1018	1395	0.237
700	4.7	40.81	30.4	0.492	1186	1889	0.173
750	4.6	40.86	-	-	-	-	-
800	3.2	40.92	26.1	0.474	1143	1800	0.180
850	3.0	40.90	28.4	0.471	930	1488	0.207
900	2.9	40.89	26.6	0.408	917	1308	0.250

Table 6.2 Summary of the physical and electrochemical properties for Pt/ACCS and Pt*/ACCS catalysts synthesized with various Pt/Co ratios.

Catalyst	Annealing condition	2θ for Pt (111) (^{o})	d_{Pt} (XRD) (nm)	Mass activity (A mg_{Pt}^{-1})	Current density at 0.6 $V_{iR\text{-}corr}$ (mA cm^{-2})
Pt/ACCS		39.87	2.9	0.193	1884
Pt_4Co_1/ACCS	800 ^{o}C 4 h w/ protective layer coating	40.29	3.8	0.329	1545
Pt_3Co_1/ACCS		40.46	3.8	0.344	1847
Pt_2Co_1/ACCS		40.92	3.4	0.474	1800
Pt_1Co_1/ACCS		41.48	3.3	0.484	1230

Table 6.3 Summary of the stability test results for Pt*/ACCS, Pt/ACCS, and commercial Pt/C catalysts.

Catalyst/Test	Cell voltage (mV)		Power density ($g_{Pt}\ kW^{-1}$)		Mass activity ($A\ mg_{Pt}^{-1}$)		ECSA ($m^2\ g_{Pt}^{-1}$)	
	Initial	Final	Initial	Final	Initial	Final	Initial	Final
Pt*/ACCS								
Support Stability (1.0-1.5 V, 5k cycles)	633 @ 1.5 A cm^{-2}	625 @ 1.5 A cm^{-2} (8 mV loss)	0.180	0.195	0.341	0.171 (50% loss)	30.5	23.9 (22% loss)
Catalyst stability (0.6-1.0 V, 30k cycles)	729 @ 0.8 A cm^{-2}	705 @ 0.8 A cm^{-2} (24 mV loss)	0.174	0.231	0.344	0.189 (45% loss)	30.1	17.4 (42% loss)
Pt/ACCS								
Support Stability (1.0-1.5 V, 5k cycles)	629 @ 1.5 A cm^{-2}	638 @ 1.5 A cm^{-2} (No loss)	0.186	0.174	0.165	0.167 (No loss)	50.0	27.5 (45% loss)
Catalyst stability (0.6-1.0 V, 30k cycles)	723 @ 0.8 A cm^{-2}	650 @ 0.8 A cm^{-2} (73 mV loss)	0.173	0.252	0.193	0.092 (52% loss)	41.0	14.0 (66% loss)
Commercial Pt/C								
Support Stability (1.0-1.5 V, 5k cycles)	481 @ 1.5 A cm^{-2}	0 @ 1.5 A cm^{-2} (481 mV loss)	0.278	3.460	0.167	0.071 (58% loss)	59.8	11.0 (82% loss)
Catalyst stability (0.6-1.0 V, 30k cycles)	696 @ 0.8 A cm^{-2}	0 @ 0.8 A cm^{-2} (696 mV loss)	0.268	0.730	0.184	0.074 (60% loss)	62.0	13.6 (78% loss)

REFERENCES

1. Grove, W.R., *On voltaic series and the combination of gases by platinum.* Philosophical Magazine and Journal of Science, Series 3, 1839. **14**(86): p. 127-130.

2. Hoogers, G., *Fuel cell technology handbook*. 2002, New York: CRC Press.

3. Borup, R., et al., *Scientific Aspects of Polymer Electrolyte Fuel Cell Durability and Degradation.* Chemical Reviews, 2007. **107**: p. 3904-3951.

4. Gasteiger, H.A., et al., *Activity benchmarks and requirements for Pt, Pt-alloy, and non-Pt oxygen reduction catalysts for PEMFCs.* Applied Catalysis B: Environmental, 2005. **56**(1-2): p. 9-35.

5. Huang, S.Y., S.M. Chang, and C.T. Yeh, *Characterization of Surface Composition of Platinum and Ruthenium Nanoalloys Dispersed on Active Carbon.* The Journal of Physical Chemistry B, 2006. **110**(1): p. 234-239.

6. Lubitz, W. and W. Tumas, *Hydrogen An overview.* Chemical Reviews, 2007. **207**(10): p. 3900-3903.

7. Popov, B.N., et al., *Power source research at USC: Development of advanced electrocatalysts for polymer electrolyte membrane fuel cells.* International Journal of Hydrogen Energy, 2011. **36**(2): p. 1794-1802.

8. Debe, M.K., *Electrocatalyst approaches and challenges for automotive fuel cells.* Nature, 2012. **486**(7401): p. 43-51.

9. Markovic, N.M., B.N. Grgur, and P.N. Ross, *Temperature-dependent hydrogen electrochemistry on platinum low-index single-crystal surfaces in acid solutions.* The Journal of Physical Chemistry B, 1997. **101**(27): p. 5405-5413.

10. Singh, R.N., R. Awasthi, and C.S. Sharma, *Review: An Overview of Recent Development of Platinum Based Cathode Materials for Direct Methanol Fuel Cells.* International Journal of Electrochemical Science, 2014. **9**: p. 5607-5639.

11. Wroblowa, H.S., Yen-Chi-Pan, and G. Razumney, *Electroreduction of oxygen: A new mechanistic criterion.* Journal of Electroanalytical Chemistry and Interfacial Electrochemistry, 1976. **69**(2): p. 195-201.

12. Zhang, J., *Recent advances in cathode electrocatalysts for PEM fuel cells.* Frontiers in Energy, 2011. **5**(2): p. 137-148.

13. Nørskov, J.K., et al., *Origin of the overpotential for oxygen reduction at a fuel-cell cathode.* The Journal of Physical Chemistry B, 2004. **108**(46): p. 17886-17892.

14. Li, X., S. Park, and B.N. Popov, *Highly stable Pt and PtPd hybrid catalysts supported on a nitrogen-modified carbon composite for fuel cell application.* Journal of Power Sources, 2010. **195**(2): p. 445-452.

15. Liu, G., et al., *A review of the development of nitrogen-modified carbon-based catalysts for oxygen reduction at USC.* Catalysis Science & Technology, 2011. **1**(2): p. 207.

16. Zhang, S., et al., *A review of accelerated stress tests of MEA durability in PEM fuel cells.* International Journal of Hydrogen Energy, 2009. **34**(1): p. 388-404.

17. Kim, H., N.P. Subramanian, and B.N. Popov, *Preparation of PEM fuel cell electrodes using pulse electrodeposition.* Journal of Power Sources, 2004. **138**(1-2): p. 14-24.

18. Li, X., et al., *Well-Dispersed Multiwalled Carbon Nanotubes Supported Platinum Nanocatalysts for Oxygen Reduction.* Electrochemical and Solid-State Letters, 2004. **7**(9): p. A286.

19. Li, X. and I.M. Hsing, *The effect of the Pt deposition method and the support on Pt dispersion on carbon nanotubes.* Electrochimica Acta, 2006. **51**(25): p. 5250-5258.

20. Shao, M., et al., *Synthesis and characterization of platinum monolayer oxygen-reduction electrocatalysts with Co–Pd core–shell nanoparticle supports.* Electrochemistry Communications, 2007. **9**(12): p. 2848-2853.

21. Shao, Y., G. Yin, and Y. Gao, *Understanding and approaches for the durability issues of Pt-based catalysts for PEM fuel cell.* Journal of Power Sources, 2007. **171**(2): p. 558-566.

22. Wee, J.-H., K.-Y. Lee, and S.H. Kim, *Fabrication methods for low-Pt-loading electrocatalysts in proton exchange membrane fuel cell systems.* Journal of Power Sources, 2007. **165**(2): p. 667-677.

23. Yu, X. and S. Ye, *Recent advances in activity and durability enhancement of Pt/C catalytic cathode in PEMFC.* Journal of Power Sources, 2007. **172**(1): p. 145-154.

24. Ball, S.C., et al., *An investigation into factors affecting the stability of carbons and carbon supported platinum and platinum/cobalt alloy catalysts during 1.2V potentiostatic hold regimes at a range of temperatures.* Journal of Power Sources, 2007. **171**(1): p. 18-25.

25. Colón-Mercado, H.R., H. Kim, and B.N. Popov, *Durability study of Pt3Ni1 catalysts as cathode in PEM fuel cells.* Electrochemistry Communications, 2004. **6**(8): p. 795-799.

26. Colón-Mercado, H.R. and B.N. Popov, *Stability of platinum based alloy cathode catalysts in PEM fuel cells.* Journal of Power Sources, 2006. **155**(2): p. 253-263.

27. Ferreira, P.J., et al., *Instability of Pt/C Electrocatalysts in Proton Exchange Membrane Fuel Cells.* Journal of The Electrochemical Society, 2005. **152**(11): p. A2256.

28. Siroma, Z., et al., *Imaging of highly oriented pyrolytic graphite corrosion accelerated by Pt particles.* Electrochemistry Communications, 2005. **7**(11): p. 1153-1156.

29. Yu, P., M. Pemberton, and P. Plasse, *PtCo/C cathode catalyst for improved durability in PEMFCs.* Journal of Power Sources, 2005. **144**(1): p. 11-20.

30. Maass, S., et al., *Carbon support oxidation in PEM fuel cell cathodes.* Journal of Power Sources, 2008. **176**(2): p. 444-451.

31. Roen, L.M., C.H. Paik, and T.D. Jarvi, *Electrocatalytic Corrosion of Carbon Support in PEMFC Cathodes.* Electrochemical and Solid-State Letters, 2004. **7**(1): p. A19.

32. Lim, K.H., et al., *Effect of operating conditions on carbon corrosion in polymer electrolyte membrane fuel cells.* Journal of Power Sources, 2009. **193**(2): p. 575-579.

33. Lim, K.H., H.-S. Oh, and H. Kim, *Use of a carbon nanocage as a catalyst support in polymer electrolyte membrane fuel cells.* Electrochemistry Communications, 2009. **11**(6): p. 1131-1134.

34. Oh, H.-S., et al., *Corrosion resistance and sintering effect of carbon supports in polymer electrolyte membrane fuel cells.* Electrochimica Acta, 2009. **54**(26): p. 6515-6521.

35. Oh, H.-S., et al., *On-line mass spectrometry study of carbon corrosion in polymer electrolyte membrane fuel cells.* Electrochemistry Communications, 2008. **10**(7): p. 1048-1051.

36. Li, X., et al., *Development of Method for Synthesis of Pt–Co Cathode Catalysts for PEM Fuel Cells.* Electrochemical and Solid-State Letters, 2007. **10**(11): p. B201.

37. Chalk, S.G. and J.F. Miller, *Key challenges and recent progress in batteries, fuel cells, and hydrogen storage for clean energy systems.* Journal of Power Sources, 2006. **159**(1): p. 73-80.

38. Wilson, M.S., et al., *Surface area loss of supported platinum in polymer electrolyte fuel cells.* Journal of the Electrochemical Society, 1993. **140**: p. 2872-2877.

39. Shao, Y., et al., *Durability Study of Pt/C and Pt/CNTs Catalysts under Simulated PEM Fuel Cell Conditions.* Journal of The Electrochemical Society, 2006. **153**(6): p. A1093.

40. Avasarala, B., R. Moore, and P. Haldar, *Surface oxidation of carbon supports due to potential cycling under PEM fuel cell conditions.* Electrochimica Acta, 2010. **55**(16): p. 4765-4771.

41. Huang, S.-Y., et al., *Development of a titanium dioxide-supported platinum catalyst with ultrahigh stability for polymer electrolyte membrane fuel cell applications.* The Journal of the American Chemical Society, 2009. **131**: p. 13898-13899.

42. Knights, S.D., et al., *Aging mechanisms and lifetime of PEFC and DMFC.* Journal of Power Sources, 2004. **127**(1-2): p. 127-134.

43. Shao, Y., et al., *Comparative investigation of the resistance to electrochemical oxidation of carbon black and carbon nanotubes in aqueous sulfuric acid solution.* Electrochimica Acta, 2006. **51**(26): p. 5853-5857.

44. Makharia, R., et al., *Durable PEM Fuel Cell Electrode Materials: Requirements and Benchmarking Methodologies.* ECS Transactions, 2006. **1**(8): p. 3-18.

45. Reiser, C.A., et al., *A Reverse-Current Decay Mechanism for Fuel Cells.* Electrochemical and Solid-State Letters, 2005. **8**(6): p. A273.

46. Eastwood, B.J., et al., *Electrochemical oxidation of a carbon black loaded polymer electrode in aqueous electrolytes.* Journal of Solid State Electrochemistry, 1999. **3**(4): p. 179-186.

47. Siroma, Z., et al., *Dissolution of Nafion® membrane and recast Nafion® film in mixtures of methanol and water.* Journal of Power Sources, 2004. **126**(1-2): p. 41-45.

48. Fowler, M.W., et al., *Issues associated with voltage degradation in a PEMFC.* Journal of New Materials for Electrochemical Systems, 2002. **5**: p. 255-262.

49. Guilminot, E., et al., *Detection of Pt[sup z+] Ions and Pt Nanoparticles Inside the Membrane of a Used PEMFC.* Journal of The Electrochemical Society, 2007. **154**(1): p. B96.

50. Debe, M.K., et al., *Durability aspects of nanostructured thin film catalysts for PEM fuel cells.* ECS Transactions, 2006. **1**(8): p. 51-66.

51. He, C., et al., *PEM fuel cell catalysts cost, performance, and durability.* The Electrochemical Society Interface, 2005. **14**: p. 41-44.

52. Huang, S.-Y., P. Ganesan, and B.N. Popov, *Electrocatalytic activity and stability of niobium-doped titanium oxide supported platinum catalyst for polymer electrolyte membrane fuel cells.* Applied Catalysis B: Environmental, 2010. **96**(1-2): p. 224-231.

53. Huang, S.-Y., P. Ganesan, and B.N. Popov, *Titania supported platinum catalyst with high electrocatalytic activity and stability for polymer electrolyte membrane fuel cell.* Applied Catalysis B: Environmental, 2011. **102**(1-2): p. 71-77.

54. Huang, S.-Y., P. Ganesan, and B.N. Popov, *Electrocatalytic Activity and Stability of Titania-Supported Platinum–Palladium Electrocatalysts for Polymer Electrolyte Membrane Fuel Cell.* ACS Catalysis, 2012. **2**(5): p. 825-831.

55. Zhang, P., S.-Y. Huang, and B.N. Popov, *Mesoporous Tin Oxide as an Oxidation-Resistant Catalyst Support for Proton Exchange Membrane Fuel Cells.* Journal of The Electrochemical Society, 2010. **157**(8): p. B1163.

56. Huang, S.-Y., P. Ganesan, and B.N. Popov, *Development of conducting polypyrrole as corrosion-resistant catalyst support for polymer electrolyte membrane fuel cell (PEMFC) application.* Applied Catalysis B: Environmental, 2009. **93**(1-2): p. 75-81.

57. Sinha, P.K., et al., *Performance of Nano Structured Thin Film (NSTF) Electrodes under Partially-Humidified Conditions.* Journal of The Electrochemical Society, 2011. **158**(7): p. B831.

58. Avasarala, B. and P. Haldar, *On the stability of TiN-based electrocatalysts for fuel cell applications.* International Journal of Hydrogen Energy, 2011. **36**(6): p. 3965-3974.

59. Ham, D.J. and J.S. Lee, *Transition Metal Carbides and Nitrides as Electrode Materials for Low Temperature Fuel Cells.* Energies, 2009. **2**(4): p. 873-899.

60. Lv, H., et al., *High stability platinum electrocatalysts with zirconia–carbon hybrid supports.* J. Mater. Chem., 2012. **22**(3): p. 1135-1141.

61. Lv, H. and S. Mu, *Nano-ceramic support materials for low temperature fuel cell catalysts.* Nanoscale, 2014. **6**(10): p. 5063-74.

62. Wu, M., et al., *Preparation and characterizations of platinum electrocatalysts supported on thermally treated CeO2–C composite support for polymer electrolyte membrane fuel cells.* Electrochimica Acta, 2014. **139**: p. 308-314.

63. Álvarez, G., et al., *Electrochemical stability of carbon nanofibers in proton exchange membrane fuel cells.* Electrochimica Acta, 2011. **56**(25): p. 9370-9377.

64. Cherstiouk, O.V., et al., *Microstructure effects on the electrochemical corrosion of carbon materials and carbon-supported Pt catalysts.* Electrochimica Acta, 2010. **55**(28): p. 8453-8460.

65. Forouzandeh, F., et al., *Evaluation of the Corrosion Resistance of Carbons for Use as PEM Fuel Cell Cathode Supports.* Journal of The Electrochemical Society, 2015. **162**(12): p. F1333-F1341.

66. He, D., et al., *Bifunctional effect of reduced graphene oxides to support active metal nanoparticles for oxygen reduction reaction and stability.* Journal of Materials Chemistry, 2012. **22**(39): p. 21298.

67. He, D., et al., *Nitrogen-doped reduced graphene oxide supports for noble metal catalysts with greatly enhanced activity and stability.* Applied Catalysis B: Environmental, 2013. **132-133**: p. 379-388.

68. Li, H., et al., *Oxidation Stability of Nanographite Materials.* Advanced Energy Materials, 2013. **3**(9): p. 1176-1179.

69. Ornelas, R., et al., *Accelerated degradation tests for Pt/C catalysts in sulfuric acid.* ECS Transactions, 2006. **3**(1): p. 633-641.

70. Wang, J., et al., *Effect of carbon black support corrosion on the durability of Pt/C catalyst.* Journal of Power Sources, 2007. **171**(2): p. 331-339.

71. Xu, F., et al., *Investigation of the Carbon Corrosion Process for Polymer Electrolyte Fuel Cells Using a Rotating Disk Electrode Technique.* Journal of The Electrochemical Society, 2010. **157**(8): p. B1138.

72. Bi, W. and T.F. Fuller, *Temperature Effects on PEM Fuel Cells Pt/C Catalyst Degradation.* ECS Transactions, 2007. **11**(1): p. 1235-1246.

73. Dhanushkodi, S.R., et al., *Carbon corrosion fingerprint development and de-convolution of performance loss according to degradation mechanism in PEM fuel cells.* Journal of Power Sources, 2013. **240**: p. 114-121.

74. Jung, J., B. Park, and J. Kim, *Durability test with fuel starvation using a Pt-CNF catalyst in PEMFC.* Nanoscale Research Letters, 2012. **7**: p. 34-41.

75. Lee, T.K., et al., *Improved durability of Pt/CNT catalysts by the low temperature self-catalyzed reduction for the PEM fuel cells.* International Journal of Hydrogen Energy, 2012. **37**(23): p. 17992-18000.

76. Selvaganesh, S.V., et al., *A Durable Graphitic-Carbon Support for Pt and Pt3Co Cathode Catalysts in Polymer Electrolyte Fuel Cells.* Journal of the Electrochemical Society, 2012. **160**(1): p. F49-F59.

77. Selvaganesh, S.V., et al., *Pristine and graphitized-MWCNTs as durable cathode-catalyst supports for PEFCs.* Journal of Solid State Electrochemistry, 2013. **18**(5): p. 1291-1305.

78. Spernjak, D., et al., *Influence of the microporous layer on carbon corrosion in the catalyst layer of a polymer electrolyte membrane fuel cell.* Journal of Power Sources, 2012. **214**: p. 386-398.

79. Tintula, K.K., et al., *Durability of Pt/C and Pt/MC-PEDOT Catalysts under Simulated Start-Stop Cycles in Polymer Electrolyte Fuel Cells.* Fuel Cells, 2013. **13**(2): p. 158-166.

80. Vinod Selvaganesh, S., et al., *Graphitic Carbon as Durable Cathode-Catalyst Support for PEFCs.* Fuel Cells, 2011. **11**(3): p. 372-384.

81. Wang, X., et al., *Durability investigation of carbon nanotube as catalyst support for proton exchange membrane fuel cell.* Journal of Power Sources, 2006. **158**(1): p. 154-159.

82. Franco, A.J., et al., *Carbon catalyst-support corrosion in polymer electrolyte fuel cells: mechanistic insights.* ECS Transactions, 2008. **13**(15): p. 35-55.

83. Pandy, A., et al., *A Carbon Corrosion Model to Evaluate the Effect of Steady State and Transient Operation of a Polymer Electrolyte Membrane Fuel Cell.* Journal of the Electrochemical Society, 2013. **160**(9): p. F972-F979.

84. Rao, C. and D. Trivedi, *Chemical and electrochemical depositions of platinum group metals and their applications.* Coordination Chemistry Reviews, 2005. **249**(5-6): p. 613-631.

85. Taylor, E.J., E.B. Anderson, and N.R.K. Vilambi, *Preparation of High-Platinum-Utilization Gas Diffusion Electrodes for Proton-Exchange-Membrane Fuel Cells.* Journal of The Electrochemical Society, 1992. **139**(5): p. L45-L46.

86. Thompson, S.D., L.R. Jordan, and M. Forsyth, *Platinum electrodeposition for polymer electrolyte membrane fuel cells.* Electrochimica Acta, 2001. **46**(10-11): p. 1657-1663.

87. Verbrugge, M.W., *Selective Electrodeposition of Catalyst within Membrane-Electrode Structures.* Journal of The Electrochemical Society, 1994. **141**(1): p. 46-53.

88. Liu, Z., et al., *Carbon-supported Pt nanoparticles as catalysts for proton exchange membrane fuel cells.* Journal of Power Sources, 2005. **139**(1-2): p. 73-78.

89. Markovic, N.M., et al., *Oxygen reduction reaction on Pt and Pt bimetallic surfaces - a selective review.* Fuel Cells, 2001. **1**(2): p. 105-116.

90. Coloma, F., et al., *Preparation of platinum supported on pregraphitized carbon blacks.* Langmuir, 1994. **10**(3): p. 750-755.

91. de Miguel, S.R., et al., *States of Pt in Pt/C catalyst precursors after impregnation, drying and reduction steps.* Applied Catalysis A: General, 1998. **170**(1): p. 93-103.

92. Fraga, M.A., et al., *Properties of Carbon-Supported Platinum Catalysts: Role of Carbon Surface Sites.* Journal of Catalysis, 2002. **209**(2): p. 355-364.

93. G.C. Torres, et al., *Effect of the carbon pre-treatment on the properties and performance for nitrobenzene hydrogenation of Pt/C catalysts.* Applied Catalysis A: General, 1997. **161**(1-2): p. 213-226.

94. Okhlopkova, L.B., et al., *Properties of Pt/C and Pd/C catalysts prepared by reduction with hydrogen of adsorbed metal chlorides.* Applied Catalysis A: General, 2000. **204**(2): p. 229-240.

95. Pai, Y.-H., et al., *Clay as a dispersion agent in anode catalyst layer for PEMFC.* Journal of Power Sources, 2006. **163**(1): p. 398-402.

96. Van Dam, H.E. and H. Van Bekkum, *Preparation of platinum on activated carbon.* Journal of Catalysis, 1991. **131**(2): p. 335-349.

97. Alegre, C., et al., *Towards an optimal synthesis route for the preparation of highly mesoporous carbon xerogel-supported Pt catalysts for the oxygen reduction reaction.* Applied Catalysis B: Environmental, 2014. **147**: p. 947-957.

98. Du, S., et al., *A simple approach for PtNi–MWCNT hybrid nanostructures as high performance electrocatalysts for the oxygen reduction reaction.* J. Mater. Chem. A, 2014. **2**(3): p. 692-698.

99. Garcia, A.C. and E.A. Ticianelli, *Investigation of the oxygen reduction reaction on Pt–WC/C electrocatalysts in alkaline media.* Electrochimica Acta, 2013. **106**: p. 453-459.

100. Rahsepar, M., M. Pakshir, and H. Kim, *Synthesis of multiwall carbon nanotubes with a high loading of Pt by a microwave-assisted impregnation method for use in the oxygen reduction reaction.* Electrochimica Acta, 2013. **108**: p. 769-775.

101. Lee, K.-S., et al., *Reversible Surface Segregation of Pt in a Pt3Au/C Catalyst and Its Effect on the Oxygen Reduction Reaction.* The Journal of Physical Chemistry C, 2013. **117**(18): p. 9164-9170.

102. A. Gamez, et al., *Oxygen reduction on well-defined platinum nanoparticles inside recast ionomer.* Electrochimica Acta, 1996. **41**(2): p. 307-314.

103. Watanabe, M. and K. Sakairi, *Electrode for polymer electrolyte electrochemical cell and process of preparing same*. 1998: US.

104. Godínez-Salomón, F., M. Hallen-López, and O. Solorza-Feria, *Enhanced electroactivity for the oxygen reduction on Ni@Pt core-shell nanocatalysts.* International Journal of Hydrogen Energy, 2012. **37**(19): p. 14902-14910.

105. Liu, H., et al., *A review of anode catalysis in the direct methanol fuel cell.* Journal of Power Sources, 2006. **155**(2): p. 95-110.

106. Petrii, O.A., *Pt–Ru electrocatalysts for fuel cells: a representative review.* Journal of Solid State Electrochemistry, 2008. **12**(5): p. 609-642.

107. T. J. Schmidt, et al., *PtRu alloy colloids as precursors for fuel cell catalysts a combined XPS, AFM, HRTEM, and RDE study.* Journal of The Electrochemical Society, 1998. **145**(3): p. 925-931.

108. Bonet, F., et al., *Synthesis of monodisperse Au, Pt, Pd, Ru and Ir nanoparticles in ethylene glycol.* Nanostructured Materials, 1999. **11**(8): p. 1277-1284.

109. Toshima, N. and Y. Wang, *Preparation and catalysis of novel colloidal dispersions of copper/noble metal bimetallic clusters.* Langmuir, 1994. **10**(12): p. 4574-4580.

110. Tang, Z., D. Geng, and G. Lu, *Size-controlled synthesis of colloidal platinum nanoparticles and their activity for the electrocatalytic oxidation of carbon monoxide.* J Colloid Interface Sci, 2005. **287**(1): p. 159-66.

111. Bock, C., et al., *Size-selected synthesis of PtRu nano-catalysts: reaction and size control mechanism.* J Am Chem Soc, 2004. **126**(25): p. 8028-37.

112. Bock, C., B. MacDougall, and Y. LePage, *Dependence of CH_3OH Oxidation Activity for a Wide Range of PtRu Alloys.* Journal of The Electrochemical Society, 2004. **151**(8): p. A1269.

113. Oh, H.-S., et al., *Investigation of carbon-supported Pt nanocatalyst preparation by the polyol process for fuel cell applications.* Electrochimica Acta, 2007. **52**(25): p. 7278-7285.

114. Oh, H.-S., J.-G. Oh, and H. Kim, *Modification of polyol process for synthesis of highly platinum loaded platinum–carbon catalysts for fuel cells.* Journal of Power Sources, 2008. **183**(2): p. 600-603.

115. Chen, W., et al., *Microwave heated polyol synthesis of carbon nanotubes supported Pt nanoparticles for methanol electrooxidation.* Materials Chemistry and Physics, 2005. **91**(1): p. 124-129.

116. Chen, W.X., J.Y. Lee, and Z. Liu, *Microwave-assisted synthesis of carbon supported Pt nanoparticles for fuel cell applications.* Chemical Communications, 2002(21): p. 2588-2589.

117. Chu, Y.-Y., et al., *Performance of Pt/C catalysts prepared by microwave-assisted polyol process for methanol electrooxidation.* Journal of Power Sources, 2010. **195**(7): p. 1799-1804.

118. Katsuki, H. and S. Komarneni, *Microwave-Hydrothermal Synthesis of Monodispersed Nanophase a-Fe2O3.* Journal of the American Ceramic Society, 2001. **84**(10): p. 2313-2317.

119. Komarneni, S., et al., *Microwave−Polyol Process for Pt and Ag Nanoparticles.* Langmuir, 2002. **18**: p. 5959-5962.

120. Lebègue, E., S. Baranton, and C. Coutanceau, *Polyol synthesis of nanosized Pt/C electrocatalysts assisted by pulse microwave activation.* Journal of Power Sources, 2011. **196**(3): p. 920-927.

121. Song, S., Y. Wang, and P.K. Shen, *Pulse-microwave assisted polyol synthesis of highly dispersed high loading Pt/C electrocatalyst for oxygen reduction reaction.* Journal of Power Sources, 2007. **170**(1): p. 46-49.

122. Tsuji, M., et al., *Microwave-assisted synthesis of metallic nanostructures in solution.* Chemistry, 2005. **11**(2): p. 440-52.

123. Yu, W., W. Tu, and H. Liu, *Synthesis of Nanoscale Platinum Colloids by Microwave Dielectric Heating.* Langmuir, 1999. **15**(1): p. 6-9.

124. Zhu, J., et al., *Microwave Assisted Preparation of CdSe, PbSe, and Cu2-xSe Nanoparticles.* The Journal of Physical Chemistry B, 2000. **104**(31): p. 7344-7347.

125. Fang, B., et al., *Homogeneous deposition of platinum nanoparticles on carbon black for proton exchange membrane fuel cell.* J Am Chem Soc, 2009. **131**(42): p. 15330-8.

126. Wang, G., et al., *Investigation of grain boundary formation in PtRu/C catalyst obtained in a polyol process with post-treatment.* International Journal of Hydrogen Energy, 2011. **36**(5): p. 3322-3332.

127. Xie, J., et al., *Microstructural Changes of Membrane Electrode Assemblies during PEFC Durability Testing at High Humidity Conditions.* Journal of The Electrochemical Society, 2005. **152**(5): p. A1011.

128. Wang, G.X., et al., *Enhancement of Ionic Conductivity of PEO Based Polymer Electrolyte by the Addition of Nanosize Ceramic Powders.* Journal of Nanoscience and Nanotechnology, 2005. **5**(7): p. 1135-1140.

129. Stevens, D.A., et al., *Ex Situ and In Situ Stability Studies of PEMFC Catalysts.* Journal of The Electrochemical Society, 2005. **152**(12): p. A2309.

130. Ahn, S.-Y., et al., *Performance and lifetime analysis of the kW-class PEMFC stack.* Journal of Power Sources, 2002. **106**(1-2): p. 295-303.

131. Liu, J., et al., *Studies on performance degradation of a direct methanol fuel cell (DMFC) in life test.* Physical Chemistry Chemical Physics, 2004. **6**(1): p. 134.

132. Antolini, E., *Formation, microstructural characteristics and stability of carbon supported platinum catalysts for low temperature fuel cells.* Journal of Materials Science, 2003. **38**(14): p. 2995-3005.

133. Yasuda, K., et al., *Platinum dissolution and deposition in the polymer electrolyte membrane of a PEM fuel cell as studied by potential cycling.* Phys Chem Chem Phys, 2006. **8**(6): p. 746-52.

134. Honji, A., et al., *Agglomeration of platinum particles supported on carbon in phosphoric acid.* Journal of The Electrochemical Society, 1988. **135**(2): p. 355-359.

135. Watanabe, M., et al., *Activity and Stability of Ordered and Disordered Co-Pt Alloys for Phosphoric Acid Fuel Cells.* Journal of The Electrochemical Society, 1994. **141**(10): p. 2659-2668.

136. Gruver, G.A., R.F. Pascoe, and H.R. Kunz, *Surface Area Loss of Platinum Supported on Carbon in Phosphoric Acid Electrolyte.* Journal of The Electrochemical Society, 1980. **127**(6): p. 1219-1224.

137. Zhai, Y., et al., *The stability of Pt/C catalyst in H3PO4/PBI PEMFC during high temperature life test.* Journal of Power Sources, 2007. **164**(1): p. 126-133.

138. Borup, R.L., et al., *PEM fuel cell electrocatalyst durability measurements.* Journal of Power Sources, 2006. **163**(1): p. 76-81.

139. Darling, R.M. and J.P. Meyers, *Kinetic Model of Platinum Dissolution in PEMFCs.* Journal of The Electrochemical Society, 2003. **150**(11): p. A1523.

140. Wang, X., R. Kumar, and D.J. Myers, *Effect of Voltage on Platinum Dissolution.* Electrochemical and Solid-State Letters, 2006. **9**(5): p. A225.

141. Mitsushima, S., et al., *Consumption Rate of Pt under Potential Cycling.* Journal of The Electrochemical Society, 2007. **154**(2): p. B153.

142. Nagy, Z. and Hoydoo You, *Applications of surface X-ray scattering to electrochemistry problems.* Electrochimica Acta, 2002. **47**(19): p. 3037-3055.

143. Ota, K.-I., S. Nishigori, and N. Kamiya, *Dissolution of platinum anodes in sulfuric acid solution.* Journal of Electroanalytical Chemistry and Interfacial Electrochemistry, 1988. **257**(1-2): p. 205-215.

144. Mathias, M.F., et al., *Two fuel cell cars in every garage?* The Electrochemical Society Interface, 2005. **14**: p. 24-35.

145. Xu, H., R. Kunz, and J.M. Fenton, *Investigation of Platinum Oxidation in PEM Fuel Cells at Various Relative Humidities.* Electrochemical and Solid-State Letters, 2007. **10**(1): p. B1.

146. Vleeming, J.H., et al., *Graphite-Supported Platinum Catalysts: Effects of Gas and Aqueous Phase Treatments* Journal of Catalysis, 1997. **166**(2): p. 148-159.

147. Wilson, M.S., J.A. Valerio, and S. Gottesfeld, *Low platinum loading electrodes for polymer electrolyte fuel cells fabricated using thermoplastic ionomers.* Electrochimica Acta, 1995. **40**(3): p. 355-363.

148. Baturina, O.A., S.R. Aubuchon, and K.J. Wynne, *Thermal Stability in Air of Pt/C Catalysts and PEM Fuel Cell Catalyst Layers.* Chemistry of Materials, 2006. **18**(6): p. 1498-1504.

149. Qi, Z. and S. Buelte, *Effect of open circuit voltage on performance and degradation of high temperature PBI–H3PO4 fuel cells.* Journal of Power Sources, 2006. **161**(2): p. 1126-1132.

150. U.S. DRIVE, *Fuel Cell Technical Team Roadmap*. 2013 [cited 2015 Oct/06]; Available from: http://energy.gov/sites/prod/files/2014/02/f8/fctt_roadmap_june2013.pdf.

151. Dicks, A.L., *The role of carbon in fuel cells.* Journal of Power Sources, 2006. **156**(2): p. 128-141.

152. Li, X., G. Liu, and B.N. Popov, *Activity and stability of non-precious metal catalysts for oxygen reduction in acid and alkaline electrolytes.* Journal of Power Sources, 2010. **195**(19): p. 6373-6378.

153. Li, X., et al., *Non-precious metal catalysts synthesized from precursors of carbon, nitrogen, and transition metal for oxygen reduction in alkaline fuel cells.* Journal of Power Sources, 2011. **196**(4): p. 1717-1722.

154. Liu, G., et al., *Development of non-precious metal oxygen-reduction catalysts for PEM fuel cells based on N-doped ordered porous carbon.* Applied Catalysis B: Environmental, 2009. **93**(1-2): p. 156-165.

155. Liu, G., et al., *Studies of oxygen reduction reaction active sites and stability of nitrogen-modified carbon composite catalysts for PEM fuel cells.* Electrochimica Acta, 2010. **55**(8): p. 2853-2858.

156. Nallathambi, V., et al., *Development of high performance carbon composite catalyst for oxygen reduction reaction in PEM Proton Exchange Membrane fuel cells.* Journal of Power Sources, 2008. **183**(1): p. 34-42.

157. Sidik, R.A., et al., *O2 reduction on graphite and nitrogen-doped graphite: experiment and theory.* The Journal of Physical Chemistry B, 2006. **110**(4): p. 1787-1793.

158. Subramanian, N.P., et al., *Studies on Co-based catalysts supported on modified carbon substrates for PEMFC cathodes.* Journal of Power Sources, 2006. **157**(1): p. 56-63.

159. Subramanian, N.P., et al., *Nitrogen-modified carbon-based catalysts for oxygen reduction reaction in polymer electrolyte membrane fuel cells.* Journal of Power Sources, 2009. **188**(1): p. 38-44.

160. Saito, Y., *Structure and absolute configurations of cobalt(III) complexes.* Pure and Applied Chemistry, 1968. **17**(1): p. 21-36.

161. Li, X., et al., *Development of durable carbon black/titanium dioxide supported macrocycle catalysts for oxygen reduction reaction.* Journal of Power Sources, 2009. **193**(2): p. 470-476.

162. Sethuraman, V.A., et al., *Importance of catalyst stability vis-à-vis hydrogen peroxide formation rates in PEM fuel cell electrodes.* Electrochimica Acta, 2009. **54**(23): p. 5571-5582.

163. Stamenkovic, V., et al., *Oxygen Reduction Reaction on Pt and Pt-Bimetallic Electrodes Covered by CO.* Journal of The Electrochemical Society, 2005. **152**(2): p. A277.

164. Maldonado, S. and K.J. Stevenson, *Influence of nitrogen doping on oxygen reduction electrocatalysis at carbon nanofiber electrodes.* The Journal of Physical Chemistry B, 2005. **109**(10): p. 4707-4716.

165. Zhu, Y.A., et al., *Modeling of fishbone-type carbon nanofibers: A theoretical study.* Carbon, 2005. **43**(8): p. 1694-1699.

166. Schwan, J., et al., *Raman spectroscopy on amorphous carbon films.* Journal of applied physics, 1996. **80**: p. 440-447.

167. Hsieh, C.-T. and H. Teng, *Influence of oxygen treatment on electric double-layer capacitance of activated carbon fabrics.* Carbon, 2002. **40**(5): p. 667-674.

168. Barbieri, O., et al., *Capacitance limits of high surface area activated carbons for double layer capacitors.* Carbon, 2005. **43**(6): p. 1303-1310.

169. Wang, Z., et al., *The synthesis of ionic-liquid-functionalized multiwalled carbon nanotubes decorated with highly dispersed Au nanoparticles and their use in oxygen reduction by electrocatalysis.* Carbon, 2008. **46**(13): p. 1687-1692.

170. Wu, B., et al., *Functionalization of carbon nanotubes by an ionic-liquid polymer: dispersion of Pt and PtRu nanoparticles on carbon nanotubes and their electrocatalytic oxidation of methanol.* Angew Chem Int Ed Engl, 2009. **48**(26): p. 4751-4.

171. Hsin, Y.L., K.C. Hwang, and C.-T. Yeh, *Poly (vinylpyrrolidone)-modified graphite carbon nanofibers as promising supports for PtRu catalysts in direct methanol fuel cells.* Journal of the American Chemical Society, 2007. **129**(32): p. 9999-10010.

172. Datsyuk, V., et al., *Chemical oxidation of multiwalled carbon nanotubes.* Carbon, 2008. **46**(6): p. 833-840.

173. Guha, A., et al., *Surface-modified carbons as platinum catalyst support for PEM fuel cells.* Carbon, 2007. **45**(7): p. 1506-1517.

174. Hull, R.V., et al., *Pt Nanoparticle Binding on Functionalized Multiwalled Carbon Nanotubes.* Chemistry of Materials, 2006. **18**(7): p. 1780-1788.

175. Maiyalagan, T., *Silicotungstic acid stabilized Pt–Ru nanoparticles supported on carbon nanofibers electrodes for methanol oxidation.* International Journal of Hydrogen Energy, 2009. **34**(7): p. 2874-2879.

176. Oh, H.-S., et al., *Effect of chemical oxidation of CNFs on the electrochemical carbon corrosion in polymer electrolyte membrane fuel cells.* International Journal of Hydrogen Energy, 2010. **35**(2): p. 701-708.

177. Xing, Y., *Synthesis and electrochemical characterization of uniformly-dispersed high loading Pt nanoparticles on sonochemically-treated carbon nanotubes.* The Journal of Physical Chemistry B, 2004. **108**(50): p. 19255-19259.

178. Xing, Y., et al., *Sonochemical oxidation of multiwalled carbon nanotubes.* Langmuir, 2005. **21**(9): p. 4185-90.

179. An, X., et al., *Stable aqueous dispersions of noncovalently functionalized graphene from graphite and their multifunctional high-performance applications.* Nano Lett, 2010. **10**(11): p. 4295-301.

180. Oh, H.-S. and H. Kim, *Efficient Synthesis of Pt Nanoparticles Supported on Hydrophobic Graphitized Carbon Nanofibers for Electrocatalysts Using Noncovalent Functionalization.* Advanced Functional Materials, 2011. **21**(20): p. 3954-3960.

181. Simmons, T.J., et al., *Noncovalent functionalization as an alternative to oxidative acid treatment of single wall carbon nanotubes with applications for polymer composites.* ACS Nano, 2009. **3**(4): p. 865-70.

182. Kangasniemi, K.H., D.A. Condit, and T.D. Jarvi, *Characterization of Vulcan Electrochemically Oxidized under Simulated PEM Fuel Cell Conditions.* Journal of The Electrochemical Society, 2004. **151**(4): p. E125.

183. Jung, W., et al., *Highly Active and Durable Co-Doped Pt/CCC Cathode Catalyst for Polymer Electrolyte Membrane Fuel Cells.* Electrochimica Acta, 2015. **167**: p. 1-12.

184. Mani, P., R. Srivastava, and P. Strasser, *Dealloyed binary PtM3 (M=Cu, Co, Ni) and ternary PtNi3M (M=Cu, Co, Fe, Cr) electrocatalysts for the oxygen reduction reaction: Performance in polymer electrolyte membrane fuel cells.* Journal of Power Sources, 2011. **196**(2): p. 666-673.

185. Yu, Z., et al., *Comparison between Dealloyed PtCo3and PtCu3Cathode Catalysts for Proton Exchange Membrane Fuel Cells.* The Journal of Physical Chemistry C, 2012. **116**(37): p. 19877-19885.

186. Antolini, E., et al., *Carbon-Supported Pt-Ni Alloys Prepared by the Borohydride Method as Electrocatalysts for DMFCs.* Electrochemical and Solid-State Letters, 2005. **8**(4): p. A226.

187. Shukla, A.K., et al., *Carbon-supported Pt–Fe alloy as a methanol-resistant oxygen-reduction catalyst for direct methanol fuel cells.* Journal of Electroanalytical Chemistry, 2004. **563**(2): p. 181-190.

188. Xiong, L., A.M. Kannan, and A. Manthiram, *Pt–M (M= Fe, Co, Ni and Cu) electrocatalysts synthesized by an aqueous route for proton exchange membrane fuel cells.* Electrochemistry Communications, 2002. **4**(11): p. 893-903.

189. Li, W., et al., *Nano-stuctured Pt–Fe/C as cathode catalyst in direct methanol fuel cell.* Electrochimica Acta, 2004. **49**(7): p. 1045-1055.

190. Soderberg, J.N., et al., *Oxygen Reduction by Sol-Derived Pt/Co-Based Alloys for PEM Fuel Cells.* Journal of The Electrochemical Society, 2005. **152**(10): p. A2017.

191. Xiong, L. and A. Manthiram, *Effect of Atomic Ordering on the Catalytic Activity of Carbon Supported PtM (M=Fe, Co, Ni, and Cu) Alloys for Oxygen Reduction in PEMFCs.* Journal of The Electrochemical Society, 2005. **152**(4): p. A697.

192. Bard, A.J. and L.R. Faulkner, *Electrochemical Methods*. 2nd edition ed. 2001, New York: John Wiley & Sons. Inc.

193. Shinozaki, K., H. Yamada, and Y. Morimoto, *Relative Humidity Dependence of Pt Utilization in Polymer Electrolyte Fuel Cell Electrodes: Effects of Electrode Thickness, Ionomer-to-Carbon Ratio, Ionomer Equivalent Weight, and Carbon Support.* Journal of The Electrochemical Society, 2011. **158**(5): p. B467.

194. Damjanovic, A. and V. Brusic, *Electrode kinetics of oxygen reduction on oxide-free platinum electrodes.* Electrochimica Acta, 1967. **12**(6): p. 615-628.

195. Sepa, D.B. and M.V. Vojnovic, *Reaction intermediates as a controlling factor in the kinetics and mechanism of oxygen reduction at platinum electrodes.* Electrochimica Acta, 1981. **26**(6): p. 781-793.

196. Wroblowa, H., et al., *Adsorption and kinetics at platinum electrodes in the presence of oxygen at zero net current.* Journal of Electroanalytical Chemistry and Interfacial Electrochemistry, 1967. **15**: p. 139-150.

197. Sharma, S. and B.G. Pollet, *Support materials for PEMFC and DMFC electrocatalysts—A review.* Journal of Power Sources, 2012. **208**: p. 96-119.

198. Honda, K., et al., *Electrochemical properties of Pt-modified nano-honeycomb diamond electrodes.* Journal of Electroanalytical Chemistry, 2001. **514**(1-2): p. 35-50.

199. Montilla, F., et al., *Platinum particles deposited on synthetic boron-doped diamond surfaces. Application to methanol oxidation.* Electrochimica Acta, 2003. **48**(25-26): p. 3891-3897.

200. Spătaru, N., et al., *Platinum Electrodeposition on Conductive Diamond Powder and Its Application to Methanol Oxidation in Acidic Media.* Journal of The Electrochemical Society, 2008. **155**(3): p. B264.

201. Han, K.I., et al., *Studies on the anode catalysts of carbon nanotube for DMFC.* Electrochimica Acta, 2004. **50**(2-3): p. 791-794.

202. Lee, K., et al., *Progress in the synthesis of carbon nanotube- and nanofiber-supported Pt electrocatalysts for PEM fuel cell catalysis.* Journal of Applied Electrochemistry, 2006. **36**(5): p. 507-522.

203. Wang, C., et al., *Proton Exchange Membrane Fuel Cells with Carbon Nanotube Based Electrodes.* Nano Letters, 2004. **4**(2): p. 345-348.

204. Rao, C.V., et al., *Synthesis and electrocatalytic oxygen reduction activity of graphene-supported Pt3Co and Pt3Cr alloy nanoparticles.* Carbon, 2011. **49**(3): p. 931-936.

205. Shao, Y., et al., *Highly durable graphene nanoplatelets supported Pt nanocatalysts for oxygen reduction.* Journal of Power Sources, 2010. **195**(15): p. 4600-4605.

206. Andersen, S.M., et al., *Durability of carbon nanofiber (CNF) & carbon nanotube (CNT) as catalyst support for Proton Exchange Membrane Fuel Cells.* Solid State Ionics, 2013. **231**: p. 94-101.

207. Ma, P.C., et al., *Enhanced electrical conductivity of nanocomposites containing hybrid fillers of carbon nanotubes and carbon black.* ACS Appl Mater Interfaces, 2009. **1**(5): p. 1090-6.

208. Antolini, E., *Carbon supports for low-temperature fuel cell catalysts.* Applied Catalysis B: Environmental, 2009. **88**(1-2): p. 1-24.

209. US Department of Energy, *DOE cell component accelerated stress test protocols for PEM fuel cells*. 2007 [cited 2015 Oct 27]; Available from: http://www1.eere.energy.gov/hydrogenandfuelcells/fuelcells/pdfs/component_durability_profile.pdf.

210. Iiyama, A., et al., *Objectives, R&D Challenge Topics and Proposed Evaluation Methods for Polymer Electrolyte Fuel Cells*. 2007: Fuel Cell Commercialization Conference of Japan.

211. Iiyama, A., et al., *Objectives, R&D Challenge Topics and Proposed Evaluation Methods for Polymer Electrolyte Fuel Cells*. 2011: Fuel Cell Commercialization Conference of Japan.

212. Ohma, A., et al., *Membrane and Catalyst Performance Targets for Automotive Fuel Cells by FCCJ Membrane, Catalyst, MEA WG.* ECS Transactions, 2011. **41**(1): p. 775-784.

213. Hashimasa, Y., Y. Matsuda, and T. Shimizu, *Comparison of Carbon Corrosion Test Methods for Polymer Electrolyte Fuel Cell.* Electrochimica Acta, 2015. **179**: p. 119-125.

214. Patterson, T.W. and R.M. Darling, *Damage to the Cathode Catalyst of a PEM Fuel Cell Caused by Localized Fuel Starvation.* Electrochemical and Solid-State Letters, 2006. **9**(4): p. A183.

215. Park, Y.-C., et al., *Investigation of the corrosion of carbon supports in polymer electrolyte fuel cells using simulated start-up/shutdown cycling.* Electrochimica Acta, 2013. **91**: p. 195-207.

216. Sugawara, Y., et al., *Dissolution Mechanism of Platinum in Sulfuric Acid Solution.* Journal of the Electrochemical Society, 2012. **159**(11): p. F779-F786.

217. Fuel cell tech team *U.S. DRIVE. Fuel cell technical team roadmap. June 2013*. 2013 [cited 2015 Oct 25]; Available from: http://energy.gov/sites/prod/files/2014/02/f8/fctt_roadmap_june2013.pdf.

218. Mukundan, R. *Accelerated Testing Validation*. 2014 [cited 2015 Oct 27]; Available from: http://www.hydrogen.energy.gov/pdfs/review14/fc016_mukundan_2014_o.pdf.

219. Hyeon, T., et al., *High-Performance Direct Methanol Fuel Cell Electrodes using Solid-Phase-Synthesized Carbon Nanocoils.* Angewandte Chemie, 2003. **115**(36): p. 4488-4492.

220. Mukerjee, S., et al., *Role of structural and electronic properties of Pt and Pt alloys on electrocatalysis of oxygen reduction An in situ XANES and EXAFS investigation.* Journal of The Electrochemical Society, 1995. **142**(5): p. 1409-1422.

221. Paulus, U.A., et al., *Oxygen reduction on high surface area Pt-based alloy catalysts in comparison to well defined smooth bulk alloy electrodes.* Electrochimica Acta, 2002. **47**(22-23): p. 3787-3798.

222. Wakabayashi, N., et al., *Temperature dependence of oxygen reduction activity at Pt-Fe, Pt-Co, and Pt-Ni alloy electrodes.* The Journal of Physical Chemistry B, 2005. **109**(12): p. 5836-5841.

223. Gottesfeld, S., *The ellipsometric characterization of Pt + Cr alloy surfaces in acid solutions.* Journal of Electroanalytical Chemistry and Interfacial Electrochemistry, 1986. **205**(1-2): p. 163-184.

224. Paffett, M.T., J.G. Beery, and S. Gottesfeld, *Oxygen reduction at $Pt_{0.65}Cr_{0.35}$, $Pt_{0.2}Cr_{0.8}$ and roughened platinum.* Journal of The Electrochemical Society, 1988. **135**(6): p. 1431-1436.

225. Jalan, V. and E.J. Taylor, *Importance of interatomic spacing in catalytic reduction of oxygen in phosphoric acid.* Journal of The Electrochemical Society, 1983. **130**(11): p. 2299-2302.

226. Mukerjee, S. and S. Srinivasan, *Enhanced electrocatalysis of oxygen reduction on platinum alloys in proton exchange membrane fuel cells.* Journal of Electroanalytical Chemistry, 1993. **357**(1-2): p. 201-224.

227. Toda, T., H. Igarashi, and M. Watanabe, *Enhancement of the electrocatalytic O2 reduction on Pt–Fe alloys.* Journal of Electroanalytical Chemistry, 1999. **460**(1-2): p. 258-262.

228. Greeley, J., et al., *Alloys of platinum and early transition metals as oxygen reduction electrocatalysts.* Nat Chem, 2009. **1**(7): p. 552-6.

229. Mun, B.S., et al., *A study of electronic structures of Pt3M (M=Ti,V,Cr,Fe,Co,Ni) polycrystalline alloys with valence-band photoemission spectroscopy.* J Chem Phys, 2005. **123**(20): p. 204717.

230. Stamenkovic, V.R., et al., *Trends in electrocatalysis on extended and nanoscale Pt-bimetallic alloy surfaces.* Nat Mater, 2007. **6**(3): p. 241-7.

231. Uribe, F.A. and T.A.Z. Jr., *A study of polymer electrolyte fuel cell performance at high voltages. Dependence on cathode catalyst layer composition and on voltage conditioning.* Electrochimica Acta, 2002. **47**(22-23): p. 3799-3806.

232. Xiong, L. and A. Manthiram, *Nanostructured Pt–M/C (M=Fe and Co) catalysts prepared by a microemulsion method for oxygen reduction in proton exchange membrane fuel cells.* Electrochimica Acta, 2005. **50**(11): p. 2323-2329.

233. Yano, H., et al., *Oxygen reduction activity of carbon-supported Pt-M (M= V, Ni, Cr, Co, and Fe) alloys prepared by nanocapsule method.* Langmuir, 2007. **23**(11): p. 6438-6445.

234. Qian, Y., et al., *PtM/C catalyst prepared using reverse micelle method for oxygen reduction reaction in PEM fuel cells.* The Journal of Physical Chemistry C, 2008. **112**(4): p. 1146-1157.

235. Rao, C.V. and B. Viswanathan, *ORR activity and direct ethanol fuel cell performance of carbon-supported Pt− M (M= Fe, Co, and Cr) alloys prepared by polyol reduction method.* The Journal of Physical Chemistry C, 2009. **113**(43): p. 18907-18913.

236. Chen, S., et al., *Enhanced activity for oxygen reduction reaction on "Pt3Co" nanoparticles: direct evidence of percolated and sandwich-segregation structures.* J Am Chem Soc, 2008. **130**(42): p. 13818-9.

237. Stamenković, V., et al., *Surface Composition Effects in Electrocatalysis: Kinetics of Oxygen Reduction on Well-Defined Pt3Ni and Pt3Co Alloy Surfaces.* The Journal of Physical Chemistry B, 2002. **106**(46): p. 11970-11979.

238. Xu, Y., A.V. Ruban, and M. Mavrikakis, *Adsorption and dissociation of O_2 on Pt-Co and Pt-Fe alloys.* Journal of the American Chemical Society, 2004. **126**(14): p. 4717-4725.

239. Stamenković, V., et al., *Surface segregation effects in electrocatalysis: kinetics of oxygen reduction reaction on polycrystalline Pt3Ni alloy surfaces.* Journal of Electroanalytical Chemistry, 2003. **554-555**: p. 191-199.

240. Chen, S., et al., *Origin of oxygen reduction reaction activity on "Pt3Co" nanoparticles- atomically resolved chemical compositions and structures.* The Journal of Physical Chemistry C, 2009. **113**(3): p. 1109-1125.

241. Stamenkovic, V.R., et al., *Effect of surface composition on electronic structure, stability, and electrocatalytic properties of Pt-transition metal alloys: Pt-skin versus Pt-skeleton surfaces.* J Am Chem Soc, 2006. **128**(27): p. 8813-9.

242. Paulus, U.A., et al., *Oxygen reduction on carbon-supported Pt-Ni and Pt-Co alloy catalysts.* The Journal of Physical Chemistry B, 2002. **106**(16): p. 4181-4191.

243. Koh, S., M.F. Toney, and P. Strasser, *Activity–stability relationships of ordered and disordered alloy phases of Pt3Co electrocatalysts for the oxygen reduction reaction (ORR).* Electrochimica Acta, 2007. **52**(8): p. 2765-2774.

244. Parthasarathy, A., et al., *Temperature dependence of the electrode kinetics of oxygen reduction at the platinum/Nafion interface - A microelectrode investigation.* Journal of The Electrochemical Society, 1992. **139**(9): p. 2530-2537.